UNIVERSITY OF CALIFORNIA
RIVERSIDE

Role of Subendothelial Matrix Stiffness and Mechanotransduction in Chronic Vascular Inflammation

A Dissertation submitted in partial satisfaction
of the requirements for the degree of

Doctor of Philosophy

in

Bioengineering

by

Harry Alexander Scott

December 2016

Dissertation Committee:
Dr. Kaustabh Ghosh, Chairperson
Dr. Jin Nam
Dr. Ilhem Messaoudi-Powers

The Dissertation of Harry Alexander Scott is approved:

Committee Chairperson

University of California, Riverside

ACKNOWLEDGEMENTS

I would like to express the deepest appreciation to my committee chairperson, Professor Kaustabh Ghosh, whom served as my Ph.D. advisor and importantly, as a mentor and role model since the beginning of my graduate studies. He has truly molded me into the independent researcher I have become today. I would also like to thank my committee members, Professor Jin Nam and Professor Ilhem Messaoudi-Powers for their guidance and constructive criticism throughout my graduate career.

Further, I would like to acknowledge the invaluable contributions of my research findings detailed in this dissertation to my long-time lab colleagues and close friends: Dr. Soroush Ardekani, Dr. Xiao Yang, Boi Quach, and the support from the Department of Bioengineering.

Finally, I would like to acknowledge that Chapter 2 has been previously published in the journal *Integrative Biology.*

DEDICATION

This dissertation is dedicated to my parents, Stan and Lou Scott, who pushed me to pursue my interest in scientific research and supported me no matter how far from home I was. I would also like to further dedicate this to my mother who suffers from Type II Diabetes Mellitus which has greatly motivated me to pursue my research in diabetes.

ABSTRACT OF THE DISSERTATION

Role of Subendothelial Matrix Stiffness and Mechanotransduction in Chronic Vascular Inflammation

by

Harry Alexander Scott

Doctor of Philosophy, Graduate Program in Bioengineering
University of California, Riverside, December 2016
Dr. Kaustabh Ghosh, Chairperson

Chronic vascular inflammation is a hallmark of various debilitating conditions such as atherosclerosis, diabetes, and emphysema. Although these conditions are marked by abnormal vascular stiffness, whether and how it contributes to vascular inflammation has largely remained unknown. The goal of this research was to address this vital gap in our mechanistic understanding of chronic vascular inflammation. Since vascular stiffness is a manifestation of subendothelial matrix stiffness and EC function is known to be regulated by matrix stiffness, the central hypothesis of this research was that abnormal subendothelial matrix stiffness alters EC mechanotransduction that, in turn, enhances EC adhesivity and leukocyte-EC adhesion, rate-limiting steps in chronic vascular inflammation. Findings from the current research revealed that ECs grown on very soft or stiff matrices elicit significantly greater monocyte adhesion that, in turn, is mediated by a preferential increase in Rho-mediated clustering of endothelial intercellular cell adhesion molecule-1 (ICAM-1) on these matrices. Subsequent mechanistic studies showed that increased monocyte-EC adhesion on stiffer subendothelial matrices results from loss of transient

receptor potential vanilloid 4 (TRPV4), a calcium ion channel that enhances the formation of endothelial nitric oxide, a Rho inhibitor. These *in vitro* data are supported by *in vivo* observations that endothelial TRPV4 is downregulated in the stiffer, inflamed aortas of atherosclerotic (ApoE-/-) and diabetic (db/db) mice. To further identify the upstream regulators of endothelial TRPV4 that contribute to EC adhesivity, the role of microRNAs (miR) was examined in an *in vitro* model of diabetic vascular inflammation. MicroRNAs are small non-coding RNA (~20–22 nucleotides) that mediate epigenetic control of gene expression. These studies showed that microRNA 203a (miR-203a), which targets TRPV4, is upregulated under high glucose conditions, resulting in TRPV4 downregulation and associated loss of endothelial nitric oxide and increased monocyte-EC adhesion. Importantly, suppression of miR-203a and the concomitant increase in TRPV4 prevented the inflammatory effects of high glucose on ECs. Taken together, these novel findings not only elucidate a key role of matrix stiffness, mechanosensitive TRPV4, and upstream epigenetic mechanisms in regulating EC adhesivity associated with chronic vascular inflammation but, crucially, identify potentially new targets (e.g. TRPV4, miR-203a) for more effective anti-inflammatory therapies in the future.

Table of Contents

List of Schematics

List of Figures

List of Abbreviations

AFM	Atomic force microscope
CAM	Cell adhesion molecules
CaM	Calmodulin
CaMKII	Calmodulin kinase II
EC	Endothelial cell
eNOS	Endothelial nitric oxide synthase
FA	Focal adhesion
FBS	Fetal bovine serum
GSK	GSK1016790A
HDL	High-density Lipoprotein
HG	High glucose
ICAM-1	Intercellular cell adhesion molecule 1
IKK	Inhibitory κB kinase
IL-1	Interleukin 1
LDL	Low-density Lipoprotein
miRNA	microRNA
Nf-kB	Nuclear factor kappa B
PFA	Paraformaldehyde
PBMs	Peripheral blood monocytes
ROCK	Rho-associated Kinase
RN	RN1734

TNF-α	Tumor necrosis factor-α
TRPV4	Transient Receptor Potential Vanilloid 4
VEGF	Vascular endothelial growth factor
Y27	Y27632

Chapter 1

Introduction

Preface

This Chapter provides a brief background of the pathogenesis of chronic vascular inflammation and discusses the potential role of subendothelial matrix stiffness in regulating endothelial adhesivity during vascular inflammation. The global aim of this doctoral research is to understand the role of subendothelial matrix stiffness and associated mechanotransduction in chronic vascular inflammation and to identify novel upstream epigenetic regulators of this mechanical control of vascular inflammation.

Significance

Chronic vascular inflammation is characterized by incessant accumulation of leukocytes at local vascular and extravascular sites. The accumulating leukocytes subsequently release various pro-inflammatory, hyperpermeability, and cytotoxic factors such as tumor necrosis factor-α (TNF-α), vascular endothelial growth factor (VEGF), and reactive oxygen species (ROS) that, together, cause significant vascular and extravascular tissue damage. Tissue degeneration resulting from chronic vascular inflammation is a major determinant of various debilitating conditions including atherosclerosis, diabetic retinopathy, and emphysema. Among these conditions, atherosclerosis and emphysema lead to significant mortality while diabetic retinopathy is the leading cause of vision loss among the working-age population. Yet, despite the enormous health and economic burden associated with these chronic inflammatory conditions, there is an unmet need to develop effective anti-inflammatory therapies that suppress vascular inflammation without causing adverse off-target effects.

Role of Endothelial Cells in Chronic Vascular Inflammation

In health, vascular endothelial cells (ECs) exhibit a very quiescent phenotype that inhibits the adhesion of circulating leukocytes. However, in response to acute infection or tissue injury, ECs participate actively in the process of vascular inflammation wherein they express surface adhesive proteins to permit leukocyte binding and extravasation. Specifically, inflammatory cytokines, such as TNF-α and IL-1, stimulate the activation of nuclear transcription factor kB (NF-kB), which acts as a master switch for endothelial

activation. This activation, or nuclear translocation, of NF-kB elicits the transcription of pro-inflammatory proteins, such as ICAM-1, which manifests as increased EC adhesivity. Typically, recruited leukocytes eradicate infectious agents or remove wound debri, thereby restoring the homeostasis of the tissue. However, if the body's immune response fails to eradicate the inflammatory source, the inflammatory cascade will continue, incessantly, to recruit additional leukocytes leading to tissue dysfunction and morbidity. Therefore, therapeutics aimed at inhibiting the adhesion of leukocytes to endothelial cells, a key step in chronic inflammation progression, present an attractive method for addressing chronic inflammatory pathologies.

Canonical Mediators of Endothelial Adhesivity

Conditions marked by chronic vascular inflammation, such as atherosclerosis, diabetes and emphysema, are characterized by increased endothelial adhesivity. Increased endothelial adhesivity supports leukocyte binding and propagation of vascular inflammation. Therefore, to develop anti-inflammatory therapeutics that target leukocyte-endothelial interaction, we must first understand the effects a disease/pathology have on endothelial adhesivity.

In atherosclerosis, elevated levels of triglycerides and cholesterol and low levels of high-density lipoproteins (HDL), which is responsible for clearing excessive triglycerides and cholesterol from the body results in dyslipidemia. Consequently, dyslipidemia elicits increased formation and extravasation of low-density lipoproteins (LDL) to the aortic wall. This presence of LDL activates the endothelium and promotes monocyte binding.

Subsequently, monocytes extravasate to the surrounding tissue to ingest the LDL and oxidized LDL (oxLDL), become foam cells, die, and ultimately form the commonly known plaque deposits.

In diabetes, a systemic vascular disease, the presence of high glucose causes endothelial cells to become dysfunctional. This manifests as increased endothelial adhesivity shown by increased ICAM-1 expression and increased pro-inflammatory cytokine production.

In emphysema, chronic tobacco smoke causes degradation of the lung tissues. This process stimulates the production of pro-inflammatory cytokines which enhances endothelial adhesivity (increased ICAM-1 expression) and recruits neutrophils to the inflamed lung tissue. The neutrophils are unable to clear the debris and chronic vascular inflammation progresses. Therefore, based on the pathogenesis of these conditions, it is important, and necessary, to further understand the mechanisms

Subendothelial Matrix Stiffness as a Potentially New Mediator of EC Adhesivity

Importantly, the aforementioned risk factors (atherosclerosis, diabetes, tobacco) not only alter EC biochemistry but are also associated with abnormal subendothelial matrix crosslinking and stiffening. Specifically, in atherosclerosis, excessive LDL formation and loss of atheroprotective apolipoprotein-E (ApoE) have been shown to contribute to arterial stiffening.[1] Diabetes, characterized by high glucose, increases endothelial LOX expression. LOX is a crosslinker for collagen and therefore enhances matrix stiffness.[2] Conversely, in

emphysema caused by tobacco smoke, LOX expression goes down which contributes to excessive matrix softening. Further, diabetes, which is a severe risk factor for retinopathy and atherosclerosis, has been linked with the stiffening of subendothelial matrix in retinal capillaries;[2] tobacco smoke, a risk factor for emphysema and AMD, disrupts the subendothelial matrix of pulmonary and choroidal capillaries and increase its compliance;[3-5] while aging is associated with increased subendothelial matrix stiffness of arteries and aortas.[6] Yet, whether and how alterations in subendothelial matrix stiffness mediate EC adhesivity and leukocyte binding associated with chronic vascular inflammation remains poorly understood.

It is important to examine the role of subendothelial matrix stiffness in EC adhesivity because past findings have implicated matrix stiffness as a key regulator of EC function.[7-9] For instance, studies have shown that excessive matrix stiffening or softening inhibits endothelial VEGFR2 expression, disrupts capillary formation, and causes endothelial barrier disruption.[10, 11] Mechanistically, such changes in subendothelial matrix stiffness alter the cytoskeleton-dependent EC-matrix force balance that, by the process of mechanotransduction, controls intracellular biochemical signaling to govern EC function at the transcriptional and/or translational levels.[9, 12] Changes in matrix stiffness also alter EC sensitivity to soluble factors and, thereby, modify cellular response.[12, 13] Further, past studies have shown that cytoskeletal tension, which is directly controlled by matrix stiffness, controls ICAM-1 clustering and leukocyte-EC binding.[14, 15] Thus, these findings raise the possibility of a causal relationship between aberrant subendothelial matrix stiffness and EC adhesivity during chronic vascular inflammation.

Hypothesis

Based on these past findings, **the working hypothesis** of this doctoral dissertation is that alterations in subendothelial matrix stiffness and associated EC mechanotransduction actively contribute to endothelial adhesivity and leukocyte-EC binding during chronic vascular inflammation.

Chapter 2

Matrix Stiffness Exerts Biphasic Control Over Monocyte-Endothelial Adhesion via Rho-mediated ICAM-1 Clustering

Preface

Matrix stiffness is a key component of mechanotransduction pathways. However, whether and how abnormal matrix stiffness influences EC activation has yet to be fully understood. This Chapter examines the effects of abnormally soft and stiff matrices on vascular inflammation and key mechanotransduction pathways regulating this phenomena.

This Chapter has been reproduced from ***Scott HA**. et al. *Integrative Biology*. 2016, Aug 8;8(8):869-78. with permission from Royal Chemistry Society.

*Adapted from manuscript: Figures 2.1-2.12

Introduction

Chronic vascular inflammation is a hallmark, and often a major determinant, of various debilitating conditions such as diabetic retinopathy, emphysema, atherosclerosis, and age-related macular degeneration (AMD).[16-18] A crucial rate-limiting event in vascular inflammation is leukocyte adhesion to activated endothelial cells (EC) that express cell adhesion molecules such as intercellular cell adhesion molecule-1 (ICAM-1).[19, 20] Past studies have revealed an important role of soluble and genetic factors in regulating endothelial activation and adhesivity.[21] However, the risk factors for the aforementioned inflammatory conditions are also associated with abnormal subendothelial matrix crosslinking (stiffness). For instance, diabetes, which increases risk for retinopathy and atherosclerosis, has been linked with the stiffening of subendothelial matrix in retinal capillaries;[2] tobacco smoke, a risk factor for emphysema and AMD, disrupts the subendothelial matrix of pulmonary and choroidal capillaries and increase its compliance;[3-5] while aging is associated with increased subendothelial matrix stiffness of arteries and aortas.[6] Yet, whether and how alterations in subendothelial matrix stiffness mediate EC adhesivity and leukocyte binding remains poorly understood.

The rationale for examining the role of matrix stiffness in EC adhesivity is further strengthened by past findings that implicate matrix stiffness as a key regulator of EC function.[7-9] For instance, excessive matrix stiffening or softening has been shown to inhibit endothelial VEGFR2 expression, disrupt capillary formation, and increase lung capillary permeability.[10, 11] Further, while matrix stiffening has been shown to disrupt endothelial junctional barrier and enhance neutrophil infiltration associated with atherosclerosis,[22]

matrix softening has been implicated in the loss of EC viability associated with tobacco-induced choriocapillaris degeneration in the eye.[5] Mechanistically, such mechanical control of EC behavior results from adjustments in the cell-matrix force balance that is established between cytoskeletal tension and the strength of matrix stiffness-dependent focal adhesions. By the process of mechanotransduction, alterations in cell-matrix force balance are transduced into distinct intracellular biochemical signaling that regulate global cellular response.[7, 8, 23] Further, cytoskeletal tension and organization, which are strongly regulated by matrix stiffness, are implicated in ICAM-1 clustering and leukocyte-EC binding.[14, 15] Thus, these findings raise the possibility of a causal relationship between aberrant matrix stiffness and EC adhesivity during vascular inflammation.

Here we show that matrix stiffness exerts biphasic control over monocyte-EC adhesion, which is significantly greater on both soft and stiff matrices. This preferential monocyte-EC adhesion on aberrant matrices correlates with increased ICAM-1 clustering that, in turn, is regulated by small GTPase Rho and its downstream target Rho-associated kinase (ROCK). Finally, we show that pharmacological inhibition of Rho/ROCK activity blocks the effects of matrix stiffness on ICAM-1 clustering-dependent monocyte-EC adhesion.

Materials and Methods

Cell Culture. Human microvascular endothelial cells (HMEC-1) were purchased from the Center for Disease Control (CDC) and grown on gelatin-coated culture dishes in medium composed of MCDB-131 basal medium (Life Technologies), 10% fetal bovine serum

(FBS; Fisherbrand), 10 mM L-Glutamine (Life Technologies), 10 ng/mL epidermal growth factor (Millipore), 1 ug/ml hydrocortisone (Sigma), and 1x antibiotic/ antimycotic supplement (Life Technologies). Human monocytic U937 cells were obtained from ATCC and grown in suspension in medium composed of RPMI-1640 basal medium (Life Technologies), 10% FBS, 10 mM HEPES (Fisherbrand), 1 mM sodium pyruvate (Cellgro), 4.5 g/L glucose (Sigma), 2 mM L-Glutamine, 1500 mg/ml sodium bicarbonate (Sigma), and 1x antibiotic/antimycotic supplement.

Fabrication of Polyacrylamide Matrices. Thin (~100 μm-thick), elastic matrices of varying stiffness were fabricated using crosslinked polyacrylamide (PA), as previously described.[2, 24, 25] Briefly, acrylamide and bis-acrylamide (crosslinker) solutions (BioRad) were mixed at different mass ratios, added onto glutaraldehyde-activated glass coverslips, and spread into a thin layer by placing a glass coverslip on top of the PA gel (for 15 min). The top coverslip was then peeled off and the resulting PA-based matrix was rinsed with HEPES buffer prior to surface modification with sulfo-SANPAH (Proteochem, Loves Park, Illinois USA) for covalent conjugation of human plasma fibronectin (3 ug/cm^2; Corning). Fibronectin (FN) was chosen as the cell-adhesive matrix protein because it is found abundantly at sites of chronic vascular inflammation.[26]

Monocyte-EC Adhesion Assay. EC plating on FN-coated matrices was adjusted to ensure that confluent monolayers were formed on all stiffness within 24h (three replicates/condition). Subsequently, confluent EC monolayers were serum-starved

overnight in medium containing MCDB-131, 2.5% FBS and 1x antibiotic/antimycotic supplement (starvation medium) to induce EC quiescence. EC monolayers were then treated with or without TNF-α (25 ng/ml; Fisher) for 5h before addition of DAPI-labeled U937 cells or human CD14+ PBMs at 125k cells/cm^2 for 30 min at 37^{o}C. Next, endothelial monolayers were rinsed three times to remove non- or weakly-adhering monocytes and fixed in 1% paraformaldehyde (PFA; Electron Microscopy Sciences). Fluorescent images ($n \geq 8$) of adherent monocytes were taken using a Nikon Eclipse Ti microscope fitted with a Nikon Digital Sight DS-Qi1Mc camera and the cell count was obtained using ImageJ (NIH). For some studies, cells were treated with ROCK inhibitor Y27632 (20 μM; Sigma) 30 min prior to the assay.

Flow Cytometry. HMEC-1s cultured on tissue culture plastic for 2d were stimulated with or without TNF-α prior to detachment and labeling with rabbit anti–ICAM-1 antibody (Santa Cruz Biotechnology) followed by fluorescently-labeled anti-Rabbit IgG (Vector Laboratories). The immunolabeled ECs were then fixed in 1% PFA for detection of ICAM-1 expression using a Cell Lab Quanta SC flow cytometer (Beckman Coulter, Brea, CA, USA). ICAM-1 expression was analyzed by FlowJo (Treestar, Inc., Ashland, OR, USA).

Western Blot. Expression of endothelial ICAM-1 and ROCK2 were determined by Western Blot. Briefly, confluent cells on matrices of varying stiffness (three replicates/condition) were lysed in RIPA buffer containing protease and phosphatase inhibitors, and the lysates were centrifuged to obtain protein supernatant. An equal amount

of protein was loaded in 10% SDS–polyacrylamide gel and the separated proteins transferred onto a nitrocellulose membrane for detection with polyclonal mouse anti-ICAM-1 antibody (Novus Biologicals, Littleton, CO) or polyclonal rabbit anti-ROCK2 (Santa Cruz Biotechnology) followed by detection with horseradish peroxidase (HRP)–conjugated secondary antibody (Vector Laboratories, Inc., Burlingame, CA). GAPDH (Sigma) was used as the loading control. Protein bands were visualized using a chemiluminescent detection kit (Thermo Scientific) coupled with a camera-based imaging system (Biospectrum AC Imaging System) while the densitometric analysis was performed by ImageJ software.

Quantitative RT PCR. Total RNA was isolated from EC monolayers grown on matrices of different stiffness (three replicates/condition) using Direct-zol RNA MiniPrep (Zymo Research, Irvine, CA, USA). cDNA was made from the RNA with High Capacity cDNA Reverse Transcription (Thermo Fisher–Applied Biosystems), and amplified with the appropriate TaqMan assay for commercially available primer for ROCK2 (HS00178154 M1; Thermo Fisher-Applied Biosystems) and ICAM-1 (HS00164932 M1; Thermo Fisher–Applied Biosystems) on the ABI 7500 Fast system (Thermo Fisher–Applied Biosystems). Relative mRNA levels were determined by the comparative cycle threshold method with normalization to GAPDH (HS02758991 G1; Thermo Fisher–Applied Biosystems).

Immunofluorescent labeling. Following U937 cell adhesion to confluent EC monolayers, the co-cultures were fixed in 1% PFA and labeled with rabbit polyclonal anti-phospho

ICAM-1 (Tyr512, GeneTex, Irvine, CA, USA), mouse monoclonal anti-ICAM-1 (Santa Cruz Biotech), or rabbit polyclonal anti-α-actinin-4 (Abcam, Cambridge, MA, USA) to visualize clustering (three replicates/condition). Clustering indices were determined by measuring target fluorescence intensity (from $n \geq 10$ images) at the U937-EC adhesion site and normalizing it to the average 'background' intensity measured from three neighboring cytoplasmic sites. U937-EC co-cultures immunolabeled with FITC-labeled anti-rabbit alone served as the negative staining control.

Rho Activity. Confluent EC monolayers grown on 200, 1000, and 4000 Pa matrices for 24h were starved overnight prior to measurement of Rho activity using a Rho G-Lisa Activity kit (Cytoskeleton Inc., Denver, CO, USA), as per manufacturer's protocol (three replicates/condition). Briefly, cell lysates were collected, measured for total protein concentration, and mixed with binding buffer (1:1) before adding to the assay plate. Surface-bound samples were then labeled with anti-RhoA primary antibody followed by a HRP-conjugated secondary antibody. Samples were incubated with the provided stop buffer prior to fluorescence detection with a Victor 2 plate reader (Perkin Elmer, Waltham, MA, USA).

Statistics. All data were obtained from multiples cells or images and from multiple replicates/condition (as indicated in each respective section) and, unless otherwise reported, expressed as mean ± standard error (SEM). Statistical significance was determined using analysis of variance (ANOVA; InStat; Graphpad Software Inc.) followed by Tukey post-hoc analysis. Results were considered significance if $p<0.05$.

Results

Matrix stiffness exerts biphasic control over monocyte-endothelial adhesion

To test the hypothesis that aberrant matrix stiffness promotes leukocyte-EC adhesion, human microvascular endothelial cells were grown to confluence on matrices of varying stiffness (for 2d; Fig. 2.1) and assessed for adhesion of human monocytic U937 cells. The stiffness of matrices ranged from 200 Pascals (Pa) to 30,000 Pa to recapitulate the wide range of matrix elasticity observed at sites of vascular inflammation, including the soft fibrin matrix formed at sites of vascular injury (~200 Pa)[27] and the stiffer subendothelial matrices characteristic of aging and atherosclerotic vessels (>4000 Pa).[1, 22]

Addition of U937 cells to TNFα-stimulated EC monolayers revealed a biphasic trend in U937 cell adhesion, with the ECs grown on 200 Pa and 4000 Pa matrices exhibiting an approximately two-fold greater ($p<0.001$) U937 cell binding than those grown on the 1000 Pa matrix (Fig. 2.2A,B). Notably, ECs grown on matrices stiffer than 4000 Pa exhibited a plateau in monocyte adhesion. The observation that monocyte-EC adhesion is the weakest on 1000-2000 Pa stiffness matrices agrees well with past measurements that reveal a similar stiffness of 'normal' subendothelial matrix.[22, 28] Further, freshly-isolated $CD14^+$ human peripheral blood monocytes (hPBMs) exhibited the same biphasic trend for EC adhesion (Fig. 2.2C), thereby confirming that U937 cells recapitulate human circulating monocytes with regards to their ability to sense differential endothelial adhesivity on matrices of varying stiffness.

To confirm that this differential effect of matrix stiffness on EC adhesivity is independent of the effects of inflammatory cytokines, we looked at monocyte-EC adhesion

in the absence of TNF-α. This was possible because, similar to lung and choroidal ECs,[29, 30] HMEC-1 exhibit low levels of baseline ICAM-1 expression[31] (Fig. 2.3), which is expected to promote monocyte binding. Indeed, monocytes adhered to EC monolayers in the absence of TNF-α. More importantly, the monocyte-EC adhesion again exhibited the same biphasic trend, with the lowest degree of monocyte adhesion seen on the normal stiffness (1000 Pa) matrix (Fig. 2.4).

This matrix stiffness-dependent biphasic regulation of monocyte-EC adhesion is not unique to microvascular ECs as human umbilical vein-derived ECs (HUVECs) also exhibited the same trend in U937 cell adhesion (Fig. 2.5), thereby raising the question whether abnormal matrix stiffness exerts similar effects on ECs across all vascular beds.

Effect of Matrix Stiffness on Endothelial ICAM-1 Expression and Clustering

Monocyte-EC adhesion is regulated by the expression and clustering of endothelial cell adhesion molecules (CAMs).[20, 32] Thus, we looked to see whether the biphasic effect of matrix stiffness on monocyte-EC adhesion was regulated by differential CAM expression and/or clustering. We focused on ICAM-1 because it is essential for firm monocyte adhesion to ECs and is upregulated in various inflammation-dependent pathological conditions.[2, 19, 33-35] Western Blot analysis revealed that short-term (2d) EC culture on aberrant matrices does not cause significant differences in ICAM-1 protein and mRNA expression (Fig. 2.6A,B), which is consistent with past findings in short-term EC culture studies.[22, 36]

To explain how abnormal matrices enhance monocyte-EC adhesion in short-term cultures independent of an increase in ICAM-1 expression, we examined the effect of matrix stiffness on endothelial ICAM-1 clustering. U937-EC co-cultures were subjected to immunofluorescent labeling of ICAM-1. Quantitative analysis of ICAM-1 fluorescence intensity at and around the sites of monocyte-EC adhesion revealed that, when compared with ECs on normal (1000 Pa) matrix, those grown on softer (200 Pa) or stiffer (4000 Pa) matrices undergo a marked increase in the degree of ICAM-1 clustering (Fig. 2.7A). Further, consistent with past findings that ICAM-1 phosphorylation contributes to ICAM-1 clustering,[35] we show that the degree of phospho-ICAM-1 (Y512) immunolabeling on the different matrices exhibits the same biphasic trend as ICAM-1 clustering (Fig. 2.7B).

We would like to point out that although we show that matrix stiffness does not alter ICAM-1 expression in short-term cultures, we have recently reported that diabetes-associated subendothelial matrix stiffening leads to NF-kB-dependent ICAM-1 upregulation in retinal ECs.[2] Since this past study was performed in long-term (10d) retinal EC cultures,[2] we hypothesized that the effect of abnormal matrix stiffness on ICAM-1 expression manifests slowly. This hypothesis was confirmed by qPCR measurements that show that EC monolayers grown on 200 Pa and 4000 Pa matrices for 5d exhibit significantly higher ICAM-1 expression than those grown on the normal 1000 Pa matrix (Fig. 2.8).

Matrix Stiffness Biphasically Regulates Rho/ROCK-mediated EC Cytoskeletal Organization

Cytoskeletal tension generated by the small GTPase Rho, via its downstream effector Rho-associated kinase (ROCK), is known to promote ICAM-1 clustering and leukocyte-EC binding.[14, 37] Since Rho/ROCK activity is tightly controlled by matrix stiffness,[22, 38] we looked to see whether the preferential increase in ICAM-1 clustering on softer and stiffer matrices corresponds to an increase in Rho activity. Our studies show that, indeed, both softer (200 Pa) and stiffer (4000 Pa) matrices cause a significant ($p<0.05$) increase in Rho activity (Fig. 2.9A) and a concomitant increase in the expression of ROCK2, the isoform of ROCK that enhances myosin-dependent cytoskeletal tension[39] (Fig. 2.9B and Fig. 2.10). Notably, this biphasic regulation of Rho/ROCK was consistent with the differential (Rho-mediated) actin cytoskeletal organization on these matrices. Specifically, as shown in Fig. 2.9C, ECs that remain round on the soft (200 Pa) matrices exhibited a dense cortical actin network, which relies on high Rho,[40, 41] while cells grown on the stiff (4000 Pa) matrices formed robust stress fibers that result from high Rho/ROCK-mediated cytoskeletal tension.

Rho/ROCK is also known to regulate the association of clustered ICAM-1 with cytoskeletal adaptor proteins that stabilize the assembly of these adhesive structures.[42] To examine this possibility in our U937-EC co-cultures, we performed immunofluorescent labeling of α-actinin-4, a key actin-binding protein that has been implicated in ICAM-1 clustering and monocyte-EC adhesion.[42, 43] Immunofluorescence imaging revealed a marked increase in the localization of α-actinin-4 at sites of adherent U937 cells on both

soft and stiff matrices (Fig. 2.9D), which correlates spatially with increased ICAM-1 clustering at these sites.

Inhibition of Rho/ROCK blocks α-actinin-4-associated ICAM-1 clustering and monocyte-EC adhesion on aberrant matrices

To determine if Rho/ROCK plays a crucial role in matrix stiffness-dependent ICAM-1 clustering and subsequent monocyte-EC adhesion, we treated ECs grown on soft (200 Pa) and stiff (4000 Pa) matrices with ROCK inhibitor Y27632 and measured ICAM-1 clustering and monocyte-EC adhesion. Pharmacological suppression of Rho/ROCK-mediated cytoskeletal tension caused a significant decrease in ICAM-1 clustering on both soft and stiff matrices (Fig. 2.11A,B). Further, our qPCR measurements revealed that the inhibitory effect of Y27632 on ICAM-1 clustering was not due to changes in ICAM-1 expression, which was similar under all conditions (Fig. 2.11C). Notably, Rho/ROCK inhibition on the abnormal matrices also led to a concomitant decrease in the clustering of phosphorylated ICAM-1 (Fig. 2.11D) and α-actinin-4 recruitment to sites of adherent U937 cells (Fig. 2.11E), thereby providing evidence for their role in ICAM-1 clustering on abnormal matrices. Predictably, this Y27632-mediated inhibition of ICAM-1 clustering caused a significant suppression of monocyte-EC adhesion on soft and stiff matrices (Fig. 2.12). Thus, these findings implicate matrix stiffness-dependent increase in Rho/ROCK activity as a key mediator of ICAM-1 clustering and monocyte-EC adhesion.

Discussion

Monocyte adhesion to activated endothelium is a hallmark of chronic vascular inflammation. Past studies aimed at elucidating the mechanisms underlying endothelial adhesivity have revealed an important role of abnormal soluble, genetic and hemodynamic factors. Our current findings implicate matrix stiffness as an independent regulator of EC adhesivity and subsequent monocyte-EC binding. Moreover, this study, coupled with our recent work,[2] reveals that abnormal matrix stiffness-dependent mechanical cues regulates EC adhesivity via both ICAM-1 clustering (rapid effect) and expression (slower effect). Given that important risk factors for chronic vascular inflammation viz. aging, diabetes, smoking, and endotoxin (sepsis), are associated with aberrant matrix stiffness and ICAM-1,[2, 4, 5, 11, 22, 44, 45] findings from our studies advocate the need to more closely examine the contribution of matrix stiffness in leukocyte-endothelial interactions.

Matrix stiffness is emerging as a key determinant of vascular development and disease. This is because alterations in matrix stiffness activate distinct mechanotransduction pathways that control EC biochemistry and function. For instance, suboptimal matrix stiffness has been shown to impair vascular endothelial growth factor (VEGF) receptor signaling and angiogenesis,[10] disrupt endothelial barrier function,[10, 22] and promote choriocapillaris degeneration associated with tobacco-induced age-related macular degeneration.[5] By demonstrating that matrix stiffness also controls monocyte-EC adhesion, our current work extends the implications of matrix-dependent mechanical cues to vascular inflammation. Since endothelial adhesivity and leukocyte-EC binding are prerequisites for leukocyte infiltration into tissues, our new findings also complement and

consolidate recent studies that have identified abnormal matrix stiffening as a key determinant of leukocyte transmigration across the endothelium.[15, 20, 22, 36]

We specifically show that both matrix softening and stiffening promote endothelial adhesivity while the intermediate stiffness sustains endothelial quiescence. This biphasic trend indicates that any alteration in normal subendothelial matrix stiffness is perceived as a divergence from normal homeostasis, which predictably triggers a spontaneous inflammatory response characterized by leukocyte-EC adhesion. It must be noted that such biphasic regulation of EC function by matrix stiffness is not unique to endothelial adhesivity. Others have reported that angiogenesis and endothelial permeability are also biphasically regulated by matrix stiffness, with excessive matrix softening or stiffening causing significant impairment in these functions.[10, 11] Thus, these findings emphasize the need to *optimize* matrix stiffness in order to achieve normal EC behavior.

Chronic vascular inflammation is associated with enhanced expression of endothelial ICAM-1, which mediates strong leukocyte binding and transmigration.[2, 14, 15, 32] Contrary to our expectation, we found that enhanced monocyte adhesion to short-term (2d) EC cultures grown on abnormal matrix stiffness is not associated with an increase in ICAM-1 expression. Although these findings are consistent with past studies that show no effects of matrix stiffness on short-term endothelial ICAM-1 expression,[22, 36] they fail to explain the significant increase in monocyte-EC adhesion we observe on soft and stiff matrices. To address this issue, we looked at the effects of matrix stiffness on ICAM-1 clustering because increases in clustering alone have been shown to enhance monocyte-EC adhesion.[14, 20, 35, 42, 43] Our study is the first to demonstrate that ECs grown on very soft or

stiff matrices exhibit significantly greater ICAM-1 clustering at sites of monocyte-EC adhesion, which is strongly associated with increased ICAM-1 phosphorylation (activity) at these sites. However, as we have shown here and reported before,[2] aberrant matrix stiffness can also cause an increase in ICAM-1 expression over time. Thus, abnormal matrix stiffness appears to play a pivotal role in vascular inflammation wherein it enhances monocyte-EC adhesion *initially* by increasing ICAM-1 clustering and activity but *subsequently* via the additional increase in ICAM-1 expression.

To further elucidate the mechanism by which matrix stiffness controls ICAM-1 clustering and EC adhesivity, we examined the role of small GTPase Rho and its downstream effector ROCK2, the ROCK isoform that enhances myosin-dependent cell contractility.[39] This is because firstly, increase in endothelial Rho/ROCK has previously been shown to promote ICAM-1 clustering and monocyte-EC adhesion,[14, 43] and secondly, Rho/ROCK is strongly regulated by matrix stiffness[22, 38] and upregulated in ECs in diabetes and aging,[22, 46] major risk factors for subendothelial matrix stiffening and vascular inflammation.[42] Our measurements reveal that ECs grown on both soft and stiff matrices exhibit significantly higher Rho activity and ROCK2 protein and mRNA expression. While matrix stiffening is commonly associated with an increase in endothelial Rho/ROCK,[22, 42, 47] which predictably correlated with robust EC spreading (via formation of actin stress fibers) in our study, the increase in Rho/ROCK on soft matrix appears less intuitive. However, past studies have reported that cell rounding, as seen on soft matrices, leads to high Rho-mediated cortical actin network, presumably to prevent membrane damage in the

poorly-spread cells.[48, 49] Consistent with this view, we found that the high endothelial Rho/ROCK on soft matrices correlates with a robust cortical actin network.

Various Rho/ROCK-associated cytoskeletal proteins are known to mediate monocyte-EC adhesion through stabilization of clustered endothelial cell adhesion molecules. Of particular relevance to our study is α-actinin-4, which has been specifically shown to mediate ICAM-1 clustering-dependent monocyte-EC adhesion.[43] Our findings reveal that both matrix softening and stiffening enhance α-actinin-4 recruitment to sites of clustered ICAM-1, presumably to strengthen ICAM-1 binding to the partnering adhesion molecule on monocytes ($\alpha_m\beta_2$). That high endothelial Rho/ROCK on soft and stiff matrices actively contributes to the preferential increase in α-actinin-4-associated ICAM-1 clustering and monocyte-EC adhesion was confirmed when treatment of ECs with a pharmacological Rho/ROCK inhibitor (Y27632) blocked these effects. This inhibitory effect of Y27632 on ICAM-1 clustering occurred independent of changes in ICAM-1 expression, thereby indicating that Rho/ROCK mediates the 'mechanical coupling' of matrix stiffness on the basal surface with ICAM-1 clustering on the apical surface.

Interestingly, past studies have shown that ICAM-1 activation and clustering can, in turn, activate Rho/ROCK in ECs.[15] Thus, our data also point towards the existence of a matrix stiffness-dependent mechanical feedback loop that sustains Rho/ROCK-ICAM-1 crosstalk and monocyte-EC adhesion. Moreover, increase in EC stiffness is also known to enhance endothelial CAM clustering via organization of F-actin and actin-binding proteins at the cytoplasmic end of CAMs.[43] Since matrix stiffness directly controls cell stiffness,[7, 50] it likely promotes endothelial CAM clustering via a similar actin-dependent mechanism.

Further, adherent leukocytes have also been shown to exert mechanical force on endothelial CAMs that is resisted by EC stiffness.[43, 51] The resulting leukocyte-EC force balance on the apical side is thought to alter leukocyte mechanotransduction and, consequently, leukocyte activation.[15] Whether matrix stiffness can modulate leukocyte-EC force balance and, subsequently, leukocyte mechanotransduction/activation (via an increase in EC stiffness), however, remains to be determined.

The findings from this study identify matrix stiffness as an independent regulator of endothelial ICAM-1 clustering and monocyte-EC adhesion via preferential activation of Rho/ROCK on soft and stiff matrices. Since the increase in α-actinin-4-associated ICAM-1 clustering in short-term (2d) EC cultures is independent of an increase in ICAM-1 expression, our findings indicate that pro-inflammatory cytokines and matrix stiffness likely cooperate to rapidly enhance monocyte-EC binding by concurrently increasing endothelial ICAM-1 expression and clustering, respectively. Finally, these new findings provide the rationale for future studies that further elucidate the mechanistic link between matrix stiffness and endothelial adhesivity and its subsequent effects on leukocyte activation associated with chronic vascular inflammation.

Figures

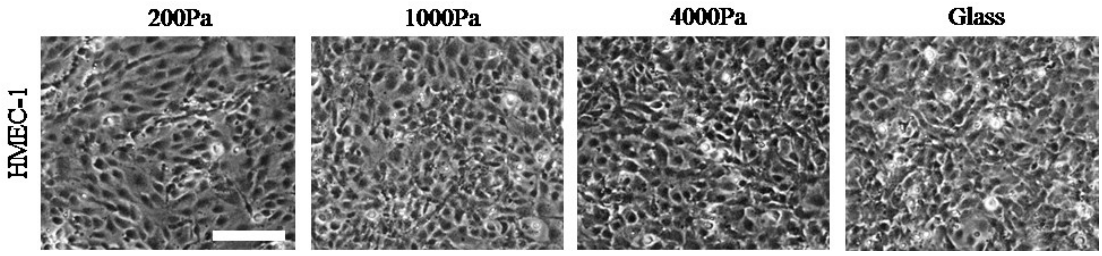

Figure 2.1. ECs form confluent monolayers on matrices of varying stiffness. Representative phase contrast images show that HMEC-1 grown on synthetic matrices of varying stiffness (for 2d) form confluent monolayers. Scale bar: 100 μm

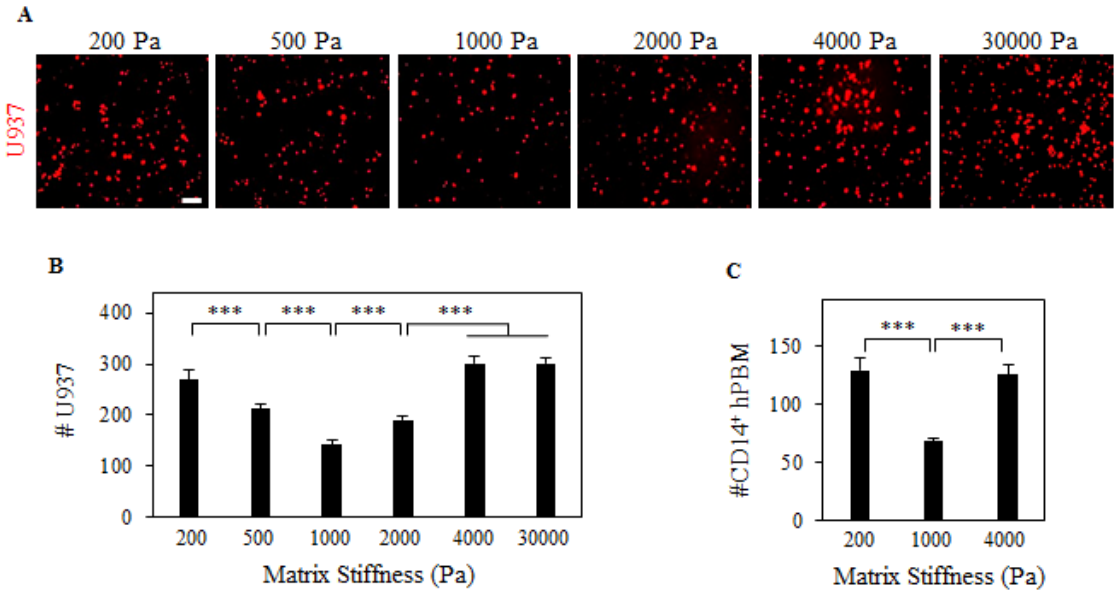

Figure 2.2. Matrix stiffness exerts biphasic control over monocyte-EC adhesion. **(A)** Representative images show fluorescently-labeled U937 cells bound to TNF-α-stimulated EC monolayers grown on matrices of varying stiffness. Scale bar: 100 μm. **(B)** Quantification of adherent U937 cells (per mm^2) reveals a biphasic trend in U937-EC adhesion (***, $p<0.001$). **(C)** Quantification of adherent fluorescently-labeled human $CD14^+$ PBMs (per mm^2) from multiple ($n\geq10$) images of PBM-EC co-cultures reveals the same biphasic trend in monocyte adhesion as observed with U937 monocytic cells (shown in B) (***, $p<0.001$).

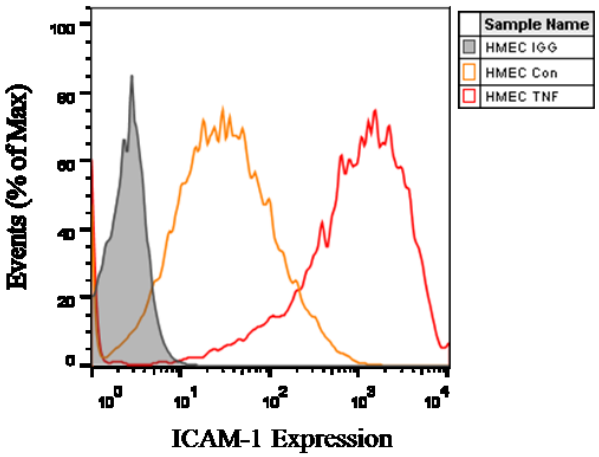

Figure 2.3. HMEC-1s express low baseline levels of ICAM-1. Surface expression of endothelial ICAM-1 was determined by flow cytometry. Representative histogram of ICAM-1 fluorescence intensity indicates that unstimulated HMEC-1s (HMEC con) express low levels of baseline ICAM-1 expression, which is markedly enhanced by TNF-α treatment (HMEC TNF). IgG was used as an isotype control.

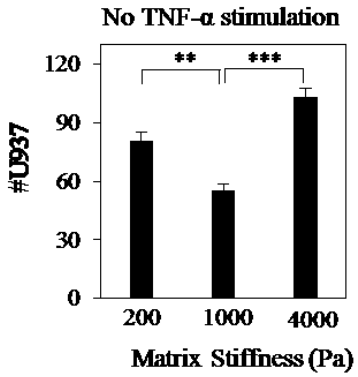

Figure 2.4. Abnormal matrix stiffness enhances monocyte-EC adhesion in the absence of pro-inflammatory cytokine. Fluorescently-labeled U937 cells were added (for 30 min) to unstimulated EC monolayers grown on different matrices for 2d. Quantification (average ± SEM; per mm^2) of adherent U937 cells from multiple ($n \geq 8$) images reveals the same biphasic trend in U937 cell-EC adhesion (***, $p<0.001$) as seen with TNF-α stimulation.

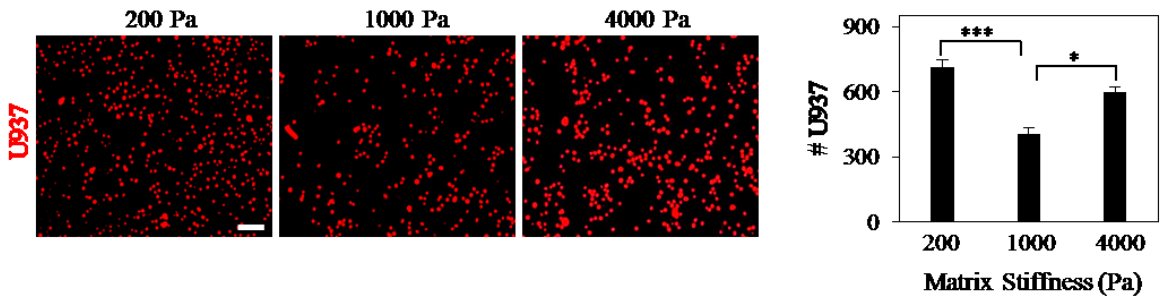

Figure 2.5. Human venous ECs also exhibit matrix stiffness-dependent biphasic regulation of monocyte-EC adhesion. Representative images show fluorescently-labeled U937 cells bound to TNF-α-stimulated HUVEC monolayers grown on synthetic matrices of varying stiffness for 2d. Scale bar: 100 μm. Quantification (average ± SEM ; per mm^2) of adherent U937 cells from multiple ($n \geq 8$) images reveals the same biphasic trend in U937 cell-EC adhesion as seen with microvascular ECs (HMEC-1) (*, $p<0.05$; ***, $p<0.001$).

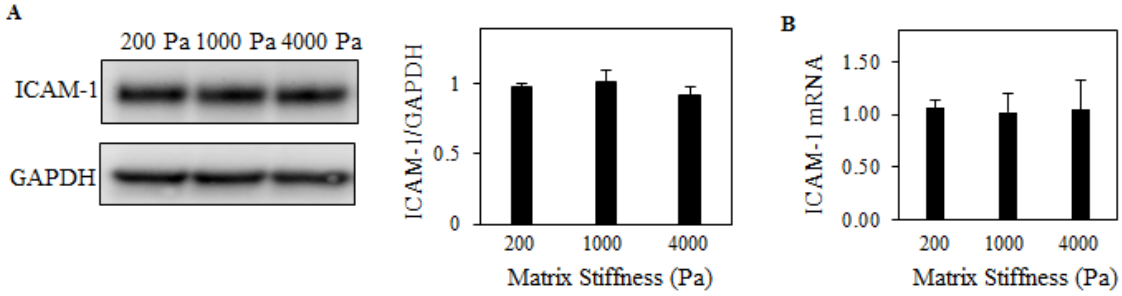

Figure 2.6. Effect of Matrix Stiffness on Endothelial ICAM-1 Expression. (A) ECs grown on the different matrices for 2d were subjected to Western Blotting for detection of ICAM-1 expression. Representative ICAM-1 protein bands (85 kDa) and their densitometric analysis (mean ± Std Dev) normalized to GAPDH (loading control) shows that matrix stiffness does not alter endothelial ICAM-1 expression in these short-term cultures. **(B)** qPCR analysis of ICAM-1 mRNA in short-term (2d) EC cultures confirms that ICAM-1 levels do not change in response to variations in matrix stiffness.

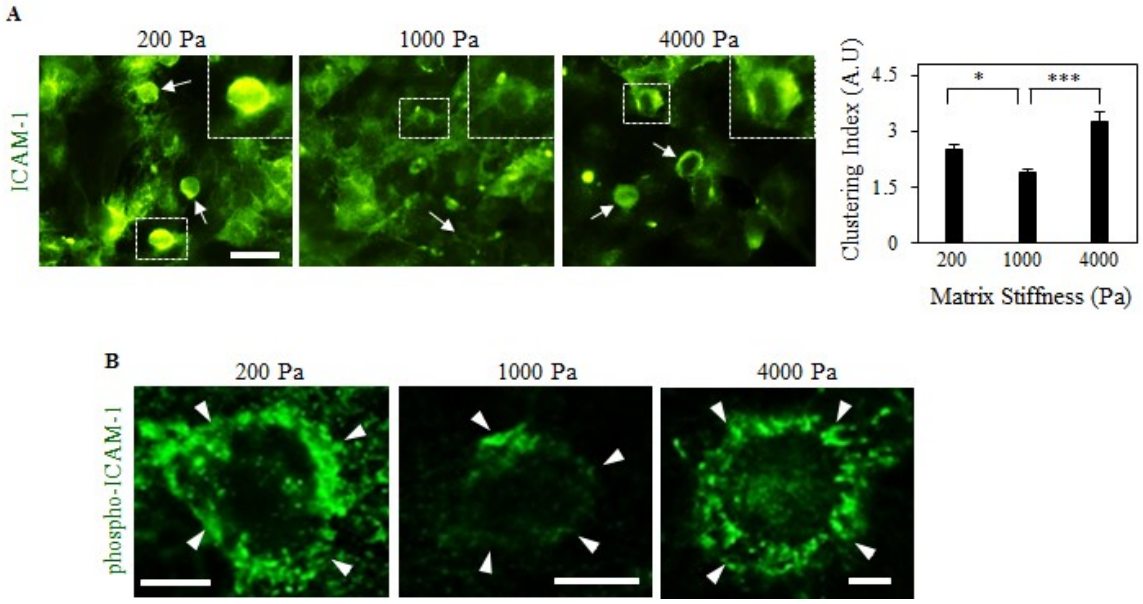

Figure 2.7. Aberrant Matrix Stiffness promotes ICAM-1 clustering. (A) U937-EC co-cultures were immunolabeled to visualize ICAM-1 clustering. Quantitative analysis of fluorescence intensity reveals that matrix softening and stiffening significantly increase endothelial ICAM-1clustering at sites of monocyte adhesions (indicated by arrows). *Inset* shows high magnification view of ICAM-1 clustering at a site of adherent monocyte (*, $p<0.05$; ***, $p<0.001$). Scale bar: 50 µm. **(B)** Confocal imaging of co-cultures immunolabeled with anti-phospho-ICAM-1 reveals that matrix softening and stiffening significantly enhance phospho-ICAM-1 clustering at sites of monocyte adhesions. Arrowheads indicate the outline of an adherent U937 cell. Scale bars: 5 µm.

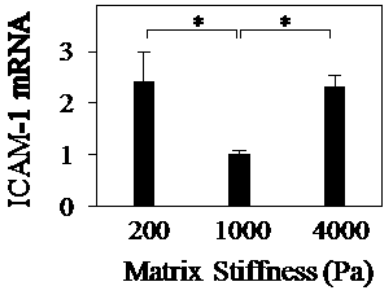

Figure 2.8. Effect of matrix stiffness on ICAM-1 expression in long-term (5d) EC cultures. qPCR analysis of ICAM-1 mRNA (three replicates/condition) shows that long-term (5d) culture of ECs on soft and stiff matrices leads to significant increase in ICAM-1 expression (*, $p<0.05$).

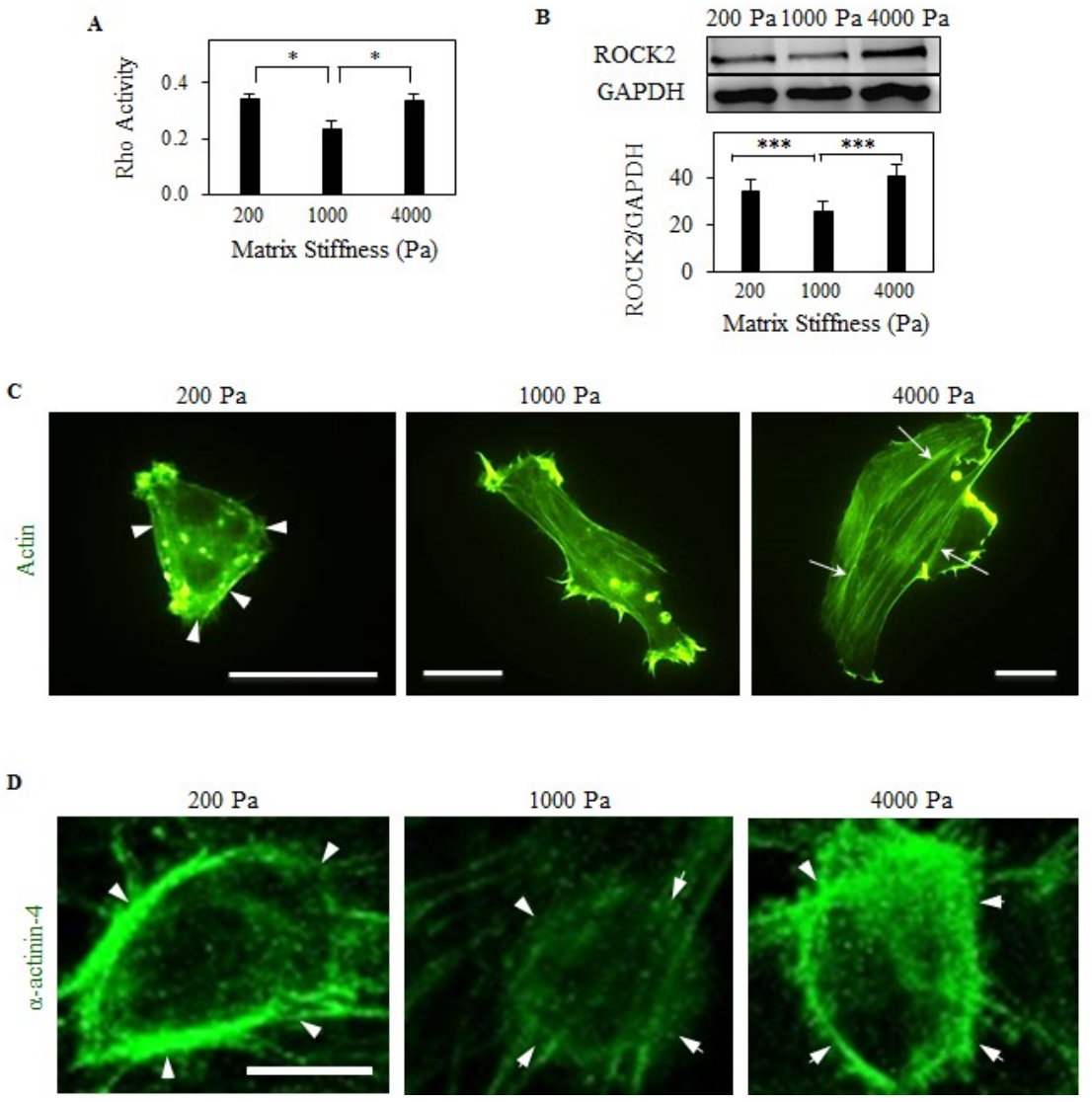
A
Rho Activity
0.4
0.2
0.0
*
*
200
1000
4000
Matrix Stiffness (Pa)
B
200 Pa 1000 Pa 4000 Pa
ROCK2
GAPDH
ROCK2/GAPDH
***
***
40
20
0
200
1000
4000
Matrix Stiffness (Pa)
C
200 Pa
1000 Pa
4000 Pa
Actin
D
200 Pa
1000 Pa
4000 Pa
α-actinin-4

Figure 2.9. Matrix stiffness biphasically regulates Rho/ROCK-mediated EC cytoskeletal organization. **(A)** ECs grown on different matrices were analyzed for Rho Activity using a Rho G-Lisa Activity kit. Quantitative analysis of Rho activity reveals that both soft (200 Pa) and stiff (4000 Pa) matrices elicit ~50% higher Rho activity when compared to normal (1000 Pa) matrix (*, $p<0.05$). **(B)** ROCK2 expression in ECs grown on matrices of different stiffness was determined by Western Blot. Representative protein bands (160 kDa) and their densitometric analysis (mean ± Std Dev) normalized to GAPDH (loading control) shows that ROCK2 expression on the different matrices follows the same biphasic trend as Rho activity (***, $p<0.001$). **(C)** Representative images of ECs labeled with phalloidin (to visualize actin) show that, when compared with cells grown on normal (1000 Pa) matrix, those grown on soft (200 Pa) matrix establish robust cortical actin network (arrowheads) while those on stiff (4000 Pa) matrix exhibit robust actin stress fibers (arrows). Scale bars: 50 μm. **(D)** U937-EC co-cultures were immunolabeled to visualize α-actinin-4 organization. Representative immunofluorescent images show increased recruitment of α-actinin-4 to sites of adherent U937 cells on soft and stiff matrices. Arrowheads indicate the outline of an adherent U937 cell. Scale bar: 10 μm.

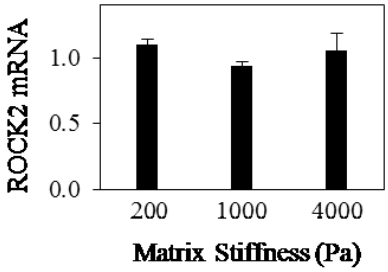

Figure 2.10. Effect of matrix stiffness on ROCK2 mRNA expression. qPCR analysis of ECs grown on different stiffness matrices (for 2d) shows that mRNA levels of ROCK2 follows the same biphasic trend as that exhibited by ROCK2 protein levels and Rho activity.

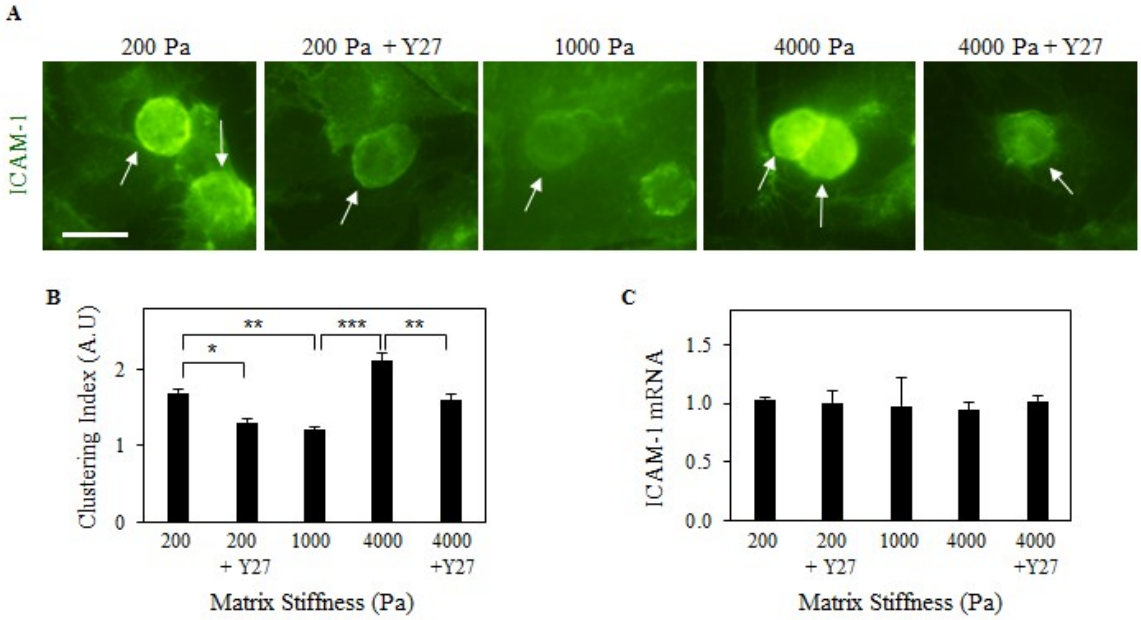
A
200 Pa
200 Pa + Y27
1000 Pa
4000 Pa
4000 Pa + Y27
ICAM-1
B
Clustering Index (A.U)
*
**
***
**
0
1
2
200
200 + Y27
1000
4000
4000 +Y27
Matrix Stiffness (Pa)
C
ICAM-1 mRNA
0.0
0.5
1.0
1.5
200
200 + Y27
1000
4000
4000 +Y27
Matrix Stiffness (Pa)
D
200 Pa
200 Pa + Y27
1000 Pa
4000 Pa
4000 Pa + Y27
phospho-ICAM-1
E
200 Pa
200 Pa + Y27
1000 Pa
4000 Pa
4000 Pa + Y27
α-actinin-4

Figure 2.11. Inhibition of endothelial Rho/ROCK blocks α-actinin-4-associated ICAM-1 clustering on abnormal matrix. (A) Representative images show anti-ICAM-1-labeled U937-EC co-cultures on different matrices following pre-treatment of ECs with or without ROCK inhibitor (Y27632). **(B)** Quantitative analysis of ICAM-1 fluorescence intensity from multiple sites of monocyte-EC adhesions (arrows) reveal that Rho/ROCK inhibition significantly blocks ICAM-1 clustering on soft and stiff matrices (*, $p<0.05$; **, $p<0.01$; ***, $p<0.001$). Scale bar: 25 μm. **(C)** qPCR analysis of ICAM-1 mRNA shows that Y27632 treatment does not alter ICAM-1 expression in short-term (2d) EC cultures. **(D, E)** U937-EC co-cultures were immunolabeled to visualize phospho-ICAM-1 and α-actinin-4. Representative confocal images show that increased phospho-ICAM-1 clustering **(D)** and α-actinin-4 recruitment **(E)** seen on the soft and stiff matrices was prevented by pretreating ECs with ROCK inhibitor (Y27632). Arrowheads indicate the outline of an adherent U937 cell. Scale bars: 5 μm **(D)**; 10 μm **(E)**.

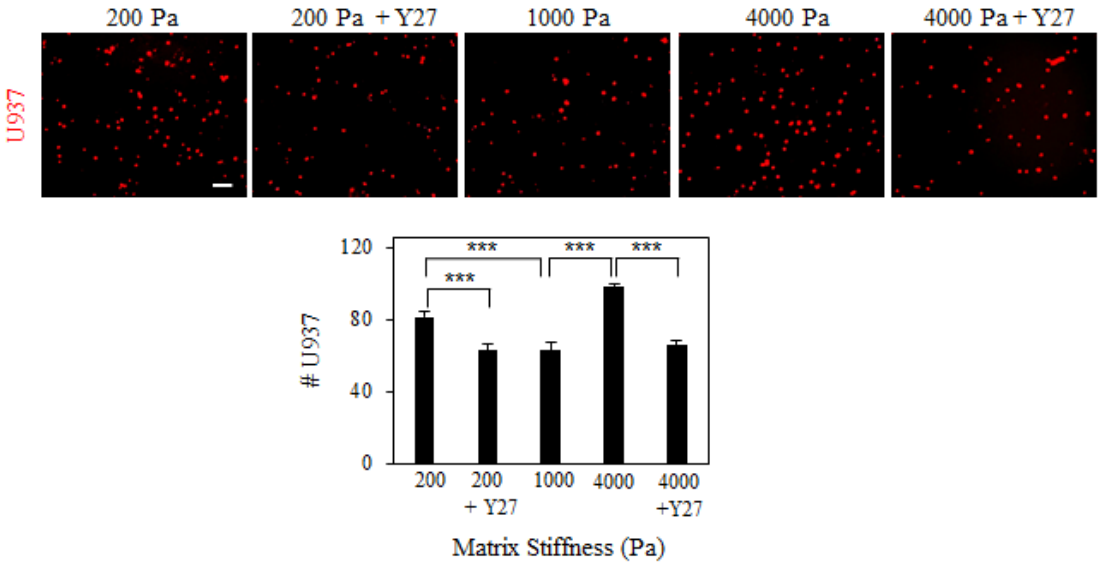

Figure 2.12. Rho/ROCK inhibition prevents the increase in monocyte-EC adhesion on abnormal matrices. Representative images show fluorescently-labeled U937 cells bound to EC monolayers pre-treated with or without Y27632 on matrices of varying stiffness. Scale bar: 100 μm. Quantification of adherent U937 cells (per mm^2) reveals that Rho/ROCK inhibition prevents the increase in EC adhesivity on soft and stiff matrices (***, $p<0.001$).

Chapter 3

Subendothelial Matrix Stiffening Promotes Vascular Inflammation via a TRPV4-Rho Axis

Preface

Studies performed in Chapter 2 showed that excessive subendothelial matrix stiffening or softening enhances monocyte-EC adhesion via an increase in Rho/ROCK-dependent ICAM-1 clustering. This Chapter aims to identify and characterize the upstream mechanotransduction pathway that mediates matrix stiffness-dependent control of endothelial adhesivity.

Figures 3.1-3.7

Introduction

Chronic inflammation contributes actively to the pathogenesis of diabetic vascular complications and cardiovascular disorders such as atherosclerosis.[17, 52] As of 2014, these conditions are known to affect over 45 million people in the US alone,[53] thus underscoring the need to curb inflammation. Historically, efforts to understand and regulate inflammation have focused on the identity and role of circulating and tissue-infiltrating leukocytes. However, increasing evidence now implicates vascular endothelial cell (EC) adhesivity as another critical determinant of inflammation as it promotes persistent leukocyte adhesion and infiltration.[16, 21]

Findings reported in Chapter 2 have revealed a previously-unknown role of matrix stiffness in EC adhesivity, as judged by increased ICAM-1 clustering and phosphorylation, and greater monocyte-EC adhesion on both very soft and stiff matrices. These effects of abnormal matrix stiffness were found to be mediated by increased Rho/ROCK activity. However, the upstream mechanotransduction pathway that mediates this Rho/ROCK-dependent control of EC adhesivity on abnormal matrices remains unknown.

Rho activity is endogenously inhibited by endothelium-derived nitric oxide (NO). Endothelial NO is produced by the constitutively active endothelial NO synthase (eNOS),[54, 55] whose expression and activity are significantly impaired at sites of chronic vascular inflammation. Indeed, loss of eNOS-derived NO has been shown to significantly enhance monocyte-EC binding. Together, these findings lead to the hypothesis that the loss of eNOS/NO by abnormal matrix stiffness leads to increased monocyte-EC binding associated with chronic vascular inflammation.

This hypothesis is supported by past findings that implicate mechanosensitive factors in the regulation of anti-inflammatory eNOS/NO.[56] Of particular relevance is the mechanosensitive Ca^{2+} channel Transient Receptor Potential Vanilloid (TRPV4). TRPV4 is a member of the transmembrane TRP family of Ca^{2+} channels that is ubiquitously expressed in ECs and known to enhance eNOS activation.[57, 58] Indeed, TRPV4 downregulation inhibits NO-dependent vasodilation[59] while inhibition of eNOS impairs the vasodilatory effects of TRPV4 stimulation.[58] Notably, endothelial TRPV4 can be mechanically activated by shear stress, osmotic pressure, and matrix-transmitted cyclic stretch;[59-61] however, whether matrix stiffness can independently regulate TRPV4 activity and/or expression is not known.

Using an ApoE-/- mouse model of atherosclerosis, a condition marked by chronic inflammation and stiffening of the aorta, here we identify a new mechanotransduction mechanism by which subendothelial matrix stiffening enhances monocyte-EC adhesion via loss of TRPV4-dependent eNOS/NO. This mechanical control of TRPV4 activity was further regulated by the activity of downstream Rho/ROCK, thus indicating the existence of a positive feedback loop that exacerbates matrix stiffening-dependent vascular inflammation. Finally, we show that pharmacological modulation of TRPV4 activity reverses the effects of matrix stiffness on EC adhesivity and monocyte-EC binding.

Materials and Methods

Animal Model. All animal studies were performed in compliance with IACUC protocols approved by UC, Riverside, and University of New Mexico. Adult (16 week-old) male

ApoE-/- mice on a C57BL6/J background (Jackson Labs) were euthanized prior to harvesting the heart. Mouse hearts were fixed and embedded in O.C.T embedding compound (Tissue Tek, Sakura FineTek) prior to freezing at -80°C. Wildtype C57BL6/J mice were used as control.

Measurement of Vascular Subendothelial Matrix Stiffness. 20 μm-thick cryosections of native aortas obtained from young adult (16-week old) ApoE-/- mice on a C57BL/6 background were subjected to stiffness measurements using a biological-grade atomic force microscope (AFM; Veeco Instruments, NY) operating in tapping mode. For these tissue measurements, a 5 μm diameter glass bead was attached to a 140 μm-long microcantilever (MLCT, Bruker) with bending spring constant of 0.1 N/m. The maximum indentation force applied to each sample was ~8 nN. Measurements were made in force-curve mode, and the cantilever deflection was measured through the photodiode difference signal (S_{def}, volts). For each region, 10 or more force curves were measured and only the linear region of force curves were considered for the analysis of subendothelial matrix stiffness. Sample stiffness was calculated as $k_{sample} = F/ z_s$, where F is the applied force and z_s the sample deformation. Average stiffness was obtained from indentations in at least 6 different subendothelial regions per aorta within 10 μm from the lumen.

Immunohistochemistry for CD11b Expression and Oil Red O. Aortas from ApoE-/- and wildtype mice were fixed in acetone and frozen (at -80°C) in optimum cutting temperature compound (O.C.T, TissueTek) prior to being cut into 5 μm thick sections.

Sections were then stained with anti-CD11b antibody followed by treatment with the chromagen 3,3-Diaminobenzidine (DAB) for 15 min. Sections were counterstained with hematoxylin. For oil red o (O.R.O), sections were immersed in 0.24% O.R.O solution in isopropanol for 25 min. Sections were then washed in 60% isopropanol until clear. Sections were counterstained with hematoxylin, treated with bluing reagent, and then treated with nuclear fast green (Sigma). Slides were dried at room temperature overnight before mounting.

Cell Culture. Human aortic endothelial cells (HAEC) were purchased from Cell Applications (CA) and grown on gelatin-coated culture dishes in medium composed of MCDB-131 basal medium (Life Technologies), 10% fetal bovine serum (FBS; Fisherbrand), 10 mM L-Glutamine (Life Technologies), 10 ng/mL epidermal growth factor (Millipore), 1 ug/ml hydrocortisone (Sigma), 4 ng/mL human basic fibroblast growth factor (Life Technologies), 100 ug/ml heparin sodium salt (Sigma) and 1x antibiotic/ antimycotic supplement (Life Technologies). Human monocytic U937 cells were obtained from ATCC and grown in suspension in medium composed of RPMI-1640 basal medium (Life Technologies), 10% FBS, 10 mM HEPES (Fisherbrand), 1 mM sodium pyruvate (Cellgro), 4.5 g/L glucose (Sigma), 2 mM L-Glutamine, 1500 mg/ml sodium bicarbonate (Sigma), and 1x antibiotic/antimycotic supplement. Mouse monocytic cells (Wehi274) were a gift from my collaborator, Dr. Reddy at City of Hope (Duarte, California). Mouse monocytes were cultured in low-glucose DMEM with 10% FBS and 1x antibiotic/antimycotic supplement.

Fabrication of Synthetic Polyacrylamide Matrices. Thin (~100 μm-thick), elastic matrices of varying stiffness were fabricated using crosslinked polyacrylamide (PA), as previously described.[2, 24, 25] Briefly, acrylamide and bis-acrylamide (crosslinker) solutions (BioRad) were mixed at different mass ratios, added onto glutaraldehyde-activated glass coverslips, and spread into a thin layer by placing a glass coverslip on top of the PA gel (for 15 min). The top coverslip was then peeled off and the resulting PA-based matrix was rinsed with HEPES buffer prior to surface modification with sulfo-SANPAH (Proteochem, Loves Park, Illinois USA) for covalent conjugation of human plasma fibronectin (3 ug/cm^2; Corning). Fibronectin (FN) was chosen as the cell-adhesive matrix protein because it is found abundantly at sites of chronic vascular inflammation.[26]

Monocyte-EC Adhesion Assay. EC plating on FN-coated matrices was adjusted to ensure that confluent monolayers were formed on all stiffness within 24h (three replicates/condition). Subsequently, confluent EC monolayers were serum-starved overnight in medium containing MCDB-131, 2.5% FBS and 1x antibiotic/antimycotic supplement (starvation medium) to induce EC quiescence. EC monolayers were then treated with or without TNF-α (25 ng/ml; Fisher) for 5h before addition of DAPI-labeled U937 cells or human CD14+ PBMs at 125k cells/cm^2 for 30 min at 37^{o}C. Next, endothelial monolayers were rinsed three times to remove non- or weakly-adhering monocytes and fixed in 1% paraformaldehyde (PFA; Electron Microscopy Sciences). Fluorescent images (n≥8) of adherent monocytes were taken using a Nikon Eclipse Ti microscope fitted with a Nikon Digital Sight DS-Qi1Mc camera and the cell count was obtained using ImageJ

(NIH). For some studies, cells were treated with GSK101790A (50 nM) 3 hr, RN1734 (25 μM) 5 hr, or Thrombin (0.25 Units/mL) 30 min prior to the assay.

Measurement of intracellular NO. ECs were plated on fibronectin-coated PA gels (in glass-bottom MatTek dish) at 15k cells/cm^2, cultured for 24h and serum-starved overnight prior to TNF-α (25 ng/ml) stimulation for 5h with or without addition of TRPV4 antagonist RN1734 (25 uM). Next, ECs were loaded with a NO-sensitive fluorescent dye DAF-FM diacetate (Life Technologies), as per manufacturer's protocol, and imaged live in Krebs-Henseleit Buffer (125 mM NaCl, 4.74 mM KCl, 2.5 mM $CaCl_2$, 1.2 mM KH_2PO_4, 1.2 mM $MgSO_4$, 5 mM $NaHCO_3$ and 10 mM Glucose (all reagents from Sigma) using Nikon Eclipse Ti epifluorescent microscope fitted with a Nikon Digital Sight DS-Qi1Mc camera. Levels of intracellular NO were quantified by measuring total fluorescence intensity using ImageJ (n>40 cells). For some studies, cells were treated with GSK101790A (50 nM) 3 hr, RN1734 (25 μM) 5 hr, or Thrombin (0.25 Units/mL) 30 min prior to the assay. For OxLDL studies, cells were treated with 20 μg/mL OxLDL for 5 days prior to assay.

IF staining for mouse endothelial TRPV4 and ROCK2. Aortic sections from ApoE-/- and wildtype mice were labeled with rabbit anti-TRPV4 (Alamone) or rabbit anti-ROCK2 (SantaCruz Biotech) primary antibody followed by conjugation with fluorescent anti-rabbit secondary antibody (Vector Labs). Immunostained samples were mounted using fluoromount and imaged using the aforementioned Nikon microscope.

Western Blot. Expression of endothelial p-eNOS, total eNOS and TRPV4 were determined by Western Blot. Briefly, confluent cells on matrices of varying stiffness (three replicates/condition) were lysed in RIPA buffer containing protease and phosphatase inhibitors, and the lysates were centrifuged to obtain protein supernatant. An equal amount of protein was loaded in 10% SDS–polyacrylamide gel and the separated proteins transferred onto a nitrocellulose membrane for detection with mouse anti-p-eNOS antibody or mouse anti-eNOS (BD Biosciences) or polyclonal rabbit anti-TRPV4 (Alamone) followed by detection with horseradish peroxidase (HRP)–conjugated secondary antibody (Vector Laboratories, Inc., Burlingame, CA). GAPDH (Sigma) was used as the loading control. Protein bands were visualized using a chemiluminescent detection kit (Thermo Scientific) coupled with a camera-based imaging system (Biospectrum AC Imaging System) while the densitometric analysis was performed by ImageJ software.

Calcium Microfluorometry. To measure TRPV4 activity subconfluent ECs grown on PA gels were loaded with Ca^{2+}-sensitive dye Fluo-4 AM (Invitrogen) in Ca^{2+} buffer (136 mM NaCl, 4.7 mM KCl, 1.2 mM $MgSO_4$, 1.1 mM $CaCl_2$, 1.2 mM KH_2PO_4, 5 mM $NaHCO_3$, 5.5 mM Glucose: Sigma, 20 mM HEPES), rinsed three times and recovered for 30 minutes in Ca^{2+} buffer. For studies where cells were pretreated with selective TRPV4 antagonist RN1734 (25 uM) or agonist GSK1016790A (50 nM) prior to dye loading, these agents were also added during the 30 min recovery period. To detect TRPV4 activity, time-lapse images (n=3) of dye-loaded cells ($n \geq 50$) were acquired every 3 sec for 1 min before addition of selective TRPV4 agonist GSK1016790A (300 nM; Sigma-Aldrich), followed

by time-lapse imaging for an additional 5 min. For studies looking at the long-term effect of TRPV4 agonist GSK1016790A, dye-loaded cells were imaged for 1 min in Ca^{2+}-free buffer followed by addition of 2.2 mM Ca^{2+} buffer (to facilitate Ca^{2+} influx). Intracellular Ca^{2+} was quantified by measuring net intracellular fluorescence intensity (using ImageJ), as previously described.[60] For OxLDL studies, cells were treated with 20 μg/mL OxLDL for 5 days prior to assay.

Rho Activity. Confluent EC monolayers grown on 1000 Pa (normal), and 4000 Pa and 10000 Pa (stiff) matrices for 24h were starved overnight prior to measurement of Rho activity using a Rho G-Lisa Activity kit (Cytoskeleton Inc., Denver, CO, USA), as per manufacturer's protocol (three replicates/condition). Briefly, cell lysates were collected, measured for total protein concentration, and mixed with binding buffer (1:1) before adding to the assay plate. Surface-bound samples were then labeled with anti-RhoA primary antibody followed by a HRP-conjugated secondary antibody. Samples were incubated with the provided stop buffer prior to fluorescence detection with a Victor 2 plate reader (Perkin Elmer, Waltham, MA, USA).

Quantitative RT PCR for ROCK2. Total RNA was isolated from Confluent EC monolayers grown on 1000 Pa (normal), and 4000 Pa and 10000 Pa (stiff) matrices using Direct-zol RNA MiniPrep (Zymo Research, Irvine, CA, USA). cDNA was made from the RNA with High Capacity cDNA Reverse Transcription (Thermo Fisher–Applied Biosystems), and amplified with the appropriate TaqMan assay for commercially available

primers for ROCK2 (HS00178154 M1; Thermo Fisher–Applied Biosystems) on the CFX Connect96 system (Bio-Rad). Relative mRNA levels were determined by the comparative cycle threshold method with normalization to GAPDH (HS02758991 G1; Thermo Fisher–Applied Biosystems).

Statistics. All data were obtained from multiples cells or images and from multiple replicates/condition (as indicated in each respective section) and, unless otherwise reported, expressed as mean ± standard error (SEM). Statistical significance was determined using analysis of variance (ANOVA; InStat; Graphpad Software Inc.) followed by Tukey post-hoc analysis. Results were considered significance if $p<0.05$.

Results

Inflammation of the aorta in ApoE-/- mice correlates with increased subendothelial matrix stiffness

To test our working hypothesis, we first measured the subendothelial matrix stiffness of aortas isolated from wildtype and atherosclerotic (ApoE-/-) mice. AFM measurements revealed that the aortas of ApoE-/- mice exhibit three-fold higher ($p<0.001$) subendothelial matrix stiffness than those of the age-matched wild type mice (Fig. 3.1A). Predictably, subendothelial matrix stiffening of the aorta correlated strongly with the accumulation of monocytes and lipid-rich plaques within the aorta of ApoE-/- mice, as indicated by $CD11b^{+}$ and oil red o staining, respectively (Fig. 3.1B). Consistent with our

in vivo observations, HAECs grown on 4000 Pa (stiff) matrices exhibited a two-fold increase ($p<0001$) in U937 monocytic cell adhesion when compared with those grown on the 1000 Pa (normal) matrix (Fig. 3.1C). The stiffness values of synthetic matrices reflect our measurements of aortic subendothelial matrix stiffness and are consistent with past measurements reported by others.[1, 22, 62] Together, these observations indicate that increased subendothelial matrix stiffness contributes to monocyte-EC adhesion in chronic vascular inflammation associated with atherosclerosis.

Inflammation of the ApoE-/- aorta is associated with higher endothelial Rho/ROCK

We have previously shown that microvascular ECs grown on stiffer matrices exhibit higher Rho/ROCK activity, which leads to greater ICAM-1 clustering and monocyte-EC adhesion. Thus, we looked to see whether the increased accumulation of $CD11b^+$ monocytes within stiffer ApoE-/- aortas and greater monocyte-EC adhesion on stiffer synthetic matrices *in vitro* are also associated with higher Rho/ROCK. Immunostaining of aortas revealed a markedly higher expression of ROCK2 in the endothelium of ApoE-/- aortas than those of their wild type counterparts (Fig. 3.2A). That the observed increase in ROCK-2 expression in ECs of ApoE-/- aortas resulted from the stiffer subendothelial matrix was confirmed when HAECs cultured on the stiff synthetic matrix exhibited an ~75% increase ($p<0.001$) in Rho activity when compared with their levels on normal matrix (Fig. 3.2B). This significant increase in Rho activity on stiff matrix led to a concomitant increase in the mRNA expression of its downstream target ROCK2, the isoform of ROCK that enhances myosin-dependent cytoskeletal tension[39] (Fig. 3.2C).

Subendothelial matrix stiffening impairs eNOS/NO in HAECs

To test the hypothesis that matrix stiffening enhances Rho/ROCK via impairment of eNOS/NO, an endogenous Rho inhibitor, ApoE-/- aortic sections were immunolabeled for p-eNOS. While wildtype mouse endothelium exhibited high levels of p-eNOS (white arrows), ApoE-/- endothelium had very low levels of endothelial p-eNOS (Fig. 3.3A). To confirm this trend in vitro, HAECs grown on normal and stiff matrices were subjected to immunoblotting for measurement of active and total levels of eNOS. Our Western Blot analysis revealed that an increase in matrix stiffness causes a significant decrease ($p<0.001$) in eNOS activity (phosphorylation) (Fig. 3.3B). This inhibitory effect of matrix stiffening on eNOS activity caused an ~50% inhibition ($p<0.01$) in intracellular NO production by HAECs grown on the stiff matrix, as independently confirmed by intracellular labeling with a NO-sensitive dye (DAF-FM diacetate) (Fig. 3.3C).

Matrix stiffening suppresses Endothelial TRPV4 activity

To elucidate the mechanosensitive mechanism underlying matrix stiffness-dependent control of eNOS/NO, we explored the role of mechanosensitive TRPV4 Ca^{2+} channel. The rationale for focusing on TRPV4 were two-fold: firstly, endothelial TRPV4 has been shown to be activated by mechanical forces such as matrix-transmitted cyclic stretch, shear stress, and osmotic pressure[61] and secondly, TRPV4 activation leads to increase in eNOS-dependent NO production.[58, 63]

Importantly, mouse aortas from wildtype and ApoE-/- mice labeled for TRPV4 showed ApoE-/- mice exhibit much lower levels of TRPV4 expression (indicated by white

arrows) compared to wildtype (Fig. 3.4A). Using Western Blot, we first showed that matrix stiffening suppresses TRPV4 expression (Fig. 3.4B). To determine TRPV4 activity, ECs grown on the normal and stiff matrices were loaded with Ca^{2+}-sensitive Fluo-4/AM dye and Ca^{2+} influx was recorded in response to a selective TRPV4 agonist GSK1016790A. Ca^{2+} microfluorometry is widely used to measure TRPV4 activity because, as we and others have reported before, constitutive TRPV4-like currents in primary ECs are small, transient, and difficult to characterize.[60, 64] As shown in Fig. 3.4C, ECs grown on stiff (4000 Pa) matrices exhibit ~50% reduction ($p<0.001$) in GSK1016790A-stimulated Ca^{2+} influx than those grown on normal (1000 Pa) matrix. This data indicates that aberrant matrix stiffness significantly impairs endothelial TPRV4 activity.

Matrix stiffening exerts comparable effects as oxidized LDL on HAECs

In the pathogenesis of atherosclerosis, matrix stiffening is one component of numerous key factors at play. One major contributor is low-density lipoproteins (LDL) or, more specifically, oxidized LDL (oxLDL). LDL in its many forms stimulates ECs to produce monocyte chemotactic protein-1 which recruits monocytes to the site of inflammation thereby furthering the pathogenesis.[65] Here I wanted to determine the predominant role of matrix stiffening in atherosclerosis and whether there existed cooperative effects with the presence of oxLDL. To do this, ECs grown on normal and stiff matrices were treated without/with oxLDL (20 μg/mL) for 5 days prior to analysis for TRPV4 expression and activity, and intracellular NO. Studies showed oxLDL treatment significantly inhibited TRPV4 expression on normal matrix stiffness, but had minimal

additional effect on stiff matrices (Fig. 3.5A). Further, this alteration in expression was mirrored in TRPV4 activity (Fig. 3.5B). Finally, treatment with oxLDL corresponded to a significant reduction in intracellular NO on normal matrix but minimal effects on stiff matrices (Fig. 3.5C). This data indicates that matrix stiffness is as potent, if not even more influential, a factor in atherosclerosis progression.

Modulation of TRPV4 activity reverses the effect of matrix stiffness on monocyte-EC adhesion

To confirm the role of TRPV4 in matrix stiffness-dependent EC adhesivity and monocyte-EC adhesion, we first treated ECs grown on normal (1000 Pa) matrix with a selective TRPV4 inhibitor RN1734 and measured TRPV4 activity, intracellular NO and monocyte-EC adhesion. As shown in Fig. 3.6A, pharmacological inhibition of TRPV4 activity caused a ~65% reduction ($p<0.001$) in Ca^{2+} influx as well as baseline Ca^{2+} levels. Consistent with past findings that TRPV4 activation enhances endothelial NO production [58], loss of TRPV4 activity produced an approximately 60% decrease ($p<0.001$) in intracellular NO levels (Fig. 3.6B). Notably, this marked suppression of endothelial NO production by TRPV4 inhibition resulted in a concomitant 2.1-fold increase ($p<0.001$) in U937 cell-EC adhesion (Fig. 3.6C). These data imply that endothelial TRPV4 activation is essential for maintenance of EC quiescence and reduced monocyte-EC binding. If so, then, conversely, pharmacological activation of TRPV4 in ECs grown on stiff (4000 Pa) matrices, which exhibit impaired TRPV4 activity, should suppress monocyte-EC adhesion.

To confirm this, we treated ECs grown on stiff matrices with a selective TRPV4 agonist GSK1016790A and examined monocyte-EC adhesion. Long-term (3h) treatment with GSK1016790A led to sustained TRPV4 activation, as demonstrated by a 2.3-fold increase ($p<0.001$) in Ca^{2+} influx in ECs on stiff matrices (Fig. 3.7A). This increase in TRPV4 corresponded to a significant increase of intracellular NO (Fig. 3.7B).

Since TRPV4 activation (by GSK1016790A) enhanced eNOS/NO, an endogenous Rho inhibitor, we asked whether GSK1016790A treatment caused inhibition of Rho activity. To do this, cells plated on stiff matrices were treated with TRPV4 selective agonist GSK1016790A for 3hr. Measurement of Rho activity revealed that pharmacological TRPV4 activation leads to significant ($p<0.001$) suppression of Rho activity on stiff matrices (Fig. 3.7C). Given the important role of Rho activity in enhancing ICAM-1 clustering and monocyte-EC adhesion on stiff matrices,[62] we predictably observed a significant decrease (45% reduction; $p<0.001$) in monocyte adhesion to GSK1016790A-treated HAECs on stiff matrices (Fig. 3.7D).

Discussion

Monocyte adhesion to NO-deficient endothelium is a hallmark of chronic vascular inflammation. Past studies aimed at elucidating the mechanisms underlying endothelial NO production and adhesivity have revealed an important role of abnormal soluble, genetic and hemodynamic factors. Our findings are the first to reveal that matrix stiffness also regulates NO-dependent monocyte-EC adhesion in a manner that is mediated by

differential activation of the mechanosensitive TRPV4 Ca^{2+} channel which is further regulated through the canonical mechanotransducer Rho/ROCK. Since many chronic inflammatory conditions such as atherosclerosis, diabetes, and emphysema are characterized by aberrant subendothelial matrix stiffness,[1, 44, 66, 67] these findings point towards the existence of a complex *mechanochemical* mechanism that drives chronic vascular inflammation.

Matrix stiffness is emerging as a key determinant of vascular development and disease. This is because alterations in matrix stiffness activate distinct mechanotransduction pathways that control EC biochemistry and function. For instance, suboptimal matrix stiffness has been shown to impair vascular endothelial growth factor (VEGF) receptor signaling and angiogenesis,[10] disrupt endothelial barrier function,[10, 22] and promote choriocapillaris degeneration associated with age-related macular degeneration.[5] By demonstrating that matrix stiffness also governs endothelial adhesivity, our current work extends the implications of matrix-dependent mechanical cues to vascular inflammation. Notably, leukocyte-endothelial adhesion is a key prerequisite for leukocyte infiltration into tissues. Thus, our new findings also complement and consolidate recent studies that have identified cell contractility and matrix stiffening as critical determinants of leukocyte transmigration across the endothelium.[15, 20, 22, 36] Given that important risk factors for inflammation viz. aging, diabetes, smoking, and endotoxin (sepsis), are associated with aberrant matrix stiffness,[5, 11, 22, 44] findings from our studies advocate the need to examine the contribution of matrix stiffness in excessive monocyte-EC adhesion associated with these inflammatory conditions. We specifically show that matrix stiffening

promotes monocyte-EC adhesion while the normal stiffness sustains endothelial quiescence. This trend indicates that any alteration in normal subendothelial matrix stiffness is perceived as a divergence from normal homeostasis, which predictably triggers a spontaneous inflammatory response mediated by the endothelium.

Chronic vascular inflammation is commonly associated with decreased bioavailability of eNOS-derived NO, a key anti-inflammatory factor that suppresses the expression and clustering of endothelial CAMs that mediate leukocyte-endothelial binding. [32] eNOS expression and activity are known to be sensitive to both inflammatory cytokines such as tumor necrosis factor-α (TNF-α) and disturbed flow characteristic of atheroprone sites.[32, 56] Our studies demonstrate that matrix stiffening also decrease eNOS phosphorylation and NO production, thereby implicating matrix stiffness as a key regulator of eNOS-dependent monocyte-EC adhesion.

To elucidate the mechanism underlying matrix stiffness-dependent monocyte-EC adhesion, we looked at the role of mechanosensitive TRPV4 Ca^{2+} channel. We focused on endothelial TRPV4 because firstly, it has been shown to be activated by physical cues such as osmotic pressure, shear stress, and matrix-transmitted cyclic stretch,[60, 61] and secondly, its activation enhances Ca^{2+}/Calmodulin-dependent eNOS activity and NO production.[58, 59] Further, although other TRP channels viz. TRPV2 and TRPC1 have been shown to exhibit stretch-induced Ca^{2+} influx when overexpressed in CHO cells and oocytes,[68, 69] inhibition of their constitutive expression in ECs causes no loss of stretch sensitivity,[60] thereby implicating TRPV4 as the predominant mechanosensitive TRP channel in ECs. Our current findings throw further light on the mechanosensitive nature of TRPV4 by

revealing that matrix stiffening suppresses TRPV4 activity and TRPV4 expression. Given this potent effect of aberrant matrix stiffness on TRPV4 activity, it is plausible that the loss of TRPV4 activity observed in mesenteric and retinal ECs of diabetic rats[66, 67] results, at least in part, from the diabetes-induced increase in subendothelial matrix stiffness.[44]

In the present study, suppressed TRPV4 activity on stiff matrices correlated directly with eNOS/NO levels and inversely with monocyte-EC adhesion. Since endothelial TRPV4 activation causes NO-dependent vasodilation in response to shear stress,[58] we looked to see whether endothelial TRPV4 activation also leads to NO-dependent control of monocyte-EC adhesion. Indeed, pharmacological inhibition of endothelial TRPV4 activity on normal matrices suppressed NO production and increased monocyte-EC adhesion while, conversely, enhancement of TRPV4 activity stiff matrices decreased monocyte-EC adhesion. Together, these new findings confirm that loss of TRPV4 activity contributes greatly to matrix stiffness-dependent mechanical control of monocyte-EC adhesion. Further, these findings also indicate a likely causal relationship between TRPV4 downregulation and basement membrane stiffening-dependent EC adhesivity observed in diabetic retinopathy,[44, 67] thereby implicating TRPV4 as a potential therapeutic target for anti-inflammatory strategies. However, care must be taken with systemic activation of TRPV4 because, as others have reported[70] and we here confirm, treatment of 'normal' ECs, which already have high endogenous TRPV4 activity, with TRPV4 agonist GSK1016790A leads to endothelial dysfunction. The exact mechanism underlying the detrimental effects of excessive GSK1016790A stimulation has, however, yet to be identified.

While these new findings reveal a hitherto unknown and pivotal mechanism by which aberrant matrix stiffness promotes monocyte-EC adhesion, they also raise several important questions that merit further examination. For instance, precisely how matrix stiffness regulates TRPV4 activity is yet to be determined. Further, although our two-day culture studies revealed that changes in TRPV4 activity are independent of changes in its expression, past studies have shown ECs from diabetic vessels, with stiffer basement membrane,[44] exhibit impaired TRPV4 expression.[66, 67] In conjunction with our data showing the same trend in atherosclerotic vessels, this raises the question whether alterations in TRPV4 expression requires cooperative effects of biochemical factors (e.g. high glucose) and aberrant matrix stiffness-dependent mechanical cues. Finally, it will be interesting, and perhaps important, to assess the extent to which TRPV4 contributes to disease pathogenesis. Addressing these questions will not only deepen our understanding of the role of TRPV4 in vascular mechanobiology but also likely lead to the development of new anti-inflammatory therapies aimed at normalizing endothelial TRPV4.

Figures

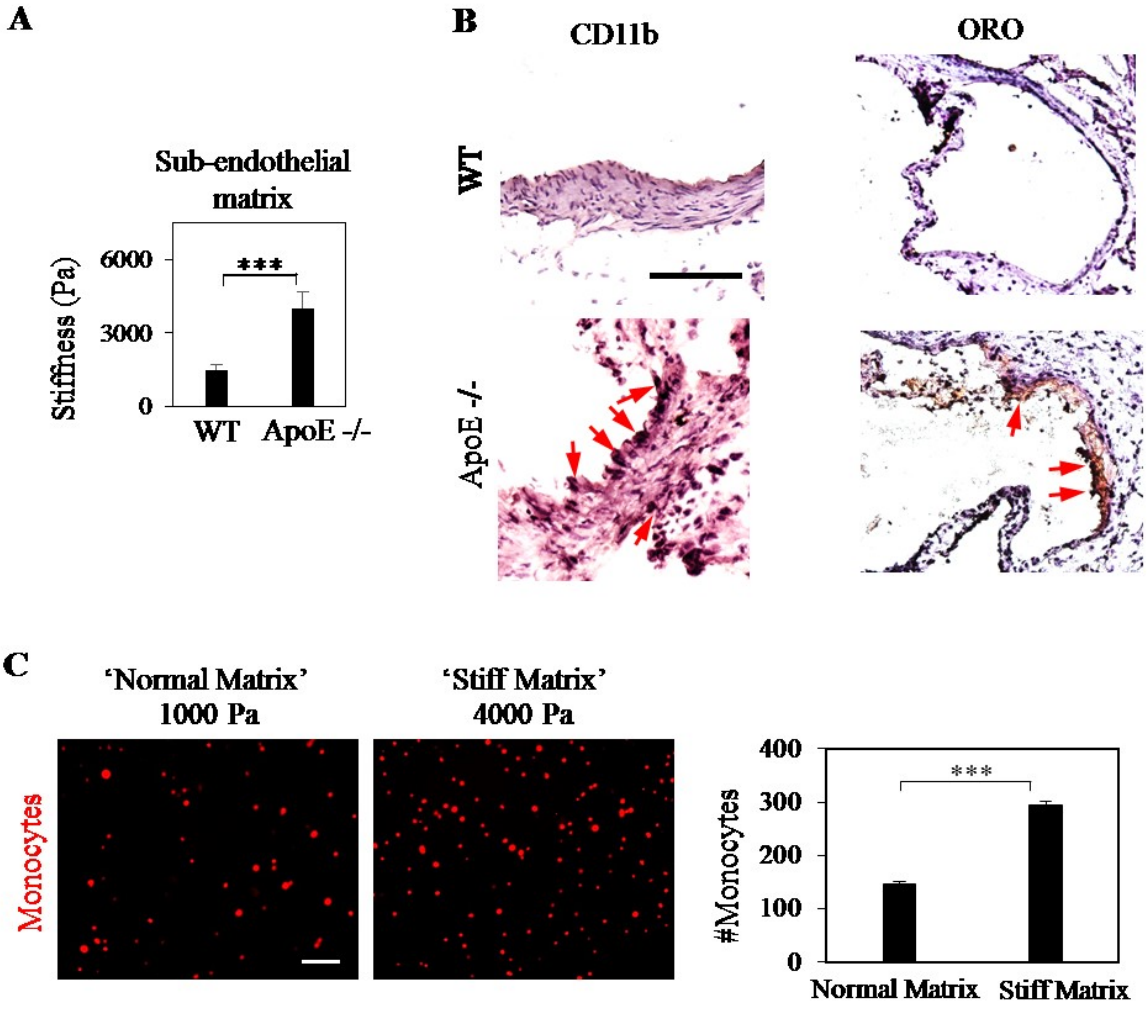
A
Sub-endothelial matrix
Stiffness (Pa)
6000
3000
0
***
WT
ApoE -/-
B
CD11b
ORO
WT
ApoE -/-
C
'Normal Matrix'
1000 Pa
'Stiff Matrix'
4000 Pa
Monocytes
#Monocytes
400
300
200
100
0
***
Normal Matrix
Stiff Matrix

Figure 3.1. Inflammation of the aorta in ApoE-/- mice correlates with increased subendothelial matrix stiffness. (A) Atomic force microscopy measurements of atherosclerotic and wildtype mouse aorta cross-sections were made at the subendothelial region of the tissue. Quantification (average ± SEM) of these measurements revealed atherosclerotic mice exhibit significantly (***, $p<0.001$) increased subendothelial matrix stiffness. **(B)** Representative images of aortic cross-sections labeled for monocytic cell marker CD11b show increased monocyte accumulation in atherosclerotic aorta compared to wildtype. Representative aortic cross-sections stained with O.R.O confirm development of atherosclerotic lesions in ApoE-/- mice. **(C)** Representative images show fluorescently-labeled U937 cells bound to endothelial monolayers cultured on 1000 Pa (normal) and 4000 Pa (stiff) matrices. Quantification of adherent U937 cells (per mm^2) reveal matrix stiffening significantly enhances U937-EC adhesion (***, $p<0.001$).

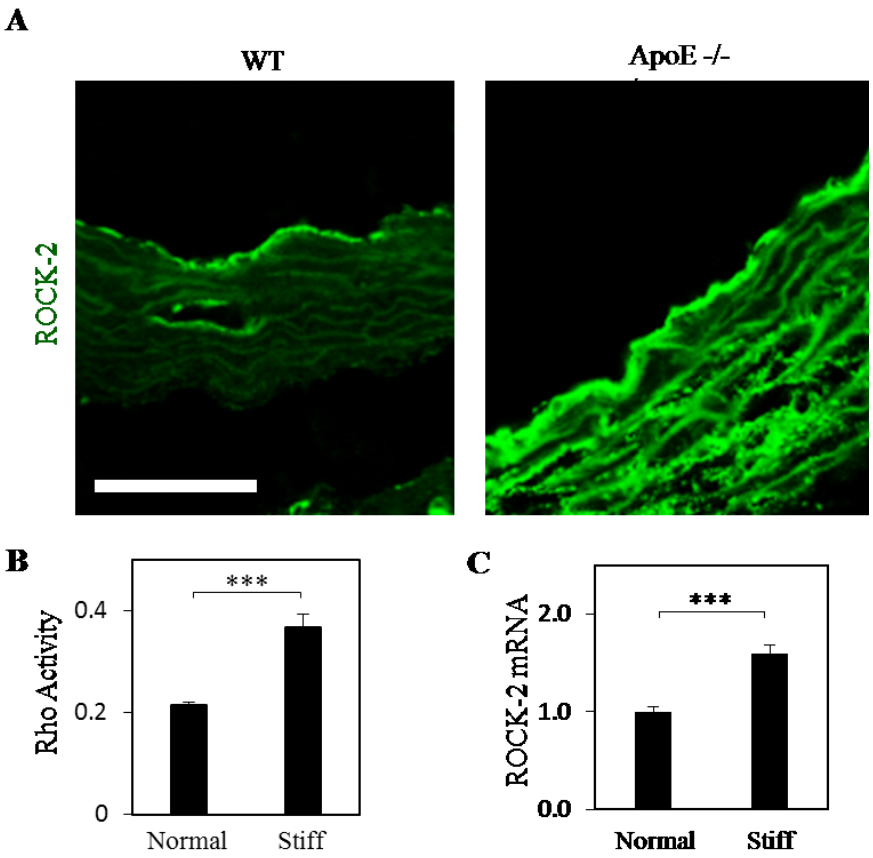

Figure 3.2. Atherosclerotic-associated matrix stiffening enhances Rho and ROCK2. **(A)** Representative images of aortic cross-sections labeled with anti-ROCK2 antibody depict ApoE-/- mice having greater endothelial ROCK-2 expression. Scale bar: 25 µm. **(B)** ECs grown on normal and stiff matrices were analyzed for Rho Activity using a Rho G-Lisa Activity kit. Quantitative analysis of Rho activity reveals that stiff (4000 Pa) matrices elicit ~60% or higher Rho activity when compared to normal (1000 Pa) matrix (***, $p<0.001$). **(C)** ROCK2 mRNA expression in ECs grown on matrices of increasing stiffness was determined by qPCR. Analysis of ROCK2 normalized to GAPDH (loading control) shows that ROCK2 mRNA expression follows the same trend as Rho activity (***, $p<0.001$).

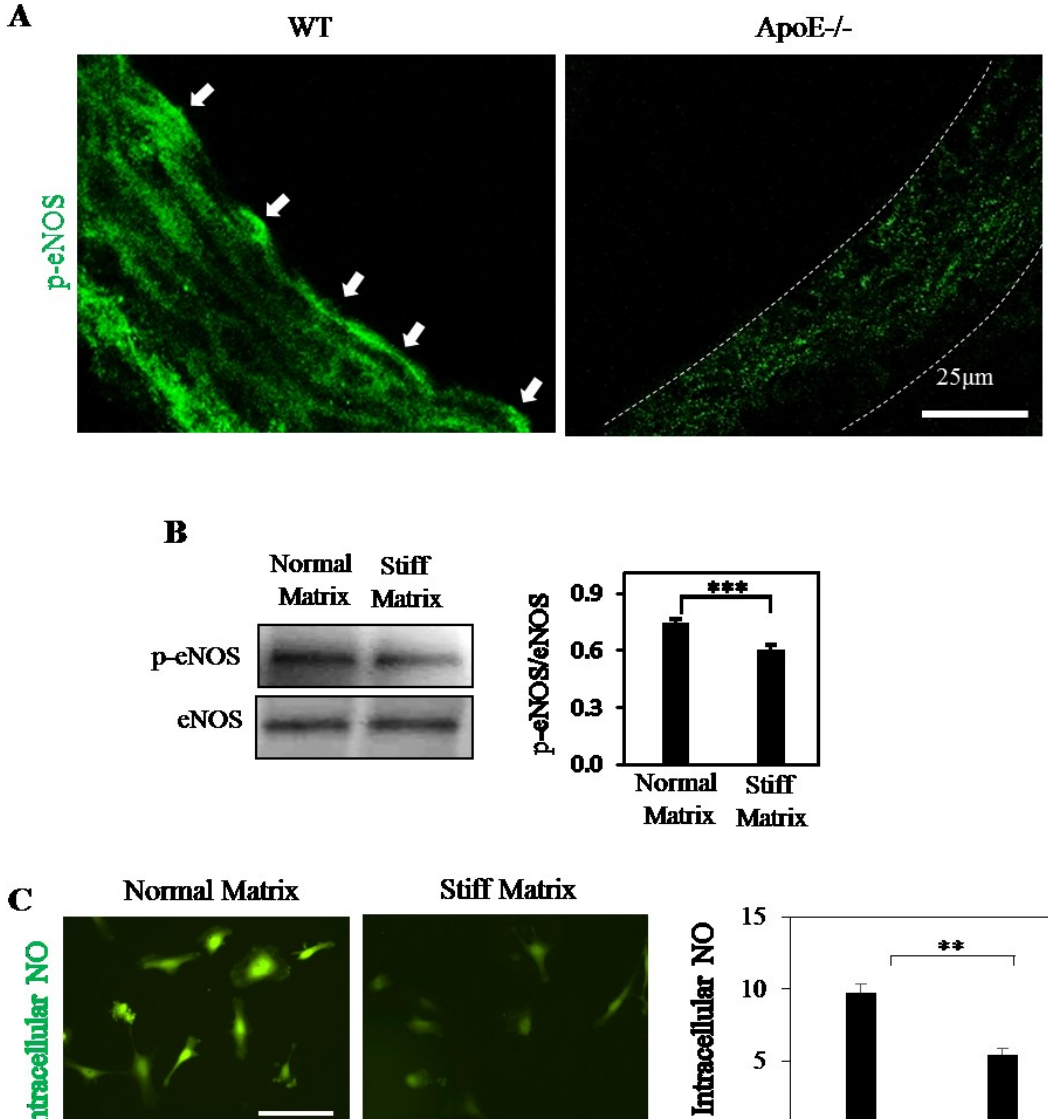
A
WT
ApoE-/-
p-eNOS
25μm
B
Normal Matrix
Stiff Matrix
p-eNOS
eNOS
p-eNOS/eNOS
0.9
0.6
0.3
0.0
***
Normal Matrix
Stiff Matrix
C
Normal Matrix
Stiff Matrix
Intracellular NO
Intracellular NO
15
10
5
0
**
Normal Matrix
Stiff Matrix

Figure 3.3. Matrix stiffening promotes monocyte-EC adhesion by suppressing eNOS-mediated NO. (A) Representative images of aortic cross-sections labeled with anti-phospho-eNOS antibody show ApoE-/- mice exhibit clear reduction in endothelial phospho-eNOS expression (p-eNOS indicated by white arrows). Scale bar: 25 μm. **(B)** Western Blot bands and their densitometric analysis show matrix stiffening also significantly (***, $p<0.001$) suppresses eNOS phosphorylation (normalized to total eNOS). **(C)** ECs were labeled with DAF-FM diacetate to measure intracellular NO. Representative fluorescent images and subsequent intensity measurements from multiple ($n\geq20$) cells reveal matrix stiffening significantly (**, $p<0.01$) suppresses intracellular NO. Scale bar: 100 μm.

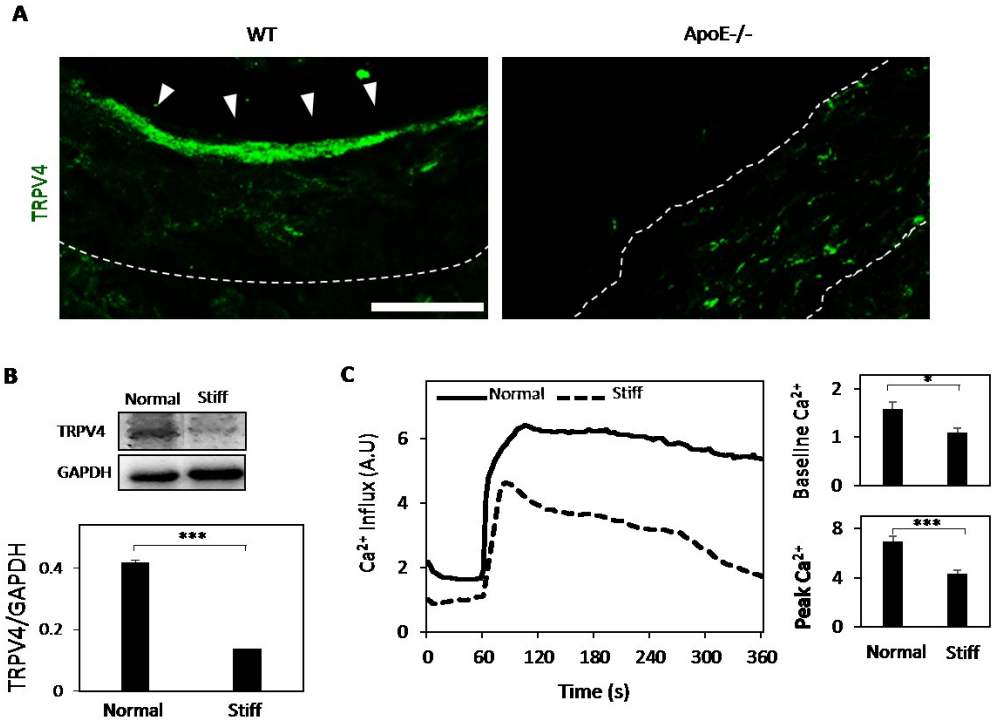

Figure 3.4. Matrix stiffening suppresses TRPV4 activity and expression. **(A)** Representative images of aortic cross-sections labeled with anti-TRPV4 antibody show ApoE-/- mice exhibit clear reduction in endothelial TRPV4 expression. Scale bar: 25 μm. **(B)** ECs grown on the different matrices were subjected to Western Blotting for levels of TRPV4 expression. Densitometric analysis (bar graph) normalized to GAPDH (loading control) showed that matrix stiffening significantly (***, $p<0.001$) reduced TRPV4 expression. **(C)** Calcium microfluorometry was performed in Fluo4-AM-loaded ECs grown on matrices of varying stiffness. Line graph from a representative cell and bar graph (average ± SEM) from multiple ($n\geq50$) cells reveal that matrix stiffening causes a significant impairment in TRPV4-dependent Ca^{2+} influx. Arrow indicates the moment selective TRPV4 agonist GSK1016790A was added to cells (*, $p<0.05$; **, $p<0.01$ and ***, $p<0.001$).

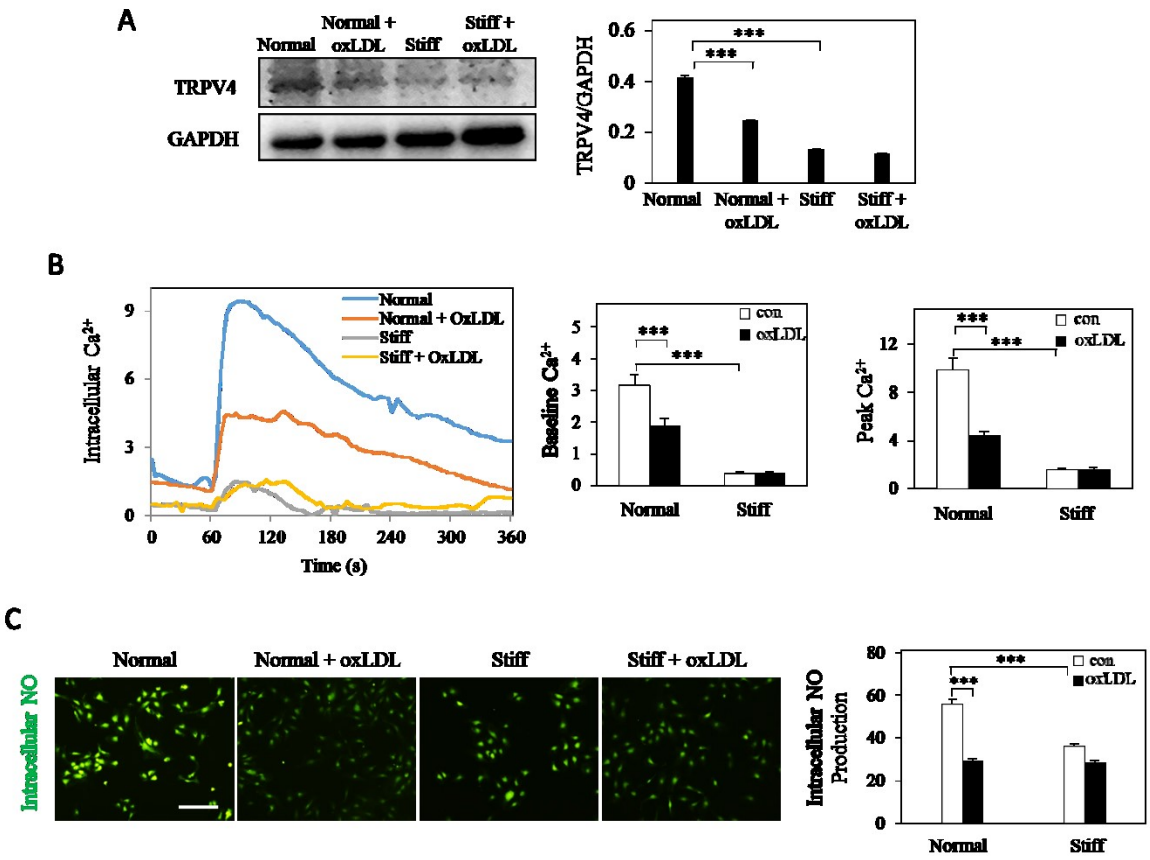
A
Normal
Normal + oxLDL
Stiff
Stiff + oxLDL
TRPV4
GAPDH
TRPV4/GAPDH
0.6
0.4
0.2
0
***
***
Normal
Normal + oxLDL
Stiff
Stiff + oxLDL
B
Intracellular Ca2+
9
6
3
0
0
60
120
180
240
300
360
Time (s)
Normal
Normal + OxLDL
Stiff
Stiff + OxLDL
Baseline Ca2+
5
4
3
2
1
0
con
oxLDL
***
***
Normal
Stiff
Peak Ca2+
12
8
4
0
con
oxLDL
***
***
Normal
Stiff
C
Intracellular NO
Normal
Normal + oxLDL
Stiff
Stiff + oxLDL
Intracellular NO Production
80
60
40
20
0
con
oxLDL
***
***
Normal
Stiff

Figure 3.5. Matrix stiffening exerts comparable effects to oxidized LDL on HAECs. **(A)** ECs grown on normal and stiff matrices were treated without/with OxLDL (20 μg/mL) for 5 days prior to collecting lysates for Western Blot. Western Blot bands and their densitometric analysis review oxLDL treatment suppresses TRPV4 expression on normal stiffness but has minimal cooperative effects on stiff matrices. **(B)** Calcium microfluorometry was performed in Fluo4-AM-loaded ECs. Line graph from a representative cell and bar graphs (average ± SEM) from multiple ($n \geq 50$) cells reveal that oxLDL causes a significant impairment in TRPV4-dependent Ca^{2+} influx on normal matrices but minimal effects on stiff matrices. (***, $p<0.001$). **(C)** ECs were labeled with DAF-FM diacetate to measure intracellular NO. Representative fluorescent images and subsequent intensity measurements from multiple ($n \geq 20$) cells reveal oxLDL significantly (***, $p<0.001$) suppresses intracellular NO on normal matrices but has minimal cooperative effect on stiff matrices. Scale bar: 100 μm.

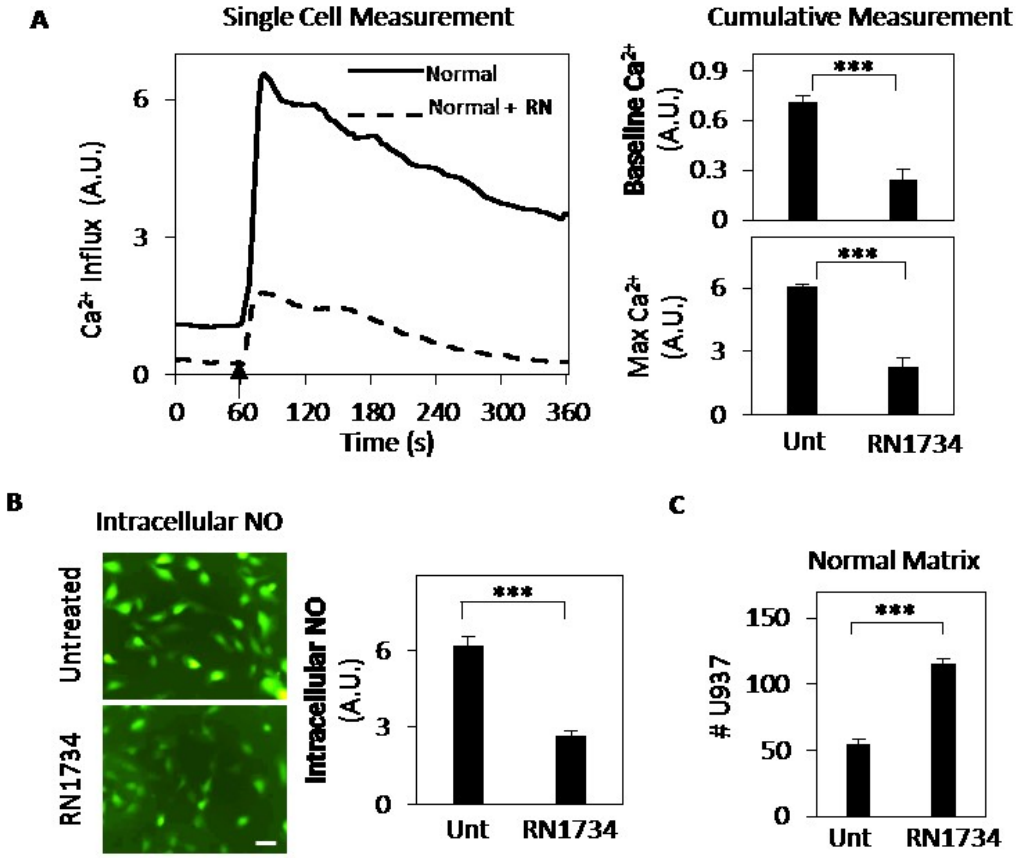
A
Single Cell Measurement
Normal
Normal + RN
Ca2+ Influx (A.U.)
Time (s)
Cumulative Measurement
Baseline Ca2+ (A.U.)
Max Ca2+ (A.U.)
***
Unt
RN1734
B
Intracellular NO
Untreated
RN1734
Intracellular NO (A.U.)
C
Normal Matrix
U937

Figure 3.6. Pharmacological suppression of TRPV4 promotes monocyte-EC adhesion. (A) Line graphs indicate GSK1016790A-stimulated (arrow) Ca^{2+} influx in representative ECs grown on normal (1000 Pa) matrix and treated without (con) or with TRPV4 antagonist RN1734 (25 μM). Bar graphs indicate average ± SEM from multiple ($n \geq 50$) cells. Note that RN1734 caused a ~65% decrease (***, $p<0.001$) in both baseline Ca^{2+} and peak Ca^{2+} influx levels **(B)** ECs grown on normal (1000 Pa) matrix were labeled with DAF-FM diacetate to measure intracellular NO. Representative fluorescent images and intensity analysis (bar graph; $n \geq 20$ cells) reveal that TRPV4 inhibition with RN1734 (25 μM) impairs endothelial NO production (***, $p<0.001$). Scale bar: 100 μm. **(C)** Quantification (average ± SEM) of adherent U937 cells from multiple ($n \geq 8$) images of U937 cell-EC co-culture reveals that TRPV4 inhibition (using RN1734; 25 μM) in ECs grown on 1000 Pa matrix causes a two-fold increase in U937 cell adhesion (***, $p<0.001$).

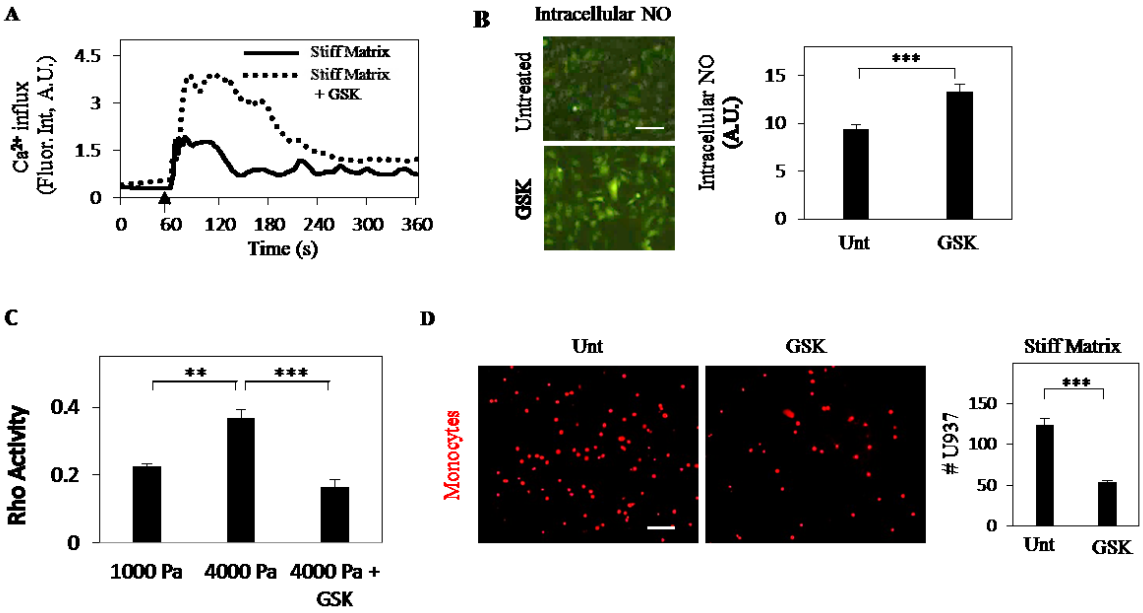
A
Ca2+ influx (Fluor. Int, A.U.)
4.5
3
1.5
0
0 60 120 180 240 300 360
Time (s)
Stiff Matrix
Stiff Matrix + GSK
B
Intracellular NO
Untreated
GSK
Intracellular NO (A.U.)
15
10
5
0
***
Unt
GSK
C
Rho Activity
0.4
0.2
0
**
***
1000 Pa
4000 Pa
4000 Pa + GSK
D
Unt
GSK
Monocytes
Stiff Matrix
U937
150
100
50
0
***
Unt
GSK

Figure 3.7. Pharmacological activation of TRPV4 suppresses endothelial activation on stiff matrices. (A) ECs grown on stiff (4000 Pa) matrices were treated with selective TRPV4 agonist GSK1016790A (50 nM; 3h) prior to Fluo4-AM loading and culture in Ca^{2+}-free buffer. Measurement of Ca^{2+} influx following addition of 50 mM $CaCl_2$ to culture medium reveals that TRPV4 channels remain activated for the extended period of 3h. Arrow indicates the moment $CaCl_2$ was added to medium. **(B)** ECs grown on stiff matrices were labeled with DAF-FM diacetate to measure intracellular NO. Representative fluorescent images and intensity analysis (bar graph; $n \geq 20$ cells) reveal that TRPV4 activation (GSK1016790A) recovers endothelial NO production (***, $p<0.001$). Scale bar: 100 μm. **(C)** ECs grown on normal and stiff matrices and treated with/without GSK1016790A were analyzed for Rho Activity using a Rho G-Lisa Activity kit. Quantitative analysis of Rho activity reveals that high Rho induced by stiff (4000 Pa) matrices elicit is significantly inhibited by stimulation of TRPV4 (**, $p<0.01$; ***, $p<0.001$). **(D)** Bar graph indicates quantification (average ± SEM) of adherent U937 cells from multiple ($n \geq 8$) images of U937 cell-EC co-culture. Note that ECs on stiff matrices treated with GSK1016790A (50 nM; 3h) exhibit ~45-55% decrease (***, $p<0.001$) in U937 cell adhesion.

Chapter 4

Epigenetic Control of TRPV4 activity and its implications for EC Adhesivity in Chronic Vascular Inflammation

Preface

Studies performed in Chapter 3 demonstrated that subendothelial matrix stiffening associated with atherosclerosis suppresses TRVP4-mediated endothelial NO production, which results in increased monocyte-EC adhesion that is characteristic of chronic inflammation of the aorta. This Chapter aims to identify the upstream epigenetic regulator of mechanosensitive TRPV4 and examine its role in EC adhesivity associated with chronic vascular inflammation.

Figures 4.1-4.8

Introduction

Abundant evidence implicates vascular inflammation in the pathogenesis of diabetes-associated cardiovascular complications such as atherosclerosis.[17, 71, 72] Aorta is a common site for diabetes-induced inflammation and atherosclerosis.[73-75] A hallmark of aortic inflammation is endothelial cell (EC) adhesivity, which is marked by increased expression and clustering of endothelial cell adhesion molecules (CAMs) such as intercellular CAM-1 (ICAM-1). The resulting ICAM-1-dependent increase in leukocyte adhesion and infiltration contributes to the development of atherosclerotic plaques via secretion of proinflammatory factors and uptake of accumulating lipids by the infiltrating leukocytes.[21, 76-78] Studies performed in Chapters 2 and 3 collectively demonstrated (a) how EC adhesivity (ICAM-1 clustering) is enhanced on abnormal subendothelial matrix stiffness associated with sites of chronic vascular inflammation, (b) the ability of mechanosensitive TRPV4 to inhibit EC adhesivity via activation of eNOS/NO. In these previous studies, the inflammatory effects of impaired TRPV4 was demonstrated using the ApoE-/- model of atherosclerosis. However, whether loss of mechanosensitive TRPV4 is also implicated in vascular inflammation associated with diabetes and, if so, the identity and inflammatory effects of its upstream regulators, remain unknown.

Protein expression and function are regulated both at the genetic and epigenetic levels. Although the effect of genetic regulation has been widely studied, increasing evidence now point towards a dominant role of epigenetic factors in mediating protein expression and function. MicroRNAs (miR), small (~20–22 nucleotides) non-coding RNA are one such epigenetic mediators. miRNAs target the 3'-untranslated region of mRNAs

with perfect or imperfect base-pairing. This pairing can either promote translational repression (inhibition) or degradation (decreased gene expression) which can alter key cellular functions.[79] Importantly, miRs are known to regulate various EC functions and diabetic vascular complications;[79, 80] thus, we hypothesize that TRPV4-mediated EC adhesivity in diabetes is also regulated by a miR-mediated epigenetic mechanism."

Studies performed using the db/db model of diabetic vascular inflammation revealed that diabetes leads to significant stiffening of aortic subendothelial matrix and loss of mechanosensitive TRPV4 in aortic ECs. *In vitro* studies using human aortic ECs confirmed that high glucose (HG), the major soluble risk factor in diabetes, increases EC adhesivity via a decrease in TRPV4-mediated endothelial NO production. Further investigation into upstream regulators of TRPV4 revealed that HG increases the levels of TRPV4-targeting microRNA 203a (miR-203a) in cultured aortic ECs, which impairs NO production and increases monocyte-EC adhesion. Finally, we show that miR-203a inhibitor reverses the inflammatory effects of HG *in vitro*. Collectively, these findings reveal a novel and crucial role of miR-203a-mediated TRPV4 regulation in EC adhesivity and vascular inflammation associated with diabetes.

Materials and Methods

Animal Model. All animal studies were performed in compliance with IACUC protocols approved by UC, Riverside, and City of Hope (Duarte, California). Adult (15 week-old) female diabetic mice (db/db) on a C57BL6/J background were purchased from Jackson

Labs. Insulin was given to all diabetics as needed to avoid catabolism (maintaining and allowing slow increase in body weight while allowing hyperglycemia as well as polyuria and hyperphagia). Extent of hyperglycemia was estimated based on fasting blood glucose levels, and blood glucose ≥300 mg/dL was considered diabetic. Average food consumption was measured daily, and body weight measured weekly. Age-matched mice (db/+) were used as non-diabetic control.

Cell Culture. Human aortic endothelial cells (HAEC) were purchased from Cell Applications (CA) and grown on gelatin-coated culture dishes in medium composed of MCDB-131 basal medium (Life Technologies), 10% fetal bovine serum (FBS; Fisherbrand), 10 mM L-Glutamine (Life Technologies), 10 ng/mL epidermal growth factor (Millipore), 1 ug/ml hydrocortisone (Sigma), 4 ng/mL human basic fibroblast growth factor (Life Technologies), 100 ug/ml heparin sodium salt (Sigma) and 1x antibiotic/ antimycotic supplement (Life Technologies). Human monocytic U937 cells were obtained from ATCC and grown in suspension in medium composed of RPMI-1640 basal medium (Life Technologies), 10% FBS, 10 mM HEPES (Fisherbrand), 1 mM sodium pyruvate (Cellgro), 4.5 g/L glucose (Sigma), 2 mM L-Glutamine, 1500 mg/ml sodium bicarbonate (Sigma), and 1x antibiotic/antimycotic supplement. Mouse monocytic cells (Wehi274) were a gift from Rama Natarajan (Beckman Research Institute of the City of Hope, Duarte, California). Mouse monocytes were cultured in low-glucose DMEM with 10% FBS and 1x antibiotic/antimycotic supplement.

miRNA Mimic and Inhibitor Transfection. HAECs were transfected using the Lipofectamine RNAiMAX transfection reagent (Invitrogen) as described in the vendor protocol. For HAECs, concentration of the lipofectamine reagent was optimized using a GFP-tagged nucleotide. Transfection efficiency was observed via fluorescent imaging, and it was found that 1.5 uL of RNAiMAX transfection reagent per 500 uL working solution was optimal. Further optimization of the concentration for the nucleotide revealed 50 nM elicited the highest fluorescence. After 72 hr, Transfected cells were harvest or used for various assays. Cells were transfected with either miR-203a mimic, miR-203a hairpin inhibitor or scrambled oligonucleotides.

Monocyte-EC Adhesion Assay. ECs were cultured for three days in medium containing normal glucose (NG, 5.5 mM glucose) or high glucose (HG, 25 mM glucose) (three replicates/condition). Subsequently, confluent EC monolayers were serum-starved overnight in medium containing MCDB-131, 2.5% FBS and 1x antibiotic/antimycotic supplement (starvation medium) to induce EC quiescence. EC monolayers were then treated with TNF-α (10 ng/ml; Fisher) for 5h before addition of DAPI-labeled U937 cells at 125k cells/cm^2 for 30 min at 37^oC. Next, endothelial monolayers were rinsed three times to remove non- or weakly-adhering monocytes and fixed in 1% paraformaldehyde (PFA; Electron Microscopy Sciences). Fluorescent images ($n \geq 8$) of adherent monocytes were taken using a Nikon Eclipse Ti microscope fitted with a Nikon Digital Sight DS-Qi1Mc camera and the cell count was obtained using ImageJ (NIH). For some studies, cells were treated with TRPV4 agonist GSK1016790A (50 nM) 3 hr prior to the assay. For monocyte

adhesion to mouse aorta, db/db or db/+ aortas were harvest from mice and cleaned. Cleaned aortas were cut, spread open and pinned to so the endothelium was face-up. Aortas were kept in a starvation medium bath and treated without/with GSK1016790A for 3 hr prior to addition of monocytes. Dapi-labeled mouse monocytes were added for 30 minutes then rinsed to remove non-adhered monocytes. Monocyte-aorta cocultures were fixed in 4% PFA overnight before imaging.

Measurement of Subendothelial Matrix Stiffness. Aortas from db/db and db/+ mice were isolated and cleaned. Each aorta was cut and pinned down to reveal the endothelium. To expose the subendothelial matrix, ECs were denuded using a cotton-tipped swab which was gently run along the whole of the aorta. Next, aortas were subjected to stiffness measurements using a biological-grade atomic force microscope (AFM; Veeco Instruments, NY) operating in tapping mode. For these tissue measurements, a 5 μm diameter glass bead was attached to a 140 μm-long microcantilever (MLCT, Bruker) with bending spring constant of 0.1 N/m. The maximum indentation force applied to each sample was ~8 nN. Measurements were made in force-curve mode, and the cantilever deflection was measured through the photodiode difference signal (S_{def}, volts). For each region, 10 or more force curves were measured and only the linear region of force curves were considered for the analysis of subendothelial matrix stiffness. Sample stiffness was calculated as $k_{sample} = F/ z_s$, where F is the applied force and z_s the sample deformation. Average stiffness was obtained from indentations in at least 10 different subendothelial regions from multiple mice.

Immunohistochemistry for TRPV4 Expression. Aortas from db/db and db/+ mice were fixed in formalin and embedded in paraffin prior to being cut into 5 μm thick sections. Prior to antibody labeling, sections were then treated with heat-activated antigen retrieval in sodium citrate buffer (10 mM Sodium citrate, 0.05% Tween, pH 6.0). Sections were then stained with anti-TRPV4 antibody followed by treatment with the chromagen 3,3-Diaminobenzidine (DAB) for 15 min. Sections were counterstained with hematoxylin.

Measurement of intracellular NO. ECs cultured under NG and HG conditions for three days were detached on the third day and plated at 15k cells/cm^2 in starvation medium overnight prior to TNF-α (10 ng/ml) stimulation for 5h. Next, ECs were loaded with a NO-sensitive fluorescent dye DAF-FM diacetate (Life Technologies), as per manufacturer's protocol, and imaged live in Krebs-Henseleit Buffer (125 mM NaCl, 4.74 mM KCl, 2.5 mM $CaCl_2$, 1.2 mM KH_2PO_4, 1.2 mM $MgSO_4$, 5 mM $NaHCO_3$ and 10 mM Glucose (all reagents from Sigma) using Nikon Eclipse Ti epifluorescent microscope fitted with a Nikon Digital Sight DS-Qi1Mc camera. Levels of intracellular NO were quantified by measuring total fluorescence intensity using ImageJ (n>40 cells)

Western Blot. Expression of endothelial TRPV4 was determined by Western Blot. Briefly, confluent cells (three replicates/condition) were lysed in RIPA buffer containing protease and phosphatase inhibitors, and the lysates were centrifuged to obtain protein supernatant. An equal amount of protein was loaded in 10% SDS–polyacrylamide gel and the separated

proteins transferred onto a nitrocellulose membrane for detection with polyclonal rabbit anti-TRPV4 (Alamone) followed by detection with horseradish peroxidase (HRP)–conjugated secondary antibody (Vector Laboratories, Inc., Burlingame, CA). GAPDH (Sigma) was used as the loading control. Protein bands were visualized using a chemiluminescent detection kit (Thermo Scientific) coupled with a camera-based imaging system (Biospectrum AC Imaging System) while the densitometric analysis was performed by ImageJ software.

Calcium Microfluorometry. Subconfluent ECs pre-cultured in NG or HG for three days were loaded with Ca^{2+}-sensitive dye Fluo-4 AM (Invitrogen) in Ca^{2+} buffer (136 mM NaCl, 4.7 mM KCl, 1.2 mM $MgSO_4$, 1.1 mM $CaCl_2$, 1.2 mM KH_2PO_4, 5 mM $NaHCO_3$, 5.5 mM Glucose: Sigma, 20 mM HEPES), rinsed three times and recovered for 30 minutes in Ca^{2+} buffer. To detect TRPV4 activity, time-lapse images (n=3) of dye-loaded cells (n≥50) were acquired every 3 sec for 1 min before addition of selective TRPV4 agonist GSK1016790A (300 nM; Sigma-Aldrich), followed by time-lapse imaging for an additional 5 min. Intracellular Ca^{2+} was quantified by measuring net intracellular fluorescence intensity (using ImageJ), as previously described. [60]

Quantitative RT PCR. Total RNA was isolated from Confluent EC monolayers cultured under the aforementioned conditions using Direct-zol RNA MiniPrep (Zymo Research, Irvine, CA, USA). For mRNA measurements, cDNA was made from the RNA with High Capacity cDNA Reverse Transcription (Thermo Fisher–Applied Biosystems), and

amplified with the appropriate TaqMan assay for commercially available primers for TRPV4 (Thermo Fisher–Applied Biosystems) on the CFX Connect96 system (Bio-Rad). Relative mRNA levels were determined by the comparative cycle threshold method with normalization to GAPDH (Thermo Fisher–Applied Biosystems). For miRNA measurements, cDNA was made using Quanta qScript miRNA cDNA synthesis kit. The primer used to determine miR-203a levels was hsa-miR-203a-5p (MIMAT0031890: AGTGGTTCTTAACAGTTCAACAGTT; IDT).

3'UTR Cloning and Luciferase Assay. To test targeting efficiency of miR-203a to TRPV4, TRPV4 3'UTR containing potential miR-203a target sequence was amplified by PCR and subcloned downstream of luciferase gene (in NotI site) of psiCHECK-2 dual luciferase vector (Promega, WI). The primer used for amplification was 5'-ATAAGAATGCGGCCGCTAAACTAT-3'. HAECs were transfected, using LTX transfection reagent as per the vendor protocol, with the Psicheck2 neat vector or the TRPV4 3'UTR clone and with either scrambled oligonucleotides or miR-203a mimic. After incubation for 3 days at 37°C, cells were lysed for 15 minutes in passive lysing buffer and then frozen at -80°C for minimum of two hours to complete the lysing process. Lysates were then measured for firefly and renilla luciferase activity using Dual-Glo Luciferase Assay (Promega, WI, USA) as per vendor protocol.

Statistics. All data were obtained from multiples cells or images and from multiple replicates/condition (as indicated in each respective section) and, unless otherwise

reported, expressed as mean ± standard error (SEM). Statistical significance was determined using analysis of variance (ANOVA; InStat; Graphpad Software Inc.) followed by Tukey post-hoc analysis. Results were considered significance if $p<0.05$.

Results

Diabetes Increases Monocyte Adhesion to Aortic Endothelium

Diabetes is characterized by abnormal matrix stiffening and composition. Here we show, for the first time, intact diabetic mouse aortas (db/db) denuded of their endothelium exhibit a 3-fold ($p<0.001$) increase in sub-endothelial matrix stiffness compared to nondiabetic (db/+) mice. (Fig. 4.1A) Diabetes-induced EC adhesivity is characterized by greater monocyte-EC adhesion. Indeed, we found that intact aortas isolated from db/db (diabetic) mice exhibited a 3-fold ($p<0.001$) greater binding of Wehi274 mouse monocytes than those isolated from age-matched db/+ (nondiabetic) mice (Fig. 4.1B). Consistent with a significant increase in monocyte adhesion to diabetic aortic endothelium, HG-treated human aortic ECs exhibited a 2-fold greater binding ($p<0.001$) of human U937 monocyte cells than their NG-treated counterparts (Fig. 4.1C). Predictably, this diabetes-induced increase in EC adhesivity was associated with a significant loss of endothelial NO bioavailability, as judged by a 82% decrease ($p<0.001$) in the intensity of NO-sensitive intracellular fluorescent dye DAF-FM diacetate (Fig. 4.1D).

Diabetes Leads to Impaired TRPV4 Expression and Activity in Aortic ECs

Studies in Chapter 3 showed that loss of endothelial NO associated with inflammation of the ApoE-/- aortas was caused by impaired endothelial TRPV4, an upstream regulator of eNOS/NO. Thus, we asked whether impaired endothelial NO in inflamed aortas of diabetic mice is also associated with loss of endothelial TRPV4. Mouse aorta sections immunolabeled for TRPV4 showed that diabetes leads to a marked reduction in endothelial TRPV4 expression (Fig. 4.2A). Consistent with this *in vivo* observation, HG-treated human aortic ECs exhibited 44% decrease ($p<0.001$) in expression of TRPV4 than their NG-treated counterparts (Fig. 4.2B). This HG-induced loss of TRPV4 expression correlated strongly with a 45% inhibition in TRPV4 activity, as judged by measurement of calcium influx in response to a TRPV4-specific agonist GSK1016790A (Fig. 4.2C).

Pharmacological Activation of Endothelial TRPV4 Prevents Monocyte-EC Adhesion Associated with Diabetes

Since diabetes- and HG-induced monocyte-EC adhesion correlates with loss of endothelial TRPV4, we looked to see whether pharmacological activation of TRPV4 in aortic ECs can block the inflammatory effects of HG and diabetes. Quantitative analysis of intracellular NO revealed that TRPV4 activation by GSK1016790A completely prevents the HG-induced decrease in endothelial NO production (Fig. 4.3A). Given the anti-inflammatory effects of endothelial NO, this GSK1016790A-mediated rescue of TRPV4 activity in HG-treated aortic ECs predictably led to a 25% inhibition ($p<0.001$) in monocyte-EC adhesion. Further, and perhaps more importantly, treatment of diabetic

aortas with GSK1016790A completely prevented the three-fold increase in monocyte-EC adhesion (Fig. 4.3C). Thus, these findings implicate TRPV4 as a potentially new target for anti-inflammatory therapies.

miRNA-203a Overexpression Contributes to High Glucose-induced Loss of Endothelial TRPV4

Given the newly-identified role of TRPV4 in the inflammation of aorta in diabetes, we next aimed to understand how HG regulates endothelial TRPV4. We focused on the role of the upstream epigenetic regulators of TRPV4, with an emphasis on TRPV4-targeting microRNAs. MicroRNAs are short, non-coding strands of nucleotides that inhibit target protein expression either by degrading the mRNA or by suppressing mRNA translation.[79] Further, microRNAs are known to be differentially regulated in diabetes.

Using target-based software (TargetScan), human microRNA-203a (miR-203a) was predicted to target human TRPV4. QPCR measurements for microRNA revealed that HG increases the levels of TRPV4-targeting miR-203a by 1.7-fold ($p<0.001$) (Fig. 4.4A). To confirm that the HG-induced overexpression of miR-203a suppresses endothelial TRPV4, ECs grown under NG conditions were transfected with a miR-203a mimic which inhibited TRPV4 expression and activity by 23% ($p<0.001$) and 64% ($p<0.05$), respectively (Fig. 4.4 B and C).

To unequivocally confirm that miR-203a targets TRPV4, the 3'UTR region of TRPV4 mRNA (Fig. 4.5A) was first cloned into the bi-luciferase PsiCheck2 vector, followed by its co-transfection into NG-treated ECs along with the miR-203a mimic or

scrambled oligonucleotides. If miR-203a specifically targeted TRPV4, it would bind the 3'UTR region of TRPV4 mRNA and suppress luciferase expression and activity. Quantitative measurement of the luciferase activity revealed that transfection of ECs with vector+miR-203a caused a significant decrease in luminescence, which was not seen with the vector+scrambled oligo transfection (Fig. 4.5B). Collectively, these data indicate that HG-induced overexpression of miR-203a leads to targeted inhibition of TRPV4 in aortic ECs.

Given our earlier finding that diabetes-induced loss of endothelial TRPV4 leads to vascular inflammation, we next asked whether the inhibitory effect of miR-203a on TRPV4 similarly leads to vascular inflammation. To address this question, NG-treated aortic ECs were transfected with miR-203a mimic prior to assessment of intracellular NO production and monocyte-EC adhesion, as previously described. Quantitative analysis of intracellular NO and adherent monocytes revealed that transfection with miR-203a mimic causes a 52% inhibition ($p<0.001$) of endothelial NO (Fig. 4.6A), which predictably leads to a 1.5-fold increase ($p<0.001$) in monocyte-EC adhesion (Fig. 4.6B).

Inhibition of miR-203a Prevents HG-Induced TRPV4 Impairment and Monocyte-EC Adhesion

Since HG-induced upregulation of endothelial miR-203a leads to TRPV4 inhibition and a concomitant increase in monocyte-EC adhesion, we reasoned that inhibiting miR-203a in aortic ECs would block these inflammatory effects of HG. To test this, HG-treated aortic ECs were transfected with a custom miR-203a hairpin inhibitor (miR-

203a-HI). QPCR analysis showed that miR-203a-HI transfection reduces miR-203a expression in HG-treated ECs to the levels seen in NG-treated cells (Fig. 4.7A). Importantly, this reduction in miR-203a levels by the hairpin inhibitor completely prevented the HG-induced decrease in TRPV4 expression (Fig. 4.7B). That this preventive effect of miR-203A-HI was not seen with the scrambled oligo sequence confirms the specificity of the hairpin inhibitor for miR-203a. Further, consistent with its profound effect on TRPV4 expression, miR-203a-HI treatment completely prevented the HG-induced loss in endothelial TRPV4 activity (Fig. 4.7C).

Predictably, the ability of miR-203a-HI to block HG-induced loss of TRPV4 resulted in complete prevention of NO impairment in HG-treated ECs (Fig. 4.8A). Consistent with the anti-inflammatory effects of endothelial NO, we finally show that miR-203a-HI transfection in HG-treated ECs successfully prevented the HG-induced increase in monocyte-EC adhesion (Fig. 4.8B). Collectively, these findings reveal a novel and crucial role of miR-203a-mediated TRPV4 regulation in EC adhesivity and monocyte-EC adhesion associated with diabetes-induced vascular inflammation.

Discussion

Chapter 4 shows, for the first time, that diabetes enhances subendothelial matrix stiffness which corresponds with increased monocyte-endothelium adhesion. Further, this increased adhesion is associated with suppression of NO production via reduced TRPV4 expression and activity. Importantly, stimulation of TRPV4 reverses the effect of diabetes

(and HG) on aortic endothelial adhesivity. Importantly, these studies were the first to show that (i) diabetic (high glucose) conditions promote miR-203a, (ii) miR-203a contributes to HG-induced suppression of TRPV4 expression and activity, and (iii) that modulation of miR-203a can reverse HG-induced EC activation. Together, these findings identify a crucial role of miR-203a in TRPV4-mediated diabetic endothelial activation and further implicate TRPV4, and perhaps miR-203a, as novel anti-inflammatory targets for management of diabetes and diabetes-associated pathologies.

Vascular inflammations is a crucial contributor in the pathogenesis of diabetes-associated pathologies such as atherosclerosis.[17, 71, 72] Further, sites of diabetic vascular inflammation is characterized by endothelial adhesivity which is attributed to increase expression and clustering of CAMs, such as ICAM-1. Chapter 2 highlighted the important role of I-CAM clustering and endothelial adhesivity and how it is regulated through abnormal matrix stiffness. Additionally, matrix stiffening has been shown to promote diabetic retinal inflammation via suppression of NO production[2] thereby implicating diabetes-associated matrix stiffening in endothelial adhesivity. Here, for the first time, I show that diabetic aorta exhibit increased subendothelial matrix stiffness. Further, this study shows that diabetes promotes monocyte adhesion to aortic endothelium. In vitro confirmation shows HG increases monocyte-HAEC adhesion which corresponded with suppressed NO production. These studies implicate matrix stiffness as a key factor regulating diabetes-associated cardiovascular complications.

Recent studies have clearly shown TRPV4 is essential for NO-dependent vasodilation.[81] Importantly, however, the studies shown in Chapter 3 are the first to identify the ability of mechanosensitive TRPV4 to inhibit EC adhesivity via activation of eNOS/NO. Notably, TRPV4 has been shown to be suppressed in the retinal vessels of diabetic rats[67] which implicates diabetes as a potential effector of TRPV4. Here, I show for the first time that diabetes suppresses TRPV4 expression in mouse aorta. Further, stimulation of TRPV4 reverses diabetes-induced endothelial adhesivity. This study implicates TRPV4 as a major determinant of chronic vascular inflammation associated with diabetes. Since retinopathy and aortic dysfunction (atherosclerosis and smooth muscle hypercontractility) are common complications of diabetes associated with loss of TRPV4, it remains to be seen whether TRPV4 downregulation is implicated in inflammation associated with diabetic nephropathy.

The studies in Chapter 3 identified matrix stiffness as a key regulator of TRPV4 expression. However, protein expression can also be regulated by genetic and epigenetic mechanisms. Specifically, microRNAs have emerged as key mediators of cell function via repression or degradation of gene expression.[79] Importantly, miRs are known to regulate shear stress-dependent EC activation and diabetic complications.[79, 80] For example, in ECs, miR-146a, which targets fibronectin, has been shown to contribute to matrix remodeling characteristic of chronic diabetes[82] and miR-200b has been shown to contribute to VEGF-mediated diabetic retinopathy.[83] Here, my studies are the first to implicate a novel role of miR-203a in diabetes-induced vascular inflammation. Further, my studies identify TRPV4

as a downstream target of miR-203a. However, given the nature of miRs, whether miR-203a targets other mediators of diabetic vascular inflammation remains to be seen.

Despite these promising findings, this study raises many important questions. For instance, how many other miRs can target TRPV4 either directly or indirectly? Since TRPV4 has upstream regulators such as integrins and possibly other focal adhesion proteins that act as direct matrix stiffness sensors, can miRs that target these proteins influence TRPV4-mediated EC function? Are miRs directly sensitive to alterations in matrix stiffness? Given that one miR can have multiple targets and that one target can be regulated by multiple miRs, a more exhaustive integrated pathway analysis may be necessary to fully examine the role and importance of miR-dependent control of diabetic vascular inflammation.

Figures

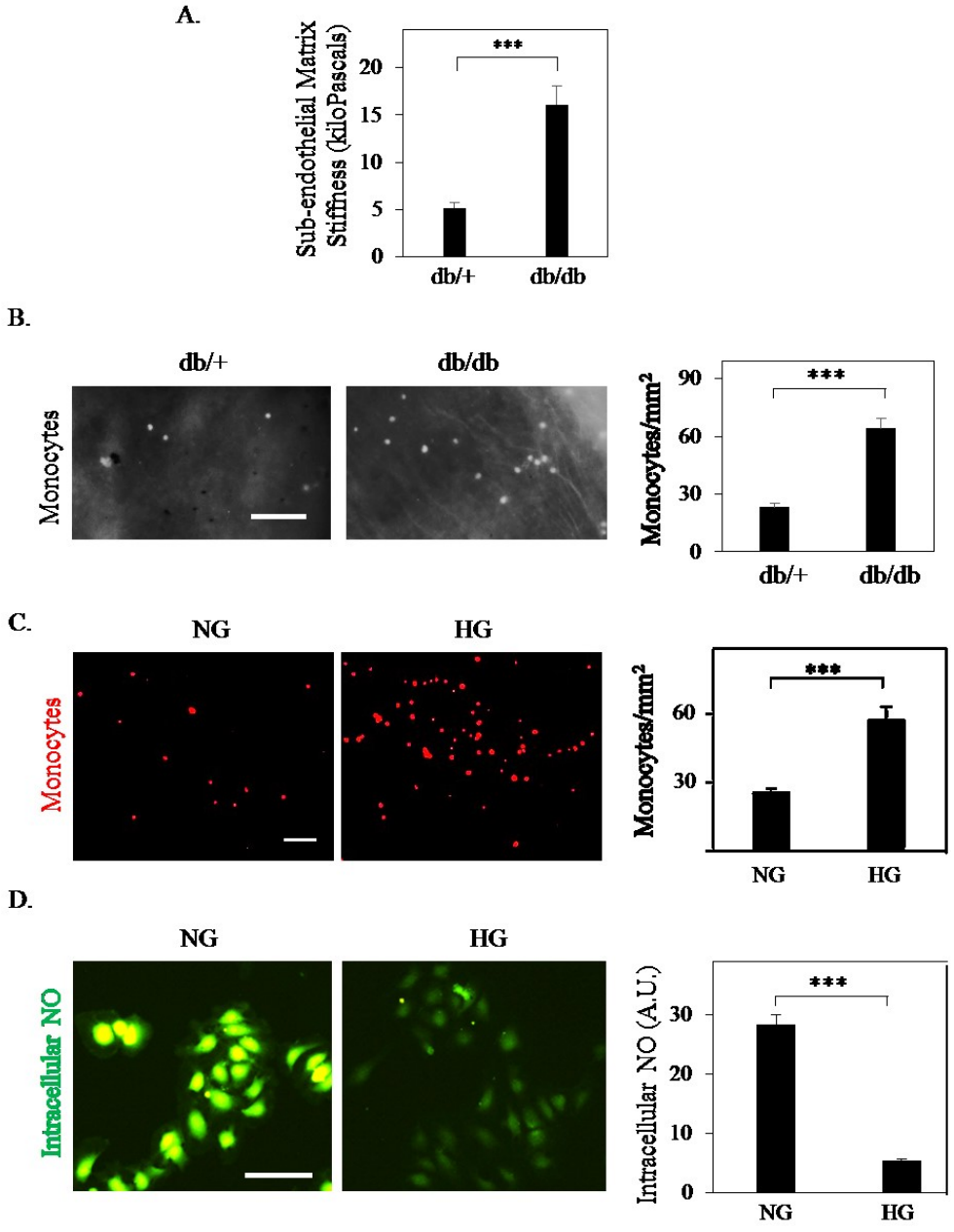
A.
Sub-endothelial Matrix Stiffness (kiloPascals)
***
20
15
10
5
0
db/+
db/db
B.
db/+
db/db
Monocytes
Monocytes/mm²
***
90
60
30
0
db/+
db/db
C.
NG
HG
Monocytes
Monocytes/mm²
***
60
30
NG
HG
D.
NG
HG
Intracellular NO
Intracellular NO (A.U.)
***
30
20
10
0
NG
HG

Figure 4.1 Diabetic conditions promote NO-mediated monocyte adhesion. **(A)** Atomic force microscopy measurements were taken of db/+ and db/db mouse aortas denuded to reveal the subendothelial matrix. Quantification (average ± SEM) of these measurements revealed diabetic mice exhibit significantly (***, $p<0.001$) increased matrix stiffness. **(B)** Representative images show fluorescently-labeled mouse monocytes bound to the aortic endothelium of normal and diabetic mice. Quantification of adherent U937 cells (per mm^2) reveal db/db mice exhibit significantly greater monocyte adhesion (***, $p<0.001$). **(C)** Representative images show fluorescently-labeled U937 cells bound to endothelial monolayers cultured in NG and HG conditions. Quantification of adherent U937 cells (per mm^2) reveal high glucose significantly enhances U937-EC adhesion (***, $p<0.001$). **(D)** ECs were labeled with DAF-FM diacetate to measure intracellular NO. Representative fluorescent images and subsequent intensity measurements from multiple ($n\geq20$) cells reveal HG significantly (**, $p<0.01$) suppresses intracellular NO. Scale bars: 100 μm.

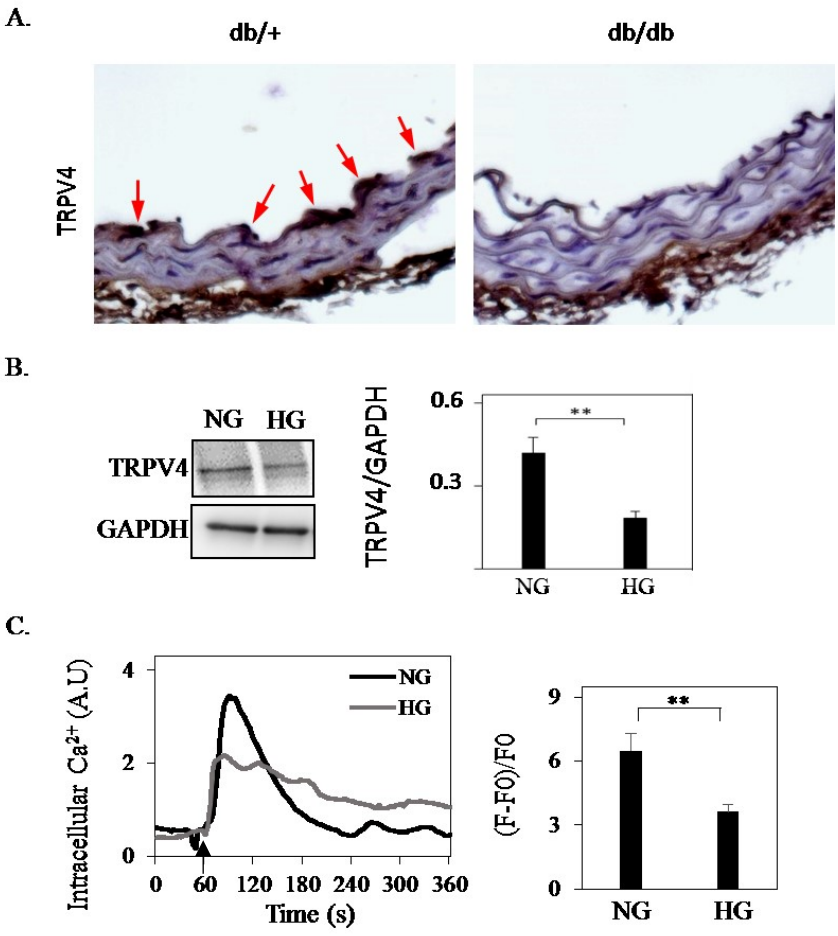
A.
db/+
db/db
TRPV4
B.
NG
HG
TRPV4
GAPDH
TRPV4/GAPDH
0.6
0.3
**
NG
HG
C.
Intracellular Ca2+ (A.U)
4
2
0
NG
HG
0
60
120
180
240
300
360
Time (s)
(F-F0)/F0
9
6
3
0
**
NG
HG

Figure 4.2. Diabetes leads to impaired TRPV4 expression and activity in aortic ECs. **(A)** Representative images of aortic cross-sections labeled with anti-TRPV4 antibody show db/db mice exhibit clear reduction in endothelial TRPV4 expression. **(B)** ECs treated with NG and HG were subjected to Western Blotting for levels of TRPV4 expression. Densitometric analysis (bar graph) normalized to GAPDH (loading control) showed that HG significantly (**, $p<0.01$) reduced TRPV4 expression. **(C)** Calcium microfluorometry was performed in Fluo4-AM-loaded ECs cultured in NG and HG conditions. Line graph from a representative cell and bar graph (average ± SEM) from multiple ($n\geq50$) cells reveal that high glucose causes a significant impairment in TRPV4-dependent Ca^{2+} influx. Arrow indicates the moment selective TRPV4 agonist GSK1016790A was added to cells (**, $p<0.01$).

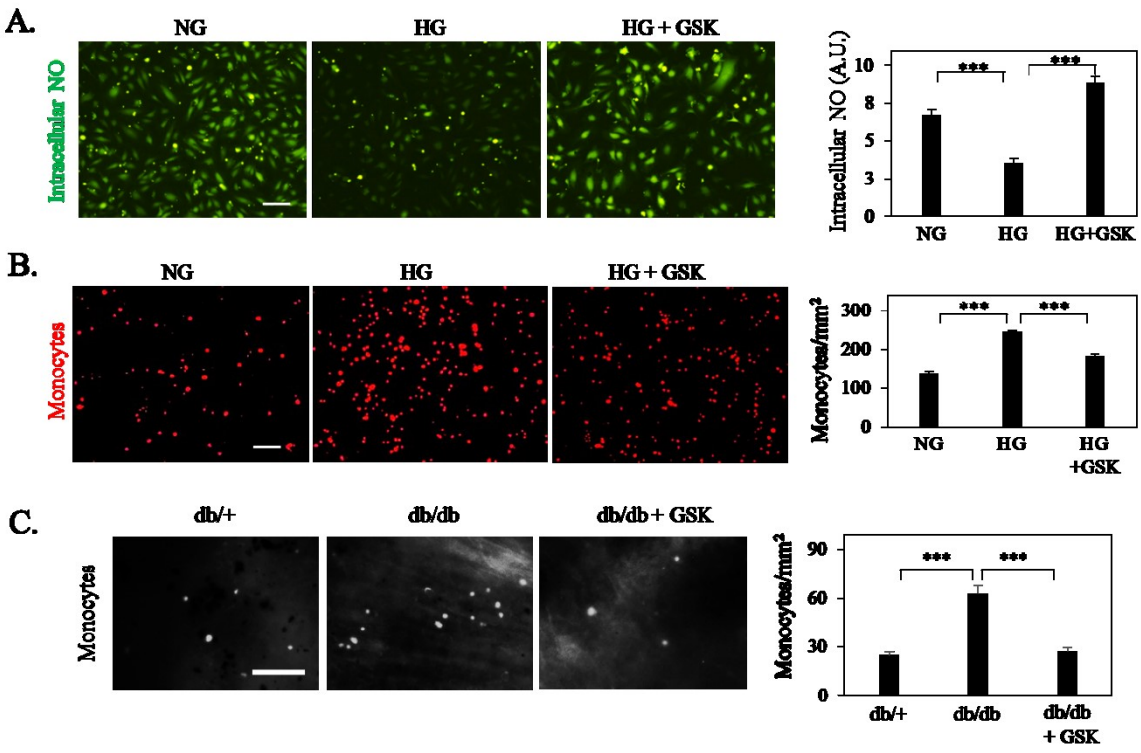

Figure 4.3. Pharmacological activation of endothelial TRPV4 prevents monocyte-EC adhesion associated with diabetes. (A) ECs in NG, HG, and HG + GSK1016790A were labeled with DAF-FM diacetate to measure intracellular NO. Representative fluorescent images and subsequent intensity measurements from multiple ($n \geq 20$) cells reveal intracellular NO suppression in HG treatment was significantly recovered (***, $p<0.001$) by TRPV4 stimulation. **(B)** Representative images and corresponding bar graph of adherent U937 cells from multiple ($n \geq 8$) images of U937 cell-EC co-culture show that TRPV4-stimulation reverses HG-induced monocyte-EC adhesion (***, $p<0.001$). **(C)** Diabetes-induced monocyte adhesion to aortic endothelium is significantly (***, $p<0.001$) reversed in GSK-stimulated diabetic aortas. Scale bars: 100 μm.

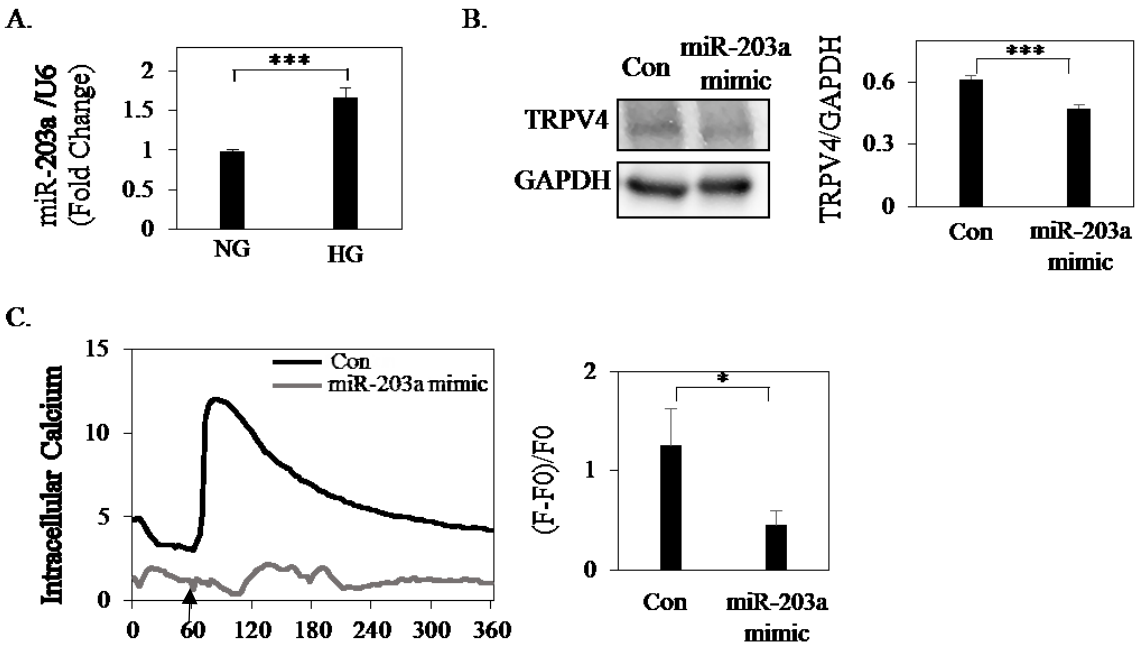
A.
miR-203a /U6
(Fold Change)
2
1.5
1
0.5
0
***
NG
HG
B.
Con
miR-203a
mimic
TRPV4
GAPDH
TRPV4/GAPDH
0.6
0.3
0
***
Con
miR-203a
mimic
C.
Intracellular Calcium
15
10
5
0
Con
miR-203a mimic
0
60
120
180
240
300
360
(F-F0)/F0
2
1
0
*
Con
miR-203a
mimic

Figure 4.4. miRNA-203a overexpression contributes to high glucose-induced loss of endothelial TRPV4. (A) RNA from ECs treated under NG and HG conditions was measured with qPCR for miR-203a expression and normalized to U6 (loading control). Analysis shows HG significantly increases miR-203a expression (***, $p<0.001$). **(B)** ECs transfected with scrambled oligonucleotides (control) or miR-203a mimic were subjected to Western Blotting for levels of TRPV4 expression. Densitometric analysis (bar graph) normalized to GAPDH (loading control) showed that miR-203a mimic significantly (**, $p<0.01$) reduced TRPV4 expression. **(C)** Calcium microfluorometry was performed in Fluo4-AM-loaded ECs transfected with scrambled oligonucleotides or miR-203a mimic. Line graph from a representative cell and bar graph (average ± SEM) from multiple ($n\geq50$) cells reveal that miR-203a enhancement causes a significant impairment in TRPV4-dependent Ca^{2+} influx. Arrow indicates the moment selective TRPV4 agonist GSK1016790A was added to cells (**, $p<0.01$).

A.

TRPV4 3'UTR 5'-ATAAGAATGCGGCCGCTAAACTAT-3'

B.

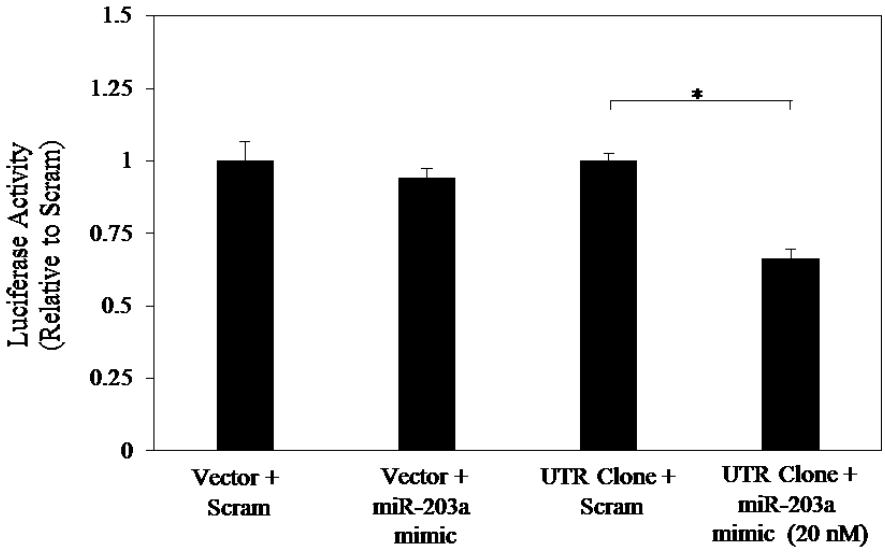

Figure 4.5. miR-203a directly targets TRPV4. (A) Sequence corresponding to the 3'UTR region of TRPV4 that was cloned into the PsiCheck2 vector for luciferase measurements. **(B)** Bar graph of ECs transfected with Psicheck2 vector or the UTR cloned vector with either scrambled oligonucleotides or miR-203a mimic. Luciferase activity measurements (Renilla/Firefly) show miR-203a reduces luciferase activity in the cloned vector which indicates targeting specificity.

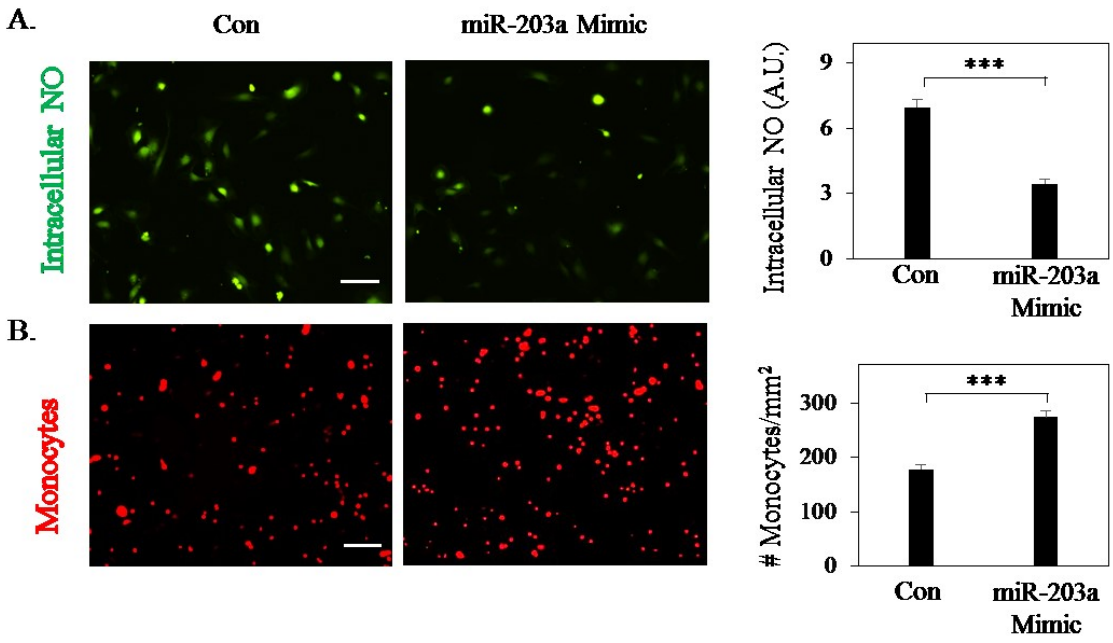

Figure 4.6. Overexpression of miR-203a promotes NO-dependent monocyte-EC adhesion. (A) Representative fluorescent images and subsequent intensity measurements from multiple (n≥20) cells reveal miR-203a significantly inhibits NO production (***, p<0.001). **(B)** Representative images and corresponding bar graph of adherent U937 cells from multiple (n≥8) images show that this miR-203a-induced NO suppression corresponds to enhanced monocyte-EC binding (***, p<0.001) Scale bars: 100 μm.

A.

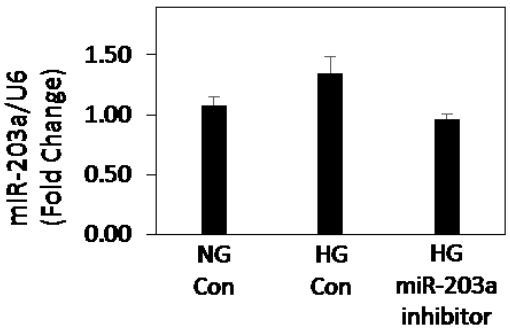
miR-203a/U6
(Fold Change)
1.50
1.00
0.50
0.00
NG
Con
HG
Con
HG
miR-203a
inhibitor

B.

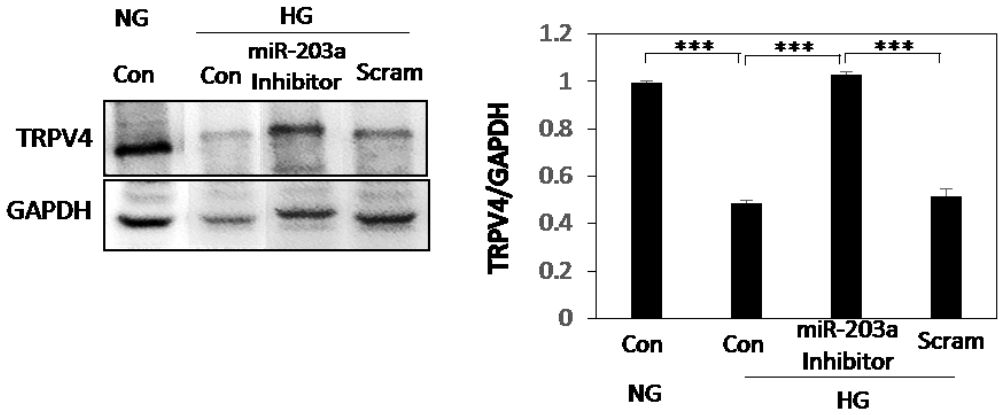
NG
HG
Con
Con
miR-203a
Inhibitor
Scram
TRPV4
GAPDH
TRPV4/GAPDH
1.2
1
0.8
0.6
0.4
0.2
0
***
***
***
Con
Con
miR-203a
Inhibitor
Scram
NG
HG

C.

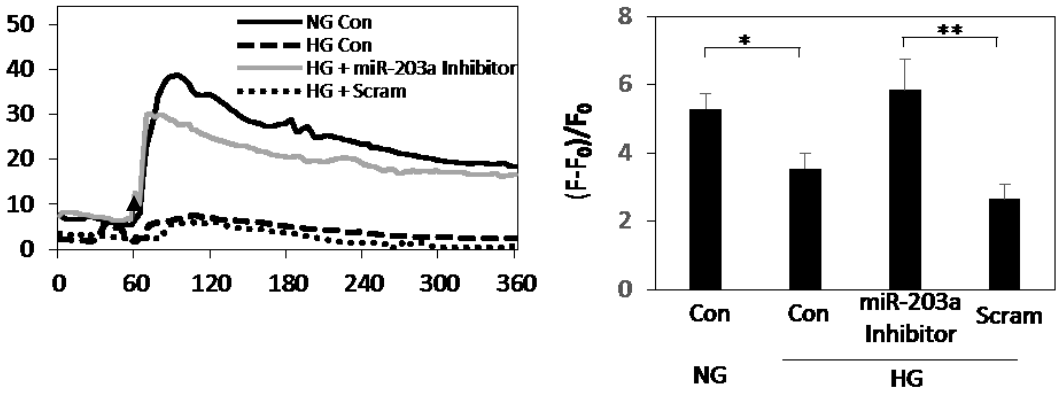
NG Con
HG Con
HG + miR-203a Inhibitor
HG + Scram
50
40
30
20
10
0
0
60
120
180
240
300
360
(F-F0)/F0
8
6
4
2
0
*
**
Con
Con
miR-203a
Inhibitor
Scram
NG
HG

Figure 4.7. Inhibition of miR-203a prevents HG-induced TRPV4 impairment. (A) RNA from ECs treated/transfected with NG, HG, HG+miR-203a inhibitor was measured with qPCR for miR-203a expression and normalized to U6 (loading control). Analysis confirms HG-induced miR-203a expression was reduced by miR-203a inhibitor (***, $p<0.001$). **(B)** HG-treated ECs transfected with scrambled oligonucleotides (control) or miR-203a inhibitor were subjected to Western Blotting for levels of TRPV4 expression. Densitometric analysis (bar graph) normalized to GAPDH (loading control) showed that miR-203a inhibitor significantly (***, $p<0.01$) reversed HG-inhibited TRPV4 expression. **(C)** Calcium microfluorometry was performed in Fluo4-AM-loaded HG-treated ECs transfected with scrambled oligonucleotides or miR-203a inhibitor. Line graph from a representative cell and bar graph (average ± SEM) from multiple ($n\geq50$) cells reveal that miR-203a inhibitor restores TRPV4-dependent Ca^{2+} influx to normal levels. Arrow indicates the moment selective TRPV4 agonist GSK1016790A was added to cells (**, $p<0.01$).

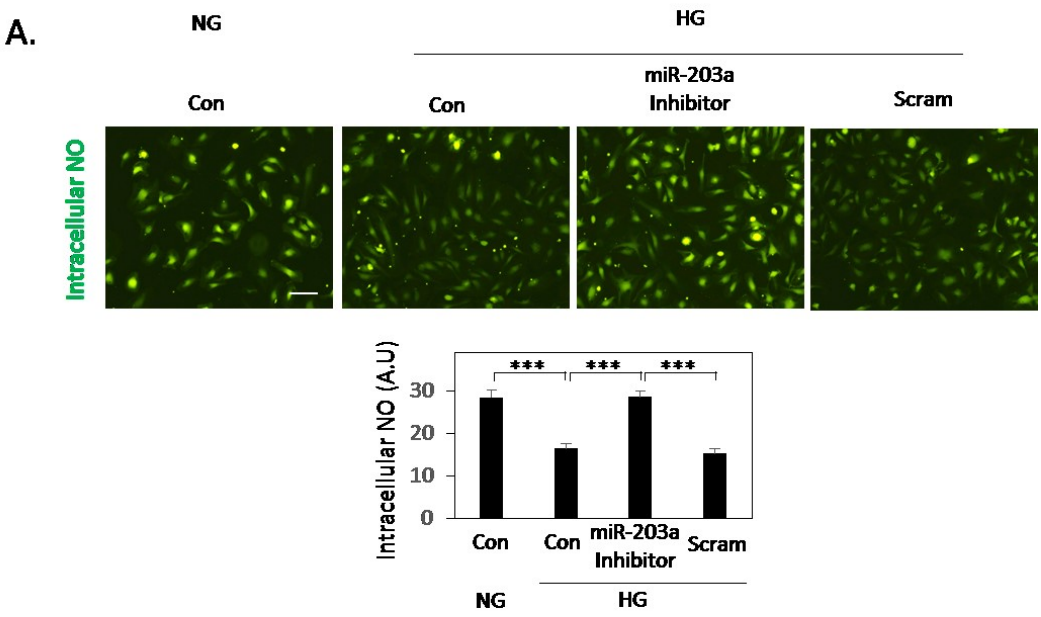
A.
NG
HG
Con
Con
miR-203a Inhibitor
Scram
Intracellular NO
Intracellular NO (A.U)
30
20
10
0
***
***
***
Con
Con
miR-203a Inhibitor
Scram
NG
HG

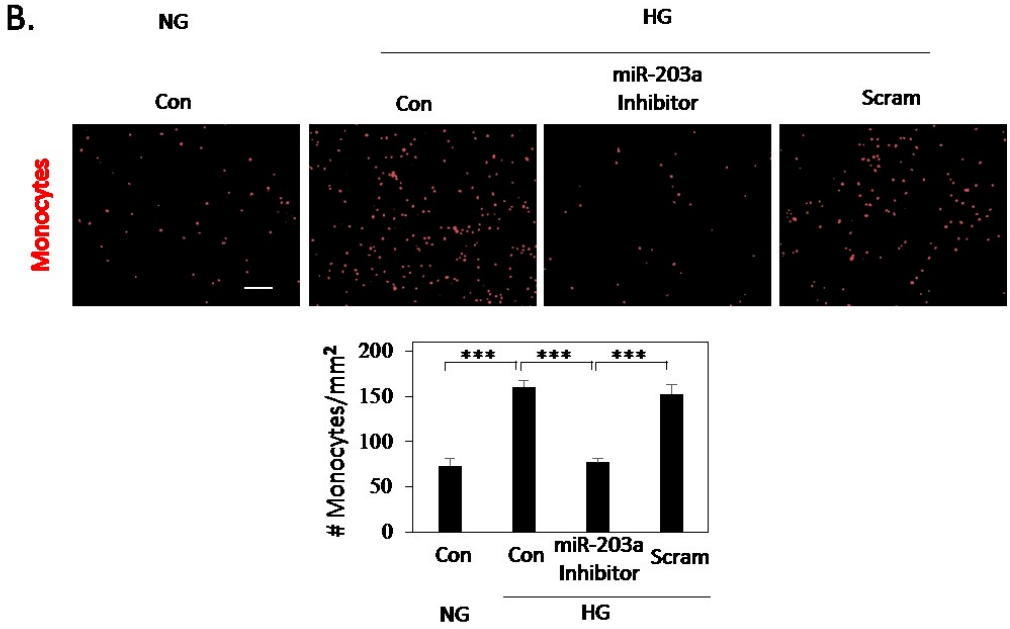
B.
NG
HG
Con
Con
miR-203a Inhibitor
Scram
Monocytes
Monocytes/mm2
200
150
100
50
0
***
***
***
Con
Con
miR-203a Inhibitor
Scram
NG
HG

Figure 4.8. Inhibition of miR-203a prevents HG-induced monocyte-EC adhesion. **(A)** Representative fluorescent images and subsequent intensity measurements from multiple ($n \geq 20$) cells reveal miR-203a-inhibition reverses HG-induced suppression of NO production (***, $p < 0.001$). **(B)** Representative images and corresponding bar graph of adherent U937 cells from multiple ($n \geq 8$) images show that inhibition of miR-203 suppressed HG-induced monocyte-EC binding (***, $p < 0.001$) Scale bars: 100 μm.

Chapter 5

Conclusion

Preface

This Chapter Summarizes the *Key Points* in the preceding Chapters and describes the working model, or the mechanistic pathway identified through this research. Further, this Chapter highlights the directions of novel research ideas that may spawn from this thesis.

Schematic 5.1

Studies in Chapter 2 show that matrix stiffness exerts biphasic control over monocyte-EC adhesion, which is significantly greater on both soft and stiff matrices. This preferential monocyte-EC adhesion on aberrant matrices correlates with increased Rho-dependent ICAM-1 clustering. Importantly, pharmacological inhibition of Rho/ROCK activity blocks the effects of matrix stiffness on ICAM-1 clustering-dependent monocyte-EC adhesion. In Chapter 3, we identify a new mechanotransduction mechanism by which subendothelial matrix stiffening enhances monocyte-EC adhesion via loss of TRPV4-dependent eNOS/NO through modulation of Rho/ROCK. Further, pharmacological modulation of TRPV4 activity reverses the effects of matrix stiffness on EC adhesivity. In Chapter 4, we showed that diabetes leads to aortic subendothelial matrix stiffening and loss of mechanosensitive TRPV4 in aortic ECs. *In vitro* studies confirmed that HG increases EC adhesivity via decreased TRPV4-mediated endothelial NO production. Further, HG increases the levels of TRPV4-targeting miR-203a in cultured aortic ECs, which impairs NO production and increases monocyte-EC adhesion. Finally, we show that inhibiting miR-203a reverses the inflammatory effects of HG *in vitro*. Collectively, these findings reveal a novel and crucial role of miR-203a-mediated mechanosensitive TRPV4 regulation in EC adhesivity and vascular inflammation associated with diabetes.

Working Model

The findings from my studies indicate a multifaceted signaling mechanism involving epigenetic, mechanical and chemical cues that links abnormal matrix stiffness

(the primal cause) and diabetes-associated pathologies characterized by monocyte-EC adhesion (the ultimate effect). Specifically, I show that abnormal matrix stiffness (Schematic 5.1A) significantly impairs TRPV4 expression and activity (Schematic 5.1B). However, precisely how subendothelial matrix stiffness controls TRPV4 remains unclear. One possibility could be through the activation of integrins found in the focal adhesion points, the point where the cell binds to the matrix. Integrins are transmembrane cell surface receptors that mediate cell adhesion to matrix molecules.[84] Importantly, these integrins can transmit external forces (such as matrix stiffness-dependent resistance force) rapidly to TRPV4 via a "hardwired" framework. It is this *physical* association between integrins and TRPV4 that confers its mechanosensitivity.[85] Importantly, in response to mechanical stimuli, TRPV4 is ultra-rapidly activated (within 4 milliseconds) which is which precedes the activation rate of any second messenger signaling pathways.[85] This implicates TRPV4 as being directly responsive to mechanical stimulus and, thus, I speculate that abnormal matrix stiffness elicits a cooperative effect between integrin-dependent and independent TRPV4 activity.

Next, TRPV4 is known to enhance eNOS activation through the calcium-dependent pathway.[57, 63] Here I show, as do others, that calcium influx induced by TRPV4 activation caused increases in cytoplasmic calcium levels (Schematic 5.1C) which is expected to activate calmodulin (CaM). CaM binds to the CaM-binding domain in eNOS which aligns the oxygenase and reductase domains and leads to NO synthesis. Additionally, CaM activates CaM kinase II (CaMKII), which phosphorylates eNOS (Schematic 5.1D) on S1179 and promotes nitric oxide (NO) synthesis (Schematic 5.1E). Thus, impaired TRPV4

activation inhibits eNOS-derived NO production and decreased endothelial NO levels in aortic ECs.

Further, eNOS-derived NO has been shown to inhibit Rho/ROCK activation via inhibition of $G_{12/13}$, a family of heterotrimeric G proteins.[86] $G_{12/13}$ stimulate Rho guanine nucleotide exchange factors (GEFs). Thus, inhibition of NO enhances $G_{12/13}$ and upregulates GEF that, in turn, activates Rho, from Rho-GDP (inactive) to Rho-GTP (active, Schematic 5.1F). Also, this increase in Rho activity leads to an increase in cytoskeleton tension via activation of its downstream effector, Rho-associated Kinase (ROCK) (Schematic 5.1G).[22] Importantly, aberrant matrix-induced Rho/ROCK alters cytoskeletal organization as well as the recruitment of α-actinin-4, an actin-binding protein, which promotes ICAM-1 phosphorylation and clustering (Schematic 5.1H). ICAM-1 clustering is key factor necessary for firm monocyte-EC adhesions (Schematic 5.1I). Additionally, ROCK activates myosin to generate contractility that increases cell stiffness (Schematic 5.1J). Together, increase in both EC and endothelial matrix stiffness contributes to overall aortic vessel stiffness.

Alternatively, and perhaps cooperatively, in a physiological state eNOS produces constitutively low levels of NO that inhibits activation of inhibitory κB kinase (IKK), the necessary enzyme complex that induces NF-κB nuclear translocation (activation) in activated ECs.[32, 55, 87] Decreased endothelial NO allows IKK to activate NF-κB and leads to downstream transcription of pro-inflammatory factors, such as TNF-α and IL-6, and increased expression of cell adhesion molecule (ICAM-1). This increase in ICAM-1 leads to enhanced monocyte-EC adhesion via binding of endothelial ICAM-1 and the $\alpha_m\beta_2$

integrin (on monocytes). Thus, perhaps there exists a long-term cooperative effect of matrix stiffening-induced suppression of NO on both Rho-associated ICAM-1 clustering and Nf-kB-induced ICAM-1 expression.

Importantly, I also show that diabetes (HG) increases miR-203a expression (Schematic 5.1K). miR-203a targets TRPV4 mRNA and ultimately suppresses both the activity and expression. However; whether miR-203a-mediate TRPV4 modulation is completely independent of matrix stiffness has yet to be determined. Recent studies have shown HG increases endothelial expression of LOX, a copper-dependent matrix crosslinker. This increase in LOX causes an increase in subendothelial matrix stiffness.[2] Perhaps, this increase in matrix stiffness elicits downstream signaling that inhibits miR-203a expression in cooperation with HG-induced effects. For now, I speculate that HG, in the short term, is enough to enhance miR-203a and suppress TRPV4; however, in the long term, there may exist a cooperative effect of matrix stiffness and high glucose conditions on enhancing miR-203a.

Finally, EC stiffness establishes a dynamic equilibrium with the subendothelial matrix stiffness; as such, an increase in EC stiffness (contractility force) can feed back to enhance matrix stiffness by pulling on integrins, which physically increase the local density and stiffness of the corresponding matrix.[25, 42] This self-propagating loop further impairs TRPV4 and downstream endothelial NO levels. The existence of this feedback mechanism between TRPV4 and Rho/ROCK signaling pathways is likely to exacerbate aortic stiffening and inflammation associated with diabetes. Therefore, future *in vivo* studies that

aim to enhance TRPV4 through a nanotechnological approach, such as site-targeted nanoliposomes or erythrocyte ghosts, may produce viable treatments for diabetes.

Future Directions

To further investigate the role of matrix stiffness in regulating epigenetic-dependent EC function, we will use small RNA-seq approach to perform transcriptome-wide miR profiling in aortic ECs grown on matrices of varying stiffness. Target prediction of differentially-expressed miRNAs (at least 2-fold) will be performed using open-sourced software such as TargetScan (www.targetscan.org) and miRanda (www.microrna.org). Focal adhesion proteins, Rho family of cytoskeletal proteins, LOX-like proteins, and TRPV family members are key mediators of mechanotransduction.[7] Thus, if miRs for these targets are found to be differentially regulated, we will verify their expression levels, as well as their target mRNA levels, by RT-qPCR. We will use Bioinformatics tools such as DAVID (NIH/NCI) and Ingenuity Pathway Analysis (IPA) to perform pathway network analysis for identification of MASTIR miRs that (a) regulate multiple mediators of EC mechanotransduction, and (b) simultaneously regulate expression of inflammatory genes such as NF-kB, cytokines, and cell adhesion molecules.

Recent studies have revealed that enhanced inflammation of diabetic (streptozotocin-induced) mice retinal capillaries correlates with higher expression of endothelial lysyl oxidase (LOX), a matrix crosslinking enzyme.[2] However, whether and how LOX contributes to diabetic aortic subendothelial stiffening has yet to be investigated.

To do this, the effect of HG (25 mM) on aortic ECs will be assessed for (a) LOX expression and activity and (b) if pharmacological inhibition of LOX (with BAPN) can reverse the effects of HG on matrix stiffness and monocyte-EC adhesion. Additionally, several LOX-targeting miRs have been reported in the literature or predicted by open-sourced software, including miR-29/-29b, -30, and -200b (LOX).[88, 89] However, whether these miRs influence target expression in diabetic ECs remains unknown. Taking a candidate miR profiling approach using PCR Arrays (Qiagen), we will first determine the levels of these miRs in human aortic ECs cultured under NG (5.5 mM) versus HG (25 mM) conditions, and confirm their levels in endothelium obtained from control and diabetic (db/db) mouse aortas. These miR levels will be compared with target mRNA levels by RT-qPCR. Further, to confirm the functional role of LOX-regulating miRNAs in diabetic EC activation, ECs will be treated with miR mimic or antagomir oligonucleotides and evaluated in functional assays, as outlined in Chapter 4.

Together with my current findings, completing these future studies will not only identify other previously-unrecognized mechanochemical mechanisms underlying diabetes-associated pathogenesis, but also further clarify the important role of matrix stiffening in aortic inflammation. Importantly, these studies have the potential to identify new targets for chronic vascular inflammation therapy.

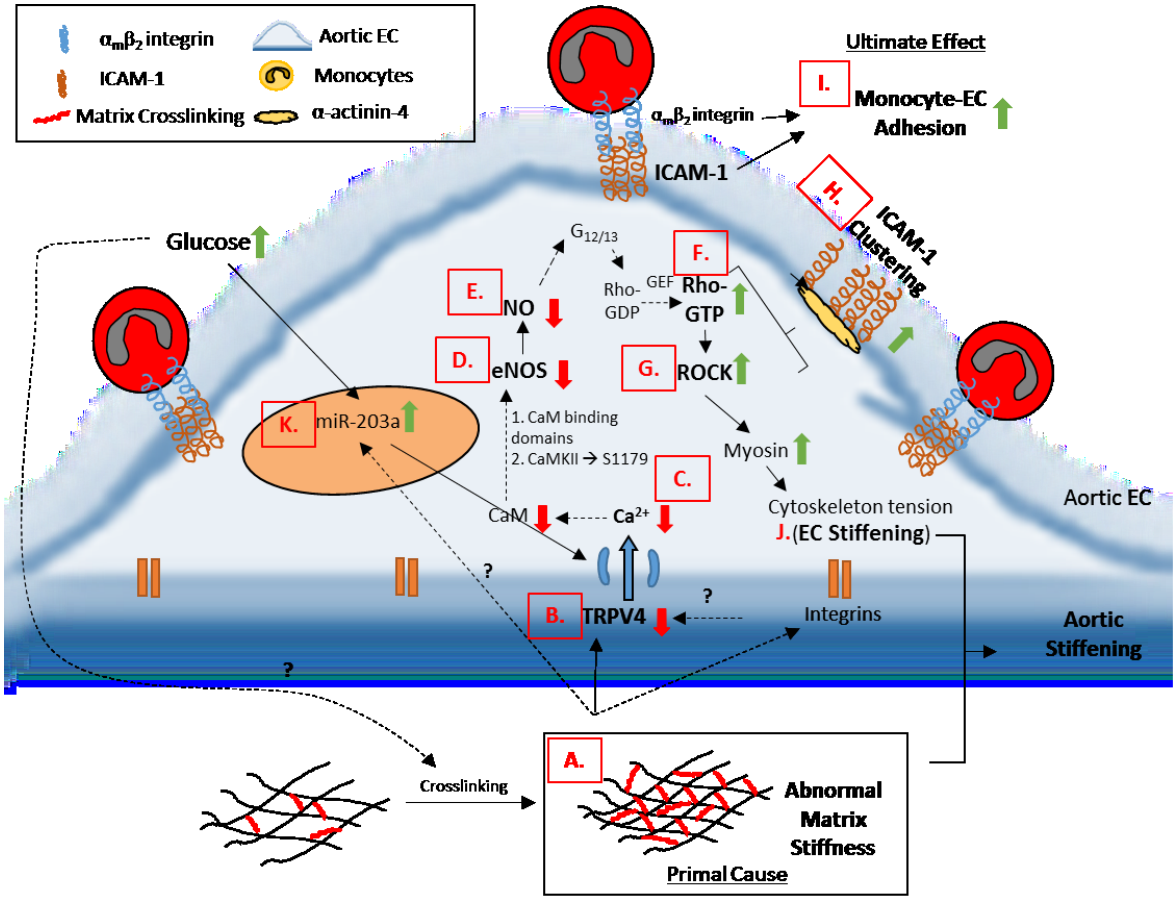

Schematic 5.1: Illustration of endothelial mechanotransduction mediating the effect of abnormal subendothelial matrix stiffness on monocyte-EC adhesion. CaM: calmodulin; CaMKII: calmodulin kinase II; IKK: inhibitory κB kinase; GEF: guanine nucleotide exchange factor; ICAM-1: Intracellular Cell Adhesion Molecule-1; miR: microRNA; NO: Nitric Oxide; ROCK: Rho-associated Kinase; TRPV4; Transient Receptor Potential Vanilloid 4

References

1. D. Kothapalli, S. L. Liu, Y. H. Bae, J. Monslow, T. Xu, E. A. Hawthorne, F. J. Byfield, P. Castagnino, S. Rao, D. J. Rader, E. Pure, M. C. Phillips, S. Lund-Katz, P. A. Janmey and R. K. Assoian, *Cell Rep*, 2012, **2**, 1259-1271.
2. X. Yang, H. A. Scott, F. Monickaraj, J. Xu, S. Ardekani, C. F. Nitta, A. Cabrera, P. G. McGuire, U. Mohideen, A. Das and K. Ghosh, *FASEB journal : official publication of the Federation of American Societies for Experimental Biology*, 2016, **30**, 601-611.
3. H. Yao, G. Arunachalam, J. W. Hwang, S. Chung, I. K. Sundar, V. L. Kinnula, J. D. Crapo and I. Rahman, *Proceedings of the National Academy of Sciences of the United States of America*, 2010, **107**, 15571-15576.
4. B. Suki, R. Jesudason, S. Sato, H. Parameswaran, A. D. Araujo, A. Majumdar, P. G. Allen and E. Bartolak-Suki, *Pulmonary pharmacology & therapeutics*, 2012, **25**, 268-275.
5. X. Yang, H. A. Scott, S. Ardekani, M. Williams, P. Talbot and K. Ghosh, *Investigative ophthalmology & visual science*, 2014, **55**, 3140-3147.
6. J. Diez, *Advances in cardiology*, 2007, **44**, 76-95.
7. K. Ghosh and D. E. Ingber, *Advanced drug delivery reviews*, 2007, **59**, 1306-1318.
8. J. Eyckmans, T. Boudou, X. Yu and C. S. Chen, *Dev Cell*, 2011, **21**, 35-47.
9. A. Mammoto, T. Mammoto and D. E. Ingber, *J Cell Sci*, 2012, **125**, 3061-3073.
10. A. Mammoto, K. M. Connor, T. Mammoto, C. W. Yung, D. Huh, C. M. Aderman, G. Mostoslavsky, L. E. Smith and D. E. Ingber, *Nature*, 2009, **457**, 1103-1108.
11. A. Mammoto, T. Mammoto, M. Kanapathipillai, C. Wing Yung, E. Jiang, A. Jiang, K. Lofgren, E. P. Gee and D. E. Ingber, *Nature communications*, 2013, **4**, 1759.
12. N. Wang, J. D. Tytell and D. E. Ingber, *Nature reviews. Molecular cell biology*, 2009, **10**, 75-82.
13. F. J. Alenghat, J. D. Tytell, C. K. Thodeti, A. Derrien and D. E. Ingber, *Journal of cellular biochemistry*, 2009, **106**, 529-538.
14. B. Wojciak-Stothard, L. Williams and A. J. Ridley, *The Journal of cell biology*, 1999, **145**, 1293-1307.
15. A. Schaefer and P. L. Hordijk, *J Cell Sci*, 2015, **128**, 2221-2230.
16. B. H. Maskrey, I. L. Megson, P. D. Whitfield and A. G. Rossi, *Arteriosclerosis, thrombosis, and vascular biology*, 2011, **31**, 1001-1006.
17. M. M. Hartge, T. Unger and U. Kintscher, *Diabetes & vascular disease research : official journal of the International Society of Diabetes and Vascular Disease*, 2007, **4**, 84-88.
18. G. Arunachalam, I. K. Sundar, J. W. Hwang, H. Yao and I. Rahman, *J Inflamm (Lond)*, 2010, **7**, 34.
19. H. Ulbrich, E. E. Eriksson and L. Lindbom, *Trends in pharmacological sciences*, 2003, **24**, 640-647.

20. M. Schnoor, *J Immunol*, 2015, **194**, 3535-3541.
21. J. S. Pober and W. C. Sessa, *Nature reviews. Immunology*, 2007, **7**, 803-815.
22. J. Huynh, N. Nishimura, K. Rana, J. M. Peloquin, J. P. Califano, C. R. Montague, M. R. King, C. B. Schaffer and C. A. Reinhart-King, *Science translational medicine*, 2011, **3**, 112ra122.
23. D. E. Ingber, N. Wang and D. Stamenovic, *Rep Prog Phys*, 2014, **77**, 046603.
24. T. Yeung, P. C. Georges, L. A. Flanagan, B. Marg, M. Ortiz, M. Funaki, N. Zahir, W. Ming, V. Weaver and P. A. Janmey, *Cell motility and the cytoskeleton*, 2005, **60**, 24-34.
25. K. Ghosh, C. K. Thodeti, A. C. Dudley, A. Mammoto, M. Klagsbrun and D. E. Ingber, *Proceedings of the National Academy of Sciences of the United States of America*, 2008, **105**, 11305-11310.
26. B. V. Shekhonin, S. P. Domogatsky, G. L. Idelson, V. E. Koteliansky and V. S. Rukosuev, *Atherosclerosis*, 1987, **67**, 9-16.
27. E. A. Ryan, L. F. Mockros, J. W. Weisel and L. Lorand, *Biophysical journal*, 1999, **77**, 2813-2826.
28. J. Peloquin, J. Huynh, R. M. Williams and C. A. Reinhart-King, *Journal of biomechanics*, 2011, **44**, 815-821.
29. J. Panes, M. A. Perry, D. C. Anderson, A. Manning, B. Leone, G. Cepinskas, C. L. Rosenbloom, M. Miyasaka, P. R. Kvietys and D. N. Granger, *The American journal of physiology*, 1995, **269**, H1955-1964.
30. D. S. McLeod, D. J. Lefer, C. Merges and G. A. Lutty, *The American journal of pathology*, 1995, **147**, 642-653.
31. E. W. Ades, F. J. Candal, R. A. Swerlick, V. G. George, S. Summers, D. C. Bosse and T. J. Lawley, *The Journal of investigative dermatology*, 1992, **99**, 683-690.
32. G. K. Kolluru, J. H. Siamwala and S. Chatterjee, *Biochimie*, 2010, **92**, 1186-1198.
33. J. M. Skeie, J. H. Fingert, S. R. Russell, E. M. Stone and R. F. Mullins, *Investigative ophthalmology & visual science*, 2010, **51**, 5336-5342.
34. C. P. Aaron, J. E. Schwartz, S. J. Bielinski, E. A. Hoffman, J. H. Austin, E. C. Oelsner, K. M. Donohue, R. Kalhan, C. Berardi, J. D. Kaufman, D. R. Jacobs, Jr., R. P. Tracy and R. G. Barr, *Respiratory medicine*, 2015, **109**, 255-264.
35. G. Liu, S. M. Vogel, X. Gao, K. Javaid, G. Hu, S. M. Danilov, A. B. Malik and R. D. Minshall, *Arteriosclerosis, thrombosis, and vascular biology*, 2011, **31**, 1342-1350.
36. K. M. Stroka and H. Aranda-Espinoza, *Blood*, 2011, **118**, 1632-1640.
37. N. Heemskerk, J. van Rijssel and J. D. van Buul, *Cell Adhesion & Migration*, 2014, **8**, 67-75.
38. M. J. Paszek, N. Zahir, K. R. Johnson, J. N. Lakins, G. I. Rozenberg, A. Gefen, C. A. Reinhart-King, S. S. Margulies, M. Dembo, D. Boettiger, D. A. Hammer and V. M. Weaver, *Cancer Cell*, 2005, **8**, 241-254.
39. P. Y. Liu and J. K. Liao, *Methods in enzymology*, 2008, **439**, 181-189.
40. K. Burridge and K. Wennerberg, *Cell*, 2004, **116**, 167-179.
41. X. Ren, W. B. Kiosses and M. A. Scwartz, *EMBO J*, 1999, **18**, 578-585.

42. S. Huveneers, M. J. Daemen and P. L. Hordijk, *Circulation research*, 2015, **116**, 895-908.
43. A. Schaefer, J. Te Riet, K. Ritz, M. Hoogenboezem, E. C. Anthony, F. P. Mul, C. J. de Vries, M. J. Daemen, C. G. Figdor, J. D. van Buul and P. L. Hordijk, *J Cell Sci*, 2014, **127**, 4470-4482.
44. X. Yang, H. Scott, F. Monickaraj, J. Xu, S. Ardekani, C. Nitta, A. Cabrera, P. McGuire, M. U, A. Das and K. Ghosh, *FASEB journal : official publication of the Federation of American Societies for Experimental Biology*, 2015, In Press.
45. D. Kothapalli, P. Castagnino, D. J. Rader, M. C. Phillips, S. Lund-Katz and R. K. Assoian, *Atherosclerosis*, 2013, **227**, 65-71.
46. R. Arita, Y. Hata, S. Nakao, T. Kita, M. Miura, S. Kawahara, S. Zandi, L. Almulki, F. Tayyari, H. Shimokawa, A. Hafezi-Moghadam and T. Ishibashi, *Diabetes*, 2009, **58**, 215-226.
47. M. Hirakawa, M. Oike, Y. Karashima and Y. Ito, *J Physiol*, 2004, **558**, 479-488.
48. K. Burridge and K. Wennerberg, *Cell*, 2004, **116**, 167-179.
49. X. D. Ren, W. B. Kiosses and M. A. Schwartz, *EMBO J*, 1999, **18**, 578-585.
50. K. Ghosh, Z. Pan, E. Guan, S. Ge, Y. Liu, T. Nakamura, X. D. Ren, M. Rafailovich and R. A. Clark, *Biomaterials*, 2007, **28**, 671-679.
51. R. Martinelli, A. S. Zeiger, M. Whitfield, T. E. Sciuto, A. Dvorak, K. J. Van Vliet, J. Greenwood and C. V. Carman, *J Cell Sci*, 2014, **127**, 3720-3734.
52. A. Zernecke and C. Weber, *Cardiovascular research*, 2010, **86**, 192-201.
53. A. S. Go, D. Mozaffarian, V. L. Roger, E. J. Benjamin, J. D. Berry, M. J. Blaha, S. Dai, E. S. Ford, C. S. Fox, S. Franco, H. J. Fullerton, C. Gillespie, S. M. Hailpern, J. A. Heit, V. J. Howard, M. D. Huffman, S. E. Judd, B. M. Kissela, S. J. Kittner, D. T. Lackland, J. H. Lichtman, L. D. Lisabeth, R. H. Mackey, D. J. Magid, G. M. Marcus, A. Marelli, D. B. Matchar, D. K. McGuire, E. R. Mohler, 3rd, C. S. Moy, M. E. Mussolino, R. W. Neumar, G. Nichol, D. K. Pandey, N. P. Paynter, M. J. Reeves, P. D. Sorlie, J. Stein, A. Towfighi, T. N. Turan, S. S. Virani, N. D. Wong, D. Woo and M. B. Turner, *Circulation*, 2014, **129**, 399-410.
54. S. Karbach, P. Wenzel, A. Waisman, T. Munzel and A. Daiber, *Current pharmaceutical design*, 2014, **20**, 3579-3594.
55. G. Cirino, S. Fiorucci and W. C. Sessa, *Trends in pharmacological sciences*, 2003, **24**, 91-95.
56. J. L. Balligand, O. Feron and C. Dessy, *Physiological reviews*, 2009, **89**, 481-534.
57. I. Jardin, N. Dionisio, J. J. Lopez, G. M. Salido and J. A. Rosado, *Current vascular pharmacology*, 2013, **11**, 480-489.
58. R. Köhler and J. Hoyer, in *TRP Ion Channel Function in Sensory Transduction and Cellular Signaling Cascades*, eds. W. Liedtke and S. Heller, Circ Press, Boca Raton, FL, 2007, ch. 27, pp. 377-388.
59. S. A. Mendoza, J. Fang, D. D. Gutterman, D. A. Wilcox, A. H. Bubolz, R. Li, M. Suzuki and D. X. Zhang, *American journal of physiology. Heart and circulatory physiology*, 2010, **298**, H466-476.
60. C. K. Thodeti, B. Matthews, A. Ravi, A. Mammoto, K. Ghosh, A. L. Bracha and D. E. Ingber, *Circulation research*, 2009, **104**, 1123-1130.

61. W. Liedtke, *Handbook of experimental pharmacology*, 2007, DOI: 10.1007/978-3-540-34891-7_28, 473-487.
62. H. A. Scott, B. Quach, X. Yang, S. Ardekani, A. P. Cabrera, R. Wilson, I. Messaoudi-Powers and K. Ghosh, *Integr Biol (Camb)*, 2016, **8**, 869-878.
63. R. K. Adapala, P. K. Talasila, I. N. Bratz, D. X. Zhang, M. Suzuki, J. G. Meszaros and C. K. Thodeti, *American journal of physiology. Heart and circulatory physiology*, 2011, **301**, H757-765.
64. J. Vriens, G. Owsianik, B. Fisslthaler, M. Suzuki, A. Janssens, T. Voets, C. Morisseau, B. D. Hammock, I. Fleming, R. Busse and B. Nilius, *Circulation research*, 2005, **97**, 908-915.
65. R. Stocker and J. Keany, *Physiol Rev*, 2003, **84**.
66. X. Ma, J. Du, P. Zhang, J. Deng, J. Liu, F. F. Lam, R. A. Li, Y. Huang, J. Jin and X. Yao, *Hypertension*, 2013, **62**, 134-139.
67. K. Monaghan, J. McNaughten, M. K. McGahon, C. Kelly, D. Kyle, P. H. Yong, J. G. McGeown and T. M. Curtis, *PLoS One*, 2015, **10**, e0128359.
68. R. Maroto, A. Raso, T. G. Wood, A. Kurosky, B. Martinac and O. P. Hamill, *Nat Cell Biol*, 2005, **7**, 179-185.
69. K. Muraki, Y. Iwata, Y. Katanosaka, T. Ito, S. Ohya, M. Shigekawa and Y. Imaizumi, *Circulation research*, 2003, **93**, 829-838.
70. R. N. Willette, W. Bao, S. Nerurkar, T. L. Yue, C. P. Doe, G. Stankus, G. H. Turner, H. Ju, H. Thomas, C. E. Fishman, A. Sulpizio, D. J. Behm, S. Hoffman, Z. Lin, I. Lozinskaya, L. N. Casillas, M. Lin, R. E. Trout, B. J. Votta, K. Thorneloe, E. S. Lashinger, D. J. Figueroa, R. Marquis and X. Xu, *J Pharmacol Exp Ther*, 2008, **326**, 443-452.
71. M. E. Assar, J. Angulo and L. Rodriguez-Manas, *The Journal of physiology*, 2016, **594**, 2125-2146.
72. N. A. Shirwany and M. H. Zou, *Front Biosci (Landmark Ed)*, 2012, **17**, 1140-1164.
73. M. A. Reddy, S. Das, C. Zhuo, W. Jin, M. Wang, L. Lanting and R. Natarajan, *Arteriosclerosis, thrombosis, and vascular biology*, 2016, **36**, 864-873.
74. M. A. Reddy, W. Jin, L. Villeneuve, M. Wang, L. Lanting, I. Todorov, M. Kato and R. Natarajan, *Arteriosclerosis, thrombosis, and vascular biology*, 2012, **32**, 721-729.
75. M. A. Reddy and R. Natarajan, *Sub-cellular biochemistry*, 2013, **61**, 435-454.
76. M. Spiecker, H. B. Peng and J. K. Liao, *The Journal of biological chemistry*, 1997, **272**, 30969-30974.
77. R. De Caterina, P. Libby, H. B. Peng, V. J. Thannickal, T. B. Rajavashisth, M. A. Gimbrone, Jr., W. S. Shin and J. K. Liao, *The Journal of clinical investigation*, 1995, **96**, 60-68.
78. H. B. Peng, P. Libby and J. K. Liao, *The Journal of biological chemistry*, 1995, **270**, 14214-14219.
79. M. Kato and R. Natarajan, *Nat Rev Nephrol*, 2014, **10**, 517-530.
80. P. Neth, M. Nazari-Jahantigh, A. Schober and C. Weber, *Cardiovascular research*, 2013, **99**, 294-303.

81. A. H. Bubolz, S. A. Mendoza, X. Zheng, N. S. Zinkevich, R. Li, D. D. Gutterman and D. X. Zhang, *Am J Physiol Heart Circ Physiol*, 2012, **302**, H634-642.
82. B. Feng, S. Chen, K. McArthur, Y. Wu, S. Sen, Q. Ding, R. Feldman and S. Chakrabarti, *Diabetes*, 2011, **60**.
83. K. McArthur, B. Feng, Y. Wu, S. Chen and S. Chakrabarti, *Diabetes*, 2011, **60**, 1314-1323.
84. A. Mammoto, T. Mammoto and D. E. Ingber, *Current opinion in hematology*, 2008, **15**, 228-234.
85. B. D. Matthews, C. K. Thodeti, J. D. Tytell, A. Mammoto, D. R. Overby and D. E. Ingber, *Integr Biol (Camb)*, 2010, **2**, 435-442.
86. H. Suzuki, K. Kimura, H. Shirai, K. Eguchi, S. Higuchi, A. Hinoki, K. Ishimaru, E. Brailoiu, D. N. Dhanasekaran, L. N. Stemmle, T. A. Fields, G. D. Frank, M. V. Autieri and S. Eguchi, *Arteriosclerosis, thrombosis, and vascular biology*, 2009, **29**, 217-224.
87. N. L. Reynaert, K. Ckless, S. H. Korn, N. Vos, A. S. Guala, E. F. Wouters, A. van der Vliet and Y. M. Janssen-Heininger, *Proceedings of the National Academy of Sciences of the United States of America*, 2004, **101**, 8945-8950.
88. J. Chou, P. Shahi and Z. Werb, *Cell Cycle*, 2013, **12**, 3262-3271.
89. M. Sun, S. Gomes, P. Chen, C. A. Frankenberger, D. Sankarasharma, C. H. Chung, K. K. Chada and M. R. Rosner, *Oncogene*, 2014, **33**, 3528-3537.